

# New Models of Dark Matter and Prospects for Measurements

by  
Timothy Cohen

A dissertation submitted in partial fulfillment  
of the requirements for the degree of  
Doctor of Philosophy  
(Physics)  
in The University of Michigan  
2011

Doctoral Committee:

Assistant Professor Aaron Pierce, Chair  
Professor Dante Eric Amidei  
Assistant Professor Henriette Elvang  
Assistant Professor Oleg Y. Gnedin  
Assistant Professor Kathryn Zurek

To all the musicians in the Downtown scene, especially Jim Black, Chris Speed, and John Hollenbeck — for filling my ears while I was busy working to fill my mind.

## ACKNOWLEDGEMENTS

I would like to thank my advisor, Aaron Pierce, for his guidance and mentorship over the last four years. Working for him has been a pleasure and has deeply altered my learning process and my approach to problem solving.

I would like to thank my collaborators on these and other projects: Henriette Elvang, Michael Kiermaier, Eric Kuflik, David Morrissey, Daniel Phalen, and Kathryn Zurek.

I would like to thank my committee members, professors Dante Amidei, Henriette Elvang, Oleg Gnedin and Kathryn Zurek, for their feedback on my work, and professors Ratin Akhoury, Gordon Kane, Leo Pando-Zayas, Finn Larsen, Jim Liu, and James Wells for always being enthusiastic to share their knowledge. I benefited from engaging conversations with the students and postdocs in our research group, especially Ibou Bah, Alberto Faraggi, Dan Feldman, Kentaro Hanaki, Sam McDermott, Phil Szepietowski, and Brian Wecht.

I would of course like to thank my brother, my parents, and my friends for support and encouragement throughout this process. In particular, I could not have survived the first three years of graduate school without Samantha and Jennifer, and cannot imagine being happy in my current life without the continuous shower of affection I receive from my darling Whitney. Much love to you all.

# TABLE OF CONTENTS

DEDICATION . . . . .	ii
ACKNOWLEDGEMENTS . . . . .	iii
LIST OF FIGURES . . . . .	vi
LIST OF TABLES . . . . .	x
LIST OF APPENDICES . . . . .	xi
<b>CHAPTER</b>	
<b>I. Introduction . . . . .</b>	<b>1</b>
1.1 Extending the Standard Model . . . . .	4
1.1.1 Supersymmetry . . . . .	5
1.1.2 Alternatives to Supersymmetry . . . . .	7
1.2 Postulating a History for the Universe . . . . .	9
1.2.1 Thermal Dark Matter . . . . .	10
1.2.2 Non-thermal Dark Matter . . . . .	12
1.2.3 Asymmetric Dark Matter . . . . .	13
1.3 Confronting Reality . . . . .	14
1.3.1 Direct Detection Experiments . . . . .	15
1.3.2 Indirect Detection Experiments . . . . .	16
1.3.3 Collider Experiments . . . . .	17
1.4 Outline . . . . .	18
<b>II. Changes in Dark Matter Properties After Freeze-Out . . . . .</b>	<b>21</b>
2.1 A late-time phase transition . . . . .	22
2.2 A Dark Matter sector . . . . .	25
2.3 Phenomenology of a Late Phase Transition . . . . .	28
2.4 Discussion . . . . .	30
<b>III. Asymmetric Dark Matter from a GeV Hidden Sector . . . . .</b>	<b>32</b>
3.1 Ingredients . . . . .	33
3.2 A Supersymmetric Model . . . . .	35
3.3 Cosmology . . . . .	38
3.3.1 After Decoupling of Asymmetry Transfer . . . . .	41
3.3.2 Cosmology of Models with $\mathcal{O}_{\text{asym}} \sim S^2 U^c D^c D^c$ . . . . .	43
3.3.3 Cosmology of Models with $\mathcal{O}_{\text{asym}} \sim S^2 (LH_u)^2$ . . . . .	45

3.3.4	Variations on the Cosmological History . . . . .	47
3.4	Direct Detection . . . . .	48
3.5	Colliders . . . . .	50
3.6	Discussion and Conclusions . . . . .	51
<b>IV.</b>	<b>Leptophilic Dark Matter from the Lepton Asymmetry . . . . .</b>	<b>53</b>
4.1	Ingredients . . . . .	54
4.2	An Explicit Model . . . . .	56
4.3	Indirect Detection Signals and Neutrino Masses . . . . .	58
4.4	Direct Detection . . . . .	60
4.5	Discussion . . . . .	61
<b>V.</b>	<b>On the Correlation Between the Spin-Independent and Spin-Dependent Direct Detection of Dark Matter . . . . .</b>	<b>62</b>
5.1	Direct Detection Preliminaries . . . . .	65
5.1.1	Spin Independent . . . . .	67
5.1.2	Spin Dependent . . . . .	68
5.2	Direct Detection of Neutralino dark matter . . . . .	70
5.3	The Argument for a Well-Tempered Neutralino . . . . .	72
5.3.1	Thermal history . . . . .	73
5.3.2	Non-thermal options . . . . .	74
5.4	Spin Dependent Cross Sections for Mixed Dark Matter . . . . .	75
5.5	Spin Independent versus Spin Dependent . . . . .	80
5.5.1	Large SI and Large SD . . . . .	82
5.5.2	Small SI and Small SD . . . . .	85
5.5.3	Large SI and Small SD . . . . .	86
5.5.4	Small SI and Large SD . . . . .	87
5.6	Conclusions . . . . .	89
<b>VI.</b>	<b>Extracting the Dark Matter Mass from Single Stage Cascade Decays at the LHC . . . . .</b>	<b>92</b>
6.1	Introduction . . . . .	92
6.2	$M_{T_2}$ Preliminaries . . . . .	95
6.3	Mass Determination from $M_{T_2}$ Bowls . . . . .	98
6.3.1	Statistical Analysis of $M_{T_2}$ Bowls . . . . .	102
6.4	Sources of Error . . . . .	104
6.4.1	Detector Effects . . . . .	106
6.4.2	Background Contamination and Cuts . . . . .	107
6.4.3	Variation in $M_{T_2}^{\max}$ . . . . .	109
6.5	Discussion and Conclusions . . . . .	111
<b>VII.</b>	<b>Summary and Conclusions . . . . .</b>	<b>114</b>
	<b>APPENDICES . . . . .</b>	<b>117</b>
	<b>BIBLIOGRAPHY . . . . .</b>	<b>132</b>

## LIST OF FIGURES

**Figure**

3.1	The spectrum of the SUSY model. We have illustrated the mass pattern of the $S/T$ multiplet (not to scale) since this splitting determines the identity of the DM. The splittings within the dark photon multiplet have been suppressed. . . . .	38
3.2	Constraints in the $\epsilon - g_d$ plane. We have shown the regions which are excluded by BBN constraints due to $\tilde{\gamma}_d \rightarrow \gamma \tilde{G}$ [134] (orange), $B$ -factories due to direct searches for $\gamma_d$ [99] (green), and precision electroweak measurements due to $\gamma_d - Z^0$ mixing [120] (brown). The red region corresponds to parameters which solve the lithium-7 problem [134]. On the left (right) we show contours where $\lambda$ is constrained so as not to reach Landau pole before $M_{\text{GUT}}$ (10 TeV) for $m_{\text{DM}} = 14.2$ GeV, $m_{\text{DM}} = 7.1$ GeV and $m_{\text{DM}} = 3.3$ GeV, assuming $\langle D_Y \rangle = 72$ GeV. The region below these contours is excluded. . . . .	44
3.3	The one-loop diagram which generates the $S$ number violating mass $b_S$ . . . . .	45
3.4	The predictions for the direct detection scattering cross sections normalized per proton ( $\sigma_p$ ) for $m_{\text{DM}} = 14.2$ GeV, 7.1 GeV and 3.3 GeV. We have plotted current/projected limits (also normalized per proton) from Xenon-10 (solid black line), Xenon-100 with 6,000 kg-days (dashed green line), Xenon-1T (dotted blue line) [133], and Majorana (dot-dashed purple line) [83]. . . . .	50
5.1	Current bounds on SI (left) and SD (right) DM-nucleon cross sections. The COUPP and XENON100 projected SD bounds are only estimates – we have scaled the current exclusion curve of COUPP by a factor of $10^{-3}$ [154] and the current SD exclusion curve of XENON10 by the factor which scales the XENON10 SI limit to the XENON100 SI limit. . . . .	66
5.2	$\sigma_{\text{SD}}^p$ , as a function of $m_\chi$ for points satisfying the relic density constraint. We have imposed gaugino mass unification and taken the decoupling limit. The shaded region above the dotted line corresponds to “large” SD and will be probed in the near term. The solid red line is the current bound from IceCube, assuming annihilation to $W^+ W^-$ . The blue hatched region is filled in if the assumption of gaugino mass unification is relaxed. The sfermion masses are taken to be $\mathcal{O}(2\text{ TeV})$ . . . . .	79

5.3	<p>The <math>\max(\sigma_{\text{SI}}^p, \sigma_{\text{SI}}^n)</math> vs. <math>\sigma_{\text{SD}}^p</math> cross sections in pb for the MSSM. The dots (in blue) and crosses (in red) correspond to <math> \mu  &lt; 500</math> GeV and <math> \mu  &gt; 500</math> GeV respectively. The horizontal (vertical) line refers to the projected sensitivity for the next generation of SI (SD) experiments. We have shaded the near-term probeable region. Note that we are neglecting the dependence of this sensitivity on the neutralino mass. We have <i>not</i> imposed the thermal relic density constraint – all points are taken to have <math>\rho_{\text{DM}} = 0.3 \text{ GeV}/\text{cm}^3</math>, regardless of thermal abundance. All sfermions have masses of <math>\mathcal{O}(2 \text{ TeV})</math>. If one takes the decoupling limit, there is a maximum value for <math>\sigma_{\text{SD}} = 3 \times 10^{-8}</math> pb. . . . .</p>	83
5.4	<p>The <math>\max(\sigma_{\text{SI}}^p, \sigma_{\text{SI}}^n)</math> vs. <math>\sigma_{\text{SD}}^p</math> cross sections in pb for the MSSM. We have imposed that the thermal abundance of the neutralinos is within <math>\pm 3\sigma</math> of the WMAP measurement. The dots (in blue) and crosses (in red) correspond to <math> \mu  &lt; 500</math> GeV and <math> \mu  &gt; 500</math> GeV respectively. The horizontal (vertical) line refers to the projected sensitivity for the next generation of SI (SD) experiments. We have shaded the near-term probeable region. Note that we are neglecting the dependence of this sensitivity on the neutralino mass. All sfermions have masses of <math>\mathcal{O}(2 \text{ TeV})</math>. . . . .</p>	84
5.5	<p>The <math>\max(\sigma_{\text{SI}}^p, \sigma_{\text{SI}}^n)</math> vs. <math>\sigma_{\text{SD}}^p</math> cross sections in pb for the MSSM with gaugino mass unification. We have imposed that the thermal abundance of the neutralinos is within <math>\pm 3\sigma</math> of the WMAP measurement. We have taken the decoupling limit (<math>m_A = 4 \text{ TeV}</math>). The dots (in blue) and crosses (in red) correspond to <math> \mu  &lt; 500</math> GeV and <math> \mu  &gt; 500</math> GeV respectively (see the text for a discussion). The horizontal (vertical) line refers to the projected sensitivity for the next generation of SI (SD) experiments. We have shaded the near-term probeable region. Note that we are neglecting the dependence of this sensitivity on the neutralino mass. All sfermions have masses of <math>\mathcal{O}(2 \text{ TeV})</math>. . . . .</p>	85
5.6	<p>Plot of the SI DD cross section for the neutralino scattering off of a proton (solid), a neutron (dashed) and both (dotted) as a function of <math>m_A</math>. For reference, the size of the SD cross section is about <math>9 \times 10^{-4}</math> pb (proton) and <math>6 \times 10^{-4}</math> pb (neutron) and <math>m_\chi = 93</math> GeV. The thermal relic density is <math>\Omega_{\text{DM}} h^2 = 0.1</math>. The minimum value for the total SI DD is <math>\sigma_{\text{SI}}^{\text{min}} = 3 \times 10^{-12}</math> pb for <math>m_A = 751</math> GeV. By changing <math>m_A</math> by 5%, the cross section becomes <math>\sim 2 \times 10^{-10}</math> pb. For small <math>m_A</math> the cross section is on the order of <math>\sigma_{\text{SI}} \sim 10^{-7}</math> pb and in the decoupling limit the cross section is on the order of <math>\sigma_{\text{SI}} \sim 10^{-9}</math> pb – the entire region where there are not any conspiratorial cancellations is within the reach of the next generation of SI experiments. . . . .</p>	90
6.1	<p>Schematic representation of the <math>n = 1</math> class of processes considered in this work, with additional Up-Stream Radiation (USR). The parent particle is the state which decays to the visible particles and the child DM particles. . . . .</p>	93
6.2	<p>Example of an <math>M_{T2}</math> bowl for 50,000 smuon pair production events with QCD USR. The parent mass is 300 GeV and the child mass is 150 GeV. The events were run through the PGS detector simulator. . . . .</p>	98
6.3	<p><math>P_T</math> of the hardest jet for slepton events with only QCD ISR. The blue dotted line is for <math>m_p = 500</math> GeV, the red dashed line is for <math>m_p = 300</math> GeV and the yellow solid line is for <math>m_p = 100</math> GeV. Note from Eq. (VI.8) that the correction to <math>M_{T2}</math> due to USR is of the form <math>P_T/m_p</math>. . . . .</p>	101

6.4	$P_T$ of the hardest jet with new colored state dominating the USR. Specifically, these colored states are squarks. The blue dotted line is for $m_{\text{col}} = 1400$ GeV, the red dotted line is for $m_{\text{col}} = 1000$ GeV and the yellow solid line is for $m_{\text{col}} = 600$ GeV. We have fixed $m_p = 300$ GeV in all cases. From Eq. (VI.8), the correction to $M_{T2}$ due to USR is of the form $P_T/m_p$ . . . . .	102
6.5	Mean and $\pm 1\text{-}\sigma$ statistical error bars for a DM mass measurement as a function of the number of signal events <i>before</i> cuts. The only source of USR is initial state radiation. The process we simulated is electroweak smuon production. The error bars will improve by $\mathcal{O}(1)$ for fermionic parents. The parent mass is 100 GeV and the child masses are 75 GeV (green), 50 GeV (blue) and 25 GeV (red) from top to bottom. The dashed lines show the actual child mass. Note that detector effects have been simulated for the underlying events and that the DM mass measurement systematically undershoots the actual value on account of these effects. . . . .	104
6.6	Same as Fig. 6.5 except that the parent mass is 300 GeV and the child masses are 225 GeV (green), 150 GeV (blue) and 75 GeV (red) from top to bottom. As explained in the text, we find that cuts designed to eliminate the background will not change these results. . . . .	105
6.7	Same as Fig. 6.5 except that the parent mass is 500 GeV and the child masses are 375 GeV (green), 250 GeV (blue) and 125 GeV (red) from top to bottom. As explained in the text, we find that cuts designed to eliminate the background will not change these results. . . . .	105
6.8	Same as Fig. 6.6 except that the dominant source of USR is new heavy colored states. These colored states are squarks which produce chargino parents and jets. The parent mass is 300 GeV and the child mass is 150 GeV for all three cases. The mass of the colored objects are 1400 GeV (green), 1000 GeV (blue) and 600 GeV (red) from top to bottom. As explained in the text, we find that cuts designed to eliminate the background will not change these results. . . . .	106
6.9	Same as Fig. 6.6 except that the underlying events are parton level. . . . .	107
6.10	$M_{T2}(\tilde{m}_c = 0)$ distribution for $t\bar{t}$ events where we have treated this as an $n = 1$ process where the $b$ -jets are USR and the $W^\pm$ are the parent particles. This plot is made before cuts and we have included detector effects. There is an endpoint at $m_W$ since the child, <i>i.e.</i> the neutrino, mass is zero in these events. . . . .	109
6.11	$M_{T2}$ bowl for 25,000 (10,000) slepton (squark) pair production events which give jets, two muons and missing energy. The bowls on the left column only have QCD ISR. The bowls on the right have additional colored states which dominate the USR, and we have taken $m_p = 300$ GeV and $m_c = 150$ GeV for these cases. Note that the cuts preserve the minimum in all cases except $m_p = 100$ GeV. Additionally, when one does a cut on $M_{T2}(\tilde{m}_c = 0)$ , the bowl will be unaffected as long as this cut is taken below $M_{T2}^{\text{max}}$ for the bowl in question. . . . .	110
6.12	Plot of $M_{T2}$ bowls allowing for variations in the $M_{T2}^{\text{max}}$ endpoint of $\pm 5\%$ and $\pm 2\%$ . All bowls are made with 50,000 smuon pair production events before cuts. For clarity we have not simulated detector effects for these events. . . . .	112
C.1	Process considered in this section. The proton momenta are $q_i$ , the parent momenta are $k_i$ , the visible momenta are $p_{v_i}$ and the child momenta are $p_{c_i}$ . . . . .	128



C.2	Various distributions for points with the same $M_{T2}$ endpoint for $pp \rightarrow \tilde{\ell}^+ \tilde{\ell}^- \rightarrow \ell^+ \ell^- \tilde{\chi}^0 \tilde{\chi}^0$ . As shown in Appendix C.2, the data only depends on $M_{T2}^{\max}$ with a slight variation due to $\hat{s}/(4m_p^2)$ . The distributions plotted are the invariant mass of the two visible particles (upper left), the total missing transverse energy (upper right), the total transverse momentum of the visible particles (lower left), and $\Delta R = \sqrt{\Delta\eta^2 + \Delta\phi^2}$ between the two visible particles (lower right). . . . .	131
-----	---	-----

## LIST OF TABLES

### Table

2.1	Benchmark phase transition parameters. . . . .	25
2.2	Benchmark parameters realizing $(\Omega_{\text{DM}} h^2)_{\text{particle}} > (\Omega_{\text{DM}} h^2)_{\text{astro}}$ . . . . .	26
6.1	Cross sections for electroweak pair production of parent particles with various masses and spins including the effects of QCD ISR. We neglect any $t$ -channel processes involving additional states. . . . .	99

# LIST OF APPENDICES

## Appendix

A.	Asymmetric Dark Matter from a GeV Hidden Sector . . . . .	118
A.1	Models with $\mathcal{O}_{\text{asym}} \sim S^2 LH_u$ are not allowed . . . . .	118
B.	On the Correlation Between the Spin-Independent and Spin-Dependent Direct Detection of Dark Matter . . . . .	120
B.1	Squark Contributions to Direct Detection . . . . .	120
B.2	The Bino/Higgsino and Wino/Higgsino Limits . . . . .	121
B.3	No-go Theorem for photino-Higgsino DM . . . . .	123
C.	Extracting the Dark Matter Mass from Single Stage Cascade Decays at the LHC . . . . .	125
C.1	Benchmark Models . . . . .	125
C.1.1	Scalar Parents . . . . .	125
C.1.2	Fermionic Parents . . . . .	126
C.1.3	Vector Parents . . . . .	128
C.2	Phase Space Dependence on $M_{T2}$ . . . . .	128

## CHAPTER I

### Introduction

One of the ultimate goals of the high energy physics community is to answer the question ‘What is the composition of our Universe?’. With the invention of quantum field theory, we have a framework within which to pose this question. The collective efforts of theorists and experimentalists have led us to a concise description which encompasses all terrestrial experimental results to date. We refer to the Lagrangian which encodes this physical picture as the Standard Model of particle physics (SM) — a theory of the strong, weak, and electromagnetic forces, and three families of matter, the quarks and leptons.

So if we can describe the composition and interactions which govern our physical world, is there anything important left to learn? As it turns out, there are a few major issues which are so far unresolved. In particular, the focus of this thesis is an attempt to understand an anomaly which has been around since 1933, when Fritz Zwicky measured the velocity of galaxies in the Coma cluster and noticed that they were moving faster than one would expect from the amount of observable luminous matter [200]. However, since it took nearly 40 years for this observation to be independently corroborated by Vera Rubin’s measurements of the rotation curves of stars in galaxies [177], this phenomenon has only been actively studied since around the time when the SM was discovered.

One plausible explanation for these phenomena is that a non-trivial portion of the matter in galaxies is dark. Further confirmation has come from gravitational lensing measurements

[194] and by studying the perturbation spectrum of the cosmic microwave background (CMB) [147]. Data from the WMAP experiment, our most precise measurement of the CMB spectrum, can be used to deduce that the so called dark matter (DM) contributes 22.9% to the total energy density of the Universe [148], *i.e.*,

$$(I.1) \quad \Omega_{\text{DM}} h^2 = 0.1126 \pm 0.0036,$$

where  $h \simeq 0.702$  parametrizes the uncertainty in the Hubble constant. Since the same data can be used to find that baryonic matter constitutes 4.6%<sup>1</sup>, approximately 83% of the matter in the Universe is dark matter. This measurement is relevant for the epoch of the CMB decoupling, when the Universe became cool enough for the first atoms to form. Using this fact we can infer that the DM cannot be non-luminous chunks of baryonic matter. Such clumps would have altered the CMB spectrum as additional visible SM matter. The DM must be something beyond what we have discovered so far.

We must also be sure that there are no non-baryonic possibilities within the SM that could account for the DM. Specifically, there is a particle within the SM which is stable and dark — the neutrino. Using the what we know about the SM, we can compute the neutrino relic density,  $\Omega_{\nu} h^2 \lesssim 4 \times 10^{-5}$  [146], which is clearly sub-dominant to  $\Omega_{\text{DM}} h^2$ . Another logical possibility which avoids all constraints is that primordial black holes (seeded by the initial over-densities in the SM matter at the end of inflation) account for the DM [111]. However, it is quite difficult to produce the correct relic density using standard big bang cosmology. Therefore, it is a well motivated assumption that the SM cannot account for the presence of DM in our Universe and new physics is necessary.

There is one potential loophole in all of the above arguments. General relativity provides the backbone of our predictions for cosmology. If there is a flaw in our understanding of how gravity behaves on large scales, we could have fooled ourselves into thinking DM is

---

<sup>1</sup>The other 72.5% is due to “dark energy.”

out there when what is really required is a modification of general relativity. However, in 2002 an observation [161], known colloquially as the “bullet cluster,” of two galaxy clusters which collided at some time in the past was made in three channels: X-rays (which measures the position of the hot interstellar gas), gravitation lensing (which traces the total mass of the cluster), and visible light (coming from the galaxies themselves). The hot gas, which accounts for the dominant visible mass of the cluster, clearly had interacted while the majority of the mass, which was no longer aligned with the gas, had not. Hence, the majority of the cluster’s matter must be collisionless matter, implying that the DM question is within the purview of particle physics.

The DM must also be able to account for the structure of the Universe. After the end of inflation, tiny inhomogeneities (due to quantum fluctuations of the field responsible for inflation) were imprinted on the density distribution of the DM. Over time these fluctuations began to collapse due to the attractive nature of gravity, eventually pulling the matter into clumps, thereby forming the skeletal structure of our network of galaxies. In order for the DM to form the mass distribution of galaxies that we observe in our Universe, it must have had a relatively low velocity, *i.e.*, it must have been “cold” at the epoch when its interactions fell out of equilibrium. For a given interaction strength, lighter states will stop interacting with larger average velocities than heavier states. Therefore, the requirement that the DM be cold implies a constraint on the DM mass<sup>2</sup>,  $m_{\text{DM}} \gtrsim \mathcal{O}(\text{keV})$ , which must be accounted for in any given model.

So a good model of DM must account for the relic density (Eq. (I.1)) and must result in cold DM. It must also be stable (at least on cosmological timescales) so that the relic density produced in the big bang would still be around today. As we will describe in Sec. 1.3 below, there are a whole host of other observational constraints which must be considered when attempting to postulate what the DM could be.

---

<sup>2</sup>In models with non-thermal warm DM the constraint is weaker:  $m_{\text{DM}} \gtrsim 550 \text{ eV}$  [193].

Given that there are various flaws of the SM, it is tempting to explore the idea that the physics of DM could be connected to seemingly unrelated extensions of the SM (see Sec. 1.1). This would allow us to understand the presence of  $\Omega_{\text{DM}} \neq 0$  as an inevitable consequence of more fundamental principles. Although these aesthetic considerations may prove to be erroneous, there are many concrete models where these correlations can motivate theoretical explorations and lead to new paradigms of thought.

Finally, since we are proposing scientific hypotheses for how our Universe might behave, we would prefer that these ideas be falsifiable. The ultimate goal of DM phenomenology is not only to construct compelling models, but to eventually have the experimental means for teasing out their structure and measuring all the relevant parameters. This will help realize our ultimate goal of understanding every aspect of the physical world.

## 1.1 Extending the Standard Model

The SM has been wildly successful at accounting for the data taken at collider experiments. However, it has additional flaws beyond the lack of an explanation for the DM.

The SM is technically unnatural [189] due to the presence of the Higgs boson mass parameter in the fundamental Lagrangian. Specifically, the Higgs boson two-point function receives a contribution to its mass which goes as the Wilsonian cutoff squared. This contribution can be interpreted as being generated by integrating out some new state which couples to the SM. For example, if we assume that there are no scales of note between the weak scale and the Planck scale, then the cutoff for the SM would be the Planck mass. In order to reproduce the mass of the  $W^\pm$  boson would then require a fine-tuning of one part in  $10^{32}$ . This is known as the “hierarchy problem.” In principle this level of tuning is allowed, but it is difficult to imagine dynamics from which it would emerge.

One can find another hint of new physics by studying the energy dependence of the SM gauge coupling constants. Assuming that the SM is a valid effective field theory up to very

high energies (on the order of  $10^{16}$  GeV), one can naively apply the SM renormalization group equations. The result is that the strong, weak, and electromagnetic forces almost meet at a point [117]. While this near unification could be an accident, it is possible that something deeper is going on. Therefore, it is not unreasonable to argue for a judicious application of new physics which would cause the couplings to unify.

A final problem stems from cosmology. We have measured that the Universe is dominated by SM matter, with essentially no anti-matter. Beginning with the big bang, one can attempt to dynamically generate this baryon asymmetry by using only the physics of the SM. However, the resulting asymmetry is far smaller than the observation. In order to understand this baryogenesis in a dynamical way will also require extending the SM.

In the following subsection we will briefly review supersymmetry, one compelling paradigm for extending the SM with the capacity to solve all of the above mentioned problems. In particular, these models often include a DM candidate. This framework will underlie some of the models utilized in later chapters of this thesis. For contrast we will end this section with a short discussion of alternatives to SUSY with an emphasis on models which include a potential DM particle.

### 1.1.1 Supersymmetry

Supersymmetry (SUSY) is a spacetime symmetry which relates particles of different spin<sup>3</sup>. In particular, it interchanges fermions with scalars and gauge bosons with fermions. Because the related particles must have identical quantum numbers under other symmetries (*e.g.* the  $SU(3) \times SU(2) \times U(1)$  gauge symmetry of the SM), none of the observed SM particles can be superpartners of each other. This tells us that SUSY must be broken, *i.e.*, the superpartners have different masses than their SM counterparts. Hence, if SUSY is a symmetry of nature, there must exist a new heavy scalar for every SM matter field,

---

<sup>3</sup>See [162] for a review.



the sleptons and squarks, and a new heavy fermion for each gauge boson, the gluino, neutralinos and charginos. Additionally, due to anomaly cancellation constraints and the requirement of a holomorphic superpotential in order to give masses to all the SM fermions, the minimal supersymmetric standard model (MSSM) must include two Higgs doublets.

Due to the SUSY relations, the scalars in these models inherit a notion of chirality from their fermionic partner. Since chiral symmetry protects the fermion masses from additive renormalization, the same becomes true for the scalars — there are no longer quadratic divergences in the scalar masses. Therefore, supersymmetrizing the SM solves the hierarchy problem, which was described above in Sec. 1.1.

One can understand this “miraculous” cancellation diagrammatically by computing the corrections to the Higgs boson mass in the MSSM. Since it has the largest Yukawa coupling, the largest contributions of this type come from loops involving the top quark. In a SUSY model, one must also include the scalar top partner, the stop squark, in the loop as well. Due to Fermi statistics, there is an overall minus sign associated with the fermion loop, and SUSY relates the coupling of the Higgs with the stop to the square of the top Yukawa coupling. All divergences from these contributions cancel among each other to all loop orders, leaving a finite correction to the Higgs mass which depends on the logarithm of the stop mass over the top mass.

SUSY solves other problems as well. Due to the inclusion of so many additional particles with SM charges, the running of the gauge couplings is altered in the MSSM once you reach the threshold of the SUSY breaking masses. When one evolves these couplings up to very high energies in the MSSM they meet at a point [88]. The MSSM automatically includes gauge coupling unification.

There are also a large number of CP violating phases available in the MSSM which could be responsible for generating the baryon asymmetry. Of course, one has to be

careful that these complex parameters do not imply violations of relevant experimental bounds, such as electric dipole measurements. Beyond this general consideration, many models of baryogenesis rely on some of the features of SUSY including the presence of additional scalars (for electroweak baryogenesis [76]) or the existence of  $D$ -flat directions (for Affleck-Dine baryogenesis [8]).

Finally, we note that SUSY is a crucial ingredient in string theory for a variety of reasons including the need to model fermionic particles. If string theory is the actual UV completion of gravity, it is possible in some string-theory based models that weak-scale SUSY would result.

Of central importance to this thesis is an additional constraint on the MSSM, known as  $R$ -parity. This is a symmetry which takes  $\phi \rightarrow \pm\phi$  where the  $+$  is for SM particles and the  $-$  is for superpartners. It is invoked to forbid renormalizable gauge invariant superpotential terms which can lead to many phenomenologically dangerous processes, including rapid proton decay.

A consequence of  $R$ -parity is that the lightest superpartner (LSP) is stable, since it could only decay into something which is odd under  $R$ -parity while only SM states are kinematically allowed. If this particle does not carry electric charge, for example if it is a neutralino, then it can be a DM candidate. In particular, the neutralino is a canonical example of a “weakly interacting massive particle” as described below in Sec. 1.2.1.

For these reasons and more, SUSY models are studied in the context of DM, cosmology, collider physics, and theoretical physics in general.

### 1.1.2 Alternatives to Supersymmetry

While other beyond the SM frameworks will not be utilized in this thesis, for the sake of completeness we will briefly mention other solutions to the hierarchy problem, emphasizing the potential connection to DM.

One possibility is that the fundamental Planck scale is actually at a TeV. This would clearly alleviate the hierarchy problem since corrections to the Higgs mass would be cut off at the weak scale. In order to explain the apparent strength of gravity the authors of [25] proposed the possible existence of one or more additional compact “large extra dimensions.” They were able to show that the “leakage” of gravity into these new dimensions would weaken its effect in the 4-dimensional effective theory. An extension of this model allows all of the SM fields to propagate in the extra dimensions — this is known as the universal extra dimension (UED) scenario [20]. One consequence of these models is that in the 4-dimensional effective theory there would exist a host of new heavy states and a new stabilizing symmetry, known as Kaluza-Klein parity. The lightest of these new particles would be stabilized by this parity and could be responsible for the DM [182].

A variation on this model is to take the new compact 5<sup>th</sup> dimension to be warped instead of flat [174]. One goal of this paradigm, known as the Randall-Sundrum (RS) scenario, is to relieve some of the fine-tuning required to achieve the weak scale which arises when one considers phenomenological constraints on the size of the extra-dimensions. While RS models allow for a rich new class of phenomenology (including a connection to technicolor models via the AdS-CFT correspondence), they do eliminate the parity of the UED model. However, it can be well motivated to extend RS to include an analogous parity which again introduces a DM candidate [9].

One final class of theories assume that the Higgs boson is a strongly coupled composite of new fermions [139]. In its modern incarnation, these are known as Little Higgs models [23]. In this scenario, the Higgs boson is a pseudo-Goldstone boson of some new global symmetry which is broken at the TeV scale. The approximate shift symmetry associated with the pseudo-Goldstone nature of this state protects it from receiving Planck sized corrections to its mass. However, the original scenario was plagued by too-large contributions to precision

electroweak observables which requires one to push up the scale of new physics, thereby reintroducing the fine-tuning problem. In order to cure this ill, a new parity ( $T$ -parity) was introduced [69]. As has been a common theme among all these scenarios (including SUSY), this new parity also provided some options for explaining the DM.

## 1.2 Postulating a History for the Universe

Given a model of particle physics, either the SM or one of the extensions mentioned above, one would like to be able to extract the physical properties of the Universe this model implies. Our modern understanding of cosmology gives a general framework within which one can address these questions in a concrete way. The relevant starting point for exploring the implications with respect to DM is the end of a period of inflation — known as the “big bang.” Immediately after the bang, it is well motivated to assume that the Universe is a thermal bath of particles at some “reheat temperature” which, due to constraints from big bang nucleosynthesis, must be greater than about 10 MeV. From this point on, the temperature falls, the Universe expands, and one must evolve these initial distributions of particles accordingly. The physics of a thermal bath in an expanding Universe is governed by the Boltzmann equation [146]:

$$(I.2) \quad \frac{dn_\psi}{dx} + 3Hn_\psi = -\langle\sigma_{\text{ann}}|v|\rangle \left(n_\psi^2 - (n_\psi^{\text{EQ}})^2\right),$$

where  $\psi$  ( $\bar{\psi}$ ) is the particle (anti-particle) whose distribution is being analyzed,  $n_\psi$  is the  $\psi$  number density,  $H$  is the Hubble parameter,  $x = m_\psi/T$ ,  $m_\psi$  is the mass of  $\psi$ , and  $\langle\sigma_{\text{ann}}|v|\rangle$  is total annihilation cross section for  $\psi + \bar{\psi}$  into anything.

Now we have a set of coupled equations for all the various particles and interactions. In order to determine some of the possibilities that can be realized, we identify two relevant rates which can potentially effect a change in number density:  $H$  (which accounts for the expansion of the Universe) and  $\Gamma_{\text{ann}} \equiv n_\psi \langle\sigma_{\text{ann}}|v|\rangle$  (which tracks the relevance of the

particle’s interactions).

From Eq. (I.2), when  $\Gamma_{\text{ann}} > H$ , the particles are in thermal equilibrium and follow the Boltzmann distribution:

$$(I.3) \quad n_\psi = \frac{1.2}{\pi^2} g T^3 \quad T > m_\psi$$

$$(I.4) \quad n_\psi = \left( \frac{m_\psi T}{2\pi} \right)^{3/2} g \exp\left( \frac{-m_\psi}{T} \right) \quad T < m_\psi,$$

where  $g$  is the number of degrees of freedom for  $\psi$ .

Conversely, when  $\Gamma_{\text{ann}} < H$  the particles no longer interact. This implies that the number density per co-moving volume is fixed, *i.e.*,  $n_\psi \sim 1/T^3$  (unless the particles are unstable and would eventually decay). Hence, this simple equation can imply a large variety of possibilities for the history of our Universe. We will outline three well motivated scenarios in the following three subsections.

### 1.2.1 Thermal Dark Matter

One possibility is known as a “thermal” history for the Universe. The paradigm proceeds in the following way: once inflation ended via reheating and subsequent thermalization, the Universe evolved from that point onwards with all particles following their thermal distributions as long as  $H < \Gamma_{\text{ann}}$  (or  $H < \Gamma_{\text{decay}}$ , where  $\Gamma_{\text{decay}}$  is the decay width for an unstable state) for each particle in the bath. Then it is a good approximation that the only changes in the relative number densities are due to epochs where  $H > \Gamma$  for a given state. For unstable particles,  $H > \Gamma_{\text{decay}}$  implying that unstable particles drop out of the thermal bath — they would decay immediately after being produced and their decay products would instantaneously re-thermalize. For stable particles, when  $H > \Gamma_{\text{ann}}$  they would undergo “freeze-out” — they would stop interacting with the bath and their number density per co-moving volume would be fixed. In a thermal Universe, this is how the DM relic density could have been generated.

Noting that in a hot thermal Universe, the energy density would be dominated by radiation (which is short hand for any relativistic degrees of freedom), one can use Einstein's equation to find that the Hubble rate is given by

$$(I.5) \quad H(T) = 1.66 g_*^{1/2} \frac{T^2}{M_{\text{Pl}}},$$

where  $g_*$  counts the number of relativistic degrees of freedom,  $T$  is the temperature, and  $M_{\text{Pl}}$  is the Planck mass. Then the epoch of freeze-out is determined by

$$(I.6) \quad H(T_{fo}) = \Gamma_{\text{ann}} = n_{\text{DM}} \langle \sigma_{\text{ann}} |v| \rangle,$$

where  $T_{fo}$  is the temperature when freeze-out occurs. As described above, observations imply that the DM is cold, *i.e.*, it is non-relativistic at freeze-out. Hence, we can approximate  $n_{\text{DM}}$  using Eq. (I.4) and we use Eq. (I.6) to find that  $T_{fo} \simeq m_{\text{DM}}/20$ . Then taking  $\langle \sigma_{\text{ann}} |v| \rangle$  to be independent of temperature and relating  $(n_{\text{DM}} m_{\text{DM}})/(s(T_0) \rho_c) = \Omega_{\text{DM}} h^2$ , where  $s(T_0)$  and  $\rho_c$  are respectively the entropy density and the critical density of the Universe today, we find that

$$(I.7) \quad \Omega_{\text{DM}} h^2 = 1.07 \times 10^9 \text{ GeV}^{-1} \frac{1}{g_*^{1/2} M_{\text{Pl}} \langle \sigma_{\text{ann}} |v| \rangle}.$$

Using the WMAP measurement given in Eq. (I.1), we find that

$$(I.8) \quad \langle \sigma_{\text{ann}} |v| \rangle^{\text{thermal}} \simeq 3 \times 10^{-26} \text{ cm}^3/\text{s}$$

under the assumption that the DM relic density is entirely due to thermal freeze-out.

This result can be interpreted as motivation for a connection to weak scale physics. The argument simply follows from the observation that  $3 \times 10^{-26} \text{ cm}^3/\text{s}$  is a typical size for interactions involving a new weakly interacting massive particle (WIMP). This hint is taken very seriously — it is often referred to as “the WIMP miracle.”

One canonical example of a WIMP is an inevitable consequence of supersymmetrizing the SM, namely the lightest neutralino (in models where it is the LSP), which is a linear

combination of the fermionic superpartner of the weak gauge bosons and the Higgs bosons. As described in Sec. 1.1.1, if  $R$ -parity is enforced, the LSP will be stable. Then for particular values of the parameters relevant for the neutralino mass and interactions,  $\langle\sigma_{\text{ann}}|v|\rangle \approx 3 \times 10^{-26} \text{ cm}^3/\text{s}$  can be realized and the neutralino can be the thermal DM. This provides an example of a well motivated DM candidate. Furthermore, the neutralino as a DM candidate implies a whole host of testable predictions for experiments which will be explored in Ch. V and Ch. VI of this thesis.

### 1.2.2 Non-thermal Dark Matter

A key assumption for the thermal story was that the Universe was radiation dominated at the epoch of DM freeze-out. However, it is possible that some long lived particle,  $\phi$ , could have been produced in the thermal bath that followed inflation, and then subsequently come to dominate the energy density of the Universe before it decayed. There are many hypothetical particles whose presence could lead to this history, *e.g.* gravitinos (the superpartner of the graviton) or string moduli (the fields which parametrize the size and shape of the compact extra dimensions in string theory). If such states exist and were produced at the big bang, they will change the thermal evolution of the Universe by releasing entropy in their decay and diluting the DM relic density. There is also the possibility that the DM could be one of the decay products of  $\phi$ . Then  $\phi$  decays would clearly change the density of DM in the Universe.

To account for the dilution, we compute the change in entropy of the Universe due to the  $\phi$  decays. To do this, one needs to find the temperature of the radiation produced as a result of the decay, known as the re-heat temperature,  $T_{\text{RH}}$ . The  $\phi$  particles will be able to decay when the age of the Universe becomes comparable to the lifetime,  $t \sim \tau_\phi$ . The Friedmann equation (which relates the Hubble constant to the energy density of the

Universe) then implies

$$(I.9) \quad H^2(t = \tau_\phi) \simeq \frac{1}{4}\tau_\phi^{-2} \simeq \frac{8\pi}{3M_{\text{Pl}}}\rho \simeq \frac{8\pi}{3M_{\text{Pl}}}\frac{\pi^2 g_*}{30}T_{\text{RH}}^4,$$

where in the last step we assumed that all of the energy of the  $\phi$  particles is transferred to radiation. Thus,

$$(I.10) \quad T_{\text{RH}} \simeq 0.55g_*^{-1/4}(M_{\text{Pl}}/\tau)^{1/2}.$$

In many models, one decay product of  $\phi$  is the DM [166]. If this is the case and the number density of DM exceeds the fixed point value

$$(I.11) \quad \frac{n_{\text{DM}}}{s} = \frac{3H}{s\langle\sigma_{\text{ann}}|v|\rangle},$$

evaluated for  $T = T_{\text{RH}}$ , then the DM will quickly annihilate down to this value for the number density. The result of being produced by the out-of-equilibrium decays is to change the thermal relic density by a factor:

$$(I.12) \quad \Omega_{\text{DM}} = \Omega_{\text{DM}}^{\text{thermal}} \left( \frac{T_{fo}}{T_{\text{RH}}} \right).$$

This implies that  $\langle\sigma_{\text{ann}}|v|\rangle \neq 3 \times 10^{-26} \text{ cm}^3/\text{s}$  for models with a non-thermal cosmological history. Since  $T_{fo} \sim m_{\text{DM}}/20 \sim 10 \text{ GeV}$  and  $T_{\text{RH}} \gtrsim 10 \text{ MeV}$  (in order to allow for big bang nucleosynthesis to proceed), this dilution factor is on the order of  $10^{-3}$ . Hence, the annihilation cross section appropriate for non-thermal DM can also be seen as associated with the weak scale (*e.g.* pure Wino DM in some SUSY models).

### 1.2.3 Asymmetric Dark Matter

Another paradigm for DM is motivated by the observation that  $\Omega_{\text{DM}} \simeq 5 \Omega_{\text{baryons}}$ . In models of asymmetric dark matter (ADM) [140], the DM carries baryon and/or lepton number and its relic density is set by the baryon asymmetry.

Given a DM-anti-DM pair, one can define a conserved (or approximately conserved) quantum number such that the DM has opposite charge from the anti-DM. We refer to



this charge as “dark matter number.” Then if an operator of the schematic form  $\mathcal{O}_{\text{asym}} = \mathcal{O}_{\text{DM}}\mathcal{O}_{B-L}$  (where  $\mathcal{O}_{\text{DM}}$  ( $\mathcal{O}_{B-L}$ ) carries non-zero DM ( $B-L$ ) number) is ever in thermal equilibrium it will spread the baryon asymmetry across the baryons and the DM. The result is that the difference in the relic densities of the DM and the baryons is primarily due to the difference  $m_{\text{DM}}$  versus  $m_{\text{proton}}$ . Thus, these models generically predict that the DM mass is roughly 5 GeV (see Ch. IV for a model where this is not the case). It is worth noting that one model building challenge comes from requiring that the symmetric component of the DM density to be sub-dominant. This is easy to understand. A WIMP, with its weak scale annihilation cross section, reproduces the full relic density, so an ADM candidate must have an annihilation rate which is a factor of  $\gtrsim 50$  larger. Once this problem is solved within a given theory, the ADM paradigm survives as a novel alternative to the WIMP.

### 1.3 Confronting Reality

Now that we have discussed many theoretical issues with a focus on DM, it is important to explore which aspects of these ideas can actually be tested. There are three classes of experiments which are relevant for disentangling the properties of the DM particle: direct detection (DD), indirect detection (ID), and collider experiments.

While normally not a part of an experimental collaboration, theorists can help make progress in many directions with respect to testing models. Two important functions of theorists are 1) to develop new models which motivate current and future experiments and 2) to respond to data by writing down new theories which can explain unexpected effects. Beyond these tasks, we can be crucial for interpreting data in the context of existing models. Often this is a non-trivial task and expertise in subtle aspects of the predictions can allow one to decide how best to approach the data. We are also responsible for identifying new classes of analysis techniques. In recent years, it has been theorists who understood the relevance of the DD spectrum for distinguishing elastic from inelastic DD models [192],

and there has been a significant effort in the theoretical community to develop new jet sub-structure methods which are relevant for the LHC.

Therefore, it is appropriate for a theoretical thesis on DM to briefly review the relevant experiments. In the following three sections we will discuss the aspects of DD, ID, and collider experiments which are important for the chapters that follow.

### 1.3.1 Direct Detection Experiments

The idea behind DD is simple. Given the above discussion on generating the relic density, it is not unreasonable to think that the DM might interact with nucleons. So, assuming that backgrounds can be eliminated, if we could watch a large bulk of nucleons for long enough eventually we would see a nucleon recoil against “nothing.” This would be the signature of a nucleus interacting with a DM particle.

There are three general classes of signal that DD experiments use to look for DM-nucleon scattering: scintillation, ionization, and phonons (or heat). Which of these is most efficient depends on the target material and the detection technology.

From the theoretical point of view, since the DM-nucleon scattering would be non-relativistic, an effective operator analysis is useful for characterizing the possibilities. As discussed in more detail in Ch. V below, the largest operators are generally those responsible for spin-independent (SI) and spin-dependent (SD) scattering:

$$(I.13) \quad \mathcal{O}_q^{\text{SI}} = c_q(\bar{\chi}\chi)(\bar{q}q),$$

$$(I.14) \quad \mathcal{O}_q^{\text{SD}} = d_q(\bar{\chi}\gamma^\mu\gamma^5\chi)(\bar{q}\gamma_\mu\gamma^5q),$$

where  $\chi$  is the DM and  $q$  is a quark. The SI scattering rate benefits from an enhancement which is proportional to the atomic number of the nucleus squared, due to the fact that  $\mathcal{O}^{\text{SI}}$  “sees” the entire nucleus instead only the quarks. Since the average expected momentum transfer is on the order of 100 MeV, the DM would not probe the internal structure of

the nucleus. This is why the limits on the resultant scattering cross section are typically stronger than for SD experiments.

If the DM is a WIMP, it is not unreasonable to expect that it could couple to the Higgs boson. This would generate a SI cross section for DM-nucleon scattering. Currently running experiments (*e.g.* XENON100 [21]) are probing rates which are naively predicted by these types of interactions, namely  $\sigma_{\text{SI}} \sim 10^{-43} \text{ cm}^2$ . There have also been some reported signals from the DAMA [54] and CoGeNT [1] experiments. While these signals could be explained by an  $\mathcal{O}(10 \text{ GeV})$  DM particle, it is difficult to build a model which is consistent with existing limits. Nevertheless, this is still an active area of research and new data will be reported on short timescales. Perhaps we will have conclusive DD signals in the near future which will require understanding in the context of models for DM.

### 1.3.2 Indirect Detection Experiments

We know that there must be DM throughout our galaxy. Assuming there is some rate for DM-DM annihilations ( $\chi^\dagger\chi \rightarrow \psi_{\text{SM}}^\dagger\psi_{\text{SM}}$ ), there is another class of experiments which have the ability to look for DM. The basic idea is that DM would annihilate throughout the galaxy, and the byproducts of this process would propagate to us. Then experiments either orbiting or based on the Earth can look for these particles. One exciting prospect is that the the annihilation rate today could be related to the  $\langle\sigma_{\text{ann}}|v|\rangle$  which appears in the derivation of the relic density in either the WIMP, Eq. (I.7), or non-thermal, Eq. (I.12) scenarios, leading to a non-trivial correlation with  $\Omega_{\text{DM}}$ . However, this statement is model dependent and would have to be corroborated by other measurements of the DM properties.

Given a determination of the expected astrophysical backgrounds (essentially assuming a power-law distribution), there are a few experiments which have detected cosmic ray spectra which do not match these standard expectations. The PAMELA experiment [7] has observed an excess in the measurement of  $e^+/(e^+ + e^-)$  around 100 GeV without

seeing an excess in anti-protons, and the Fermi collaboration [4] has seen an excess in the electron channel which extends to energies up to nearly a TeV. Explaining these anomalies is an active area of research. The PAMELA signal requires a DM annihilation cross section which is two orders of magnitude above the thermal value for a WIMP in order to reproduce the size of the excess. The predominant annihilation should be to leptons to explain the lack of anti-protons. In Ch. IV we will provide a DM model which satisfies both of these criteria.

Perhaps the biggest issue with mapping ID onto DM models is the problem of understanding the astrophysical sources of uncertainty. In order to extract a DM signal, we must be able to determine both the continuum background and the contribution from additional (unknown?) astrophysical processes which generate cosmic rays. The exact distribution of DM in our galaxy is another source of uncertainty, since this is an important input in the calculation of the cosmic ray spectra produced by DM annihilations. With the exception of a sharp  $\gamma$ -ray line with energy  $m_{\text{DM}}/2$ , it is not possible to argue that a discovery through only ID is possible. However, these experiments do allow us to both motivate novel types of models and to constrain well known scenarios in relevant regions of parameter space.

### 1.3.3 Collider Experiments

The last class of experiments which are relevant in the context of DM searches are colliders. Again assuming that the DM interacts with the SM, the idea is simply to exploit a process of the type  $\psi_{\text{SM}}^\dagger \psi_{\text{SM}} \rightarrow \chi\chi + X$ , where  $X$  is any number of SM states. Then, since the DM interacts so weakly, it will pass through the detector without leaving behind any trace. We will be able to measure the rest of the event, namely  $X$ , which we can use to infer the missing momentum. At a hadron collider, such as the large hadron collider (LHC) which is currently running at CERN, the momentum of the colliding partons along the direction parallel to the beam is unknown. Therefore, the only constraint that can be

inferred is on the transverse missing momentum. This makes it a difficult proposition to explore DM at hadron colliders since we wish to extract the properties of a state which we will not directly measure.

We have some experience with these types of measurements from past discoveries. A notable example is the  $W^\pm$  boson which can decay to a lepton and an (invisible) neutrino. To extract the mass from events with a single  $s$ -channel  $W^\pm$ , a new kinematic variable, the transverse mass  $\left(M_T = \sqrt{m^2 + |\vec{p}_T|^2}\right)$  was proposed, where  $m$  is the mass of the visible particle being produced and  $\vec{p}_T$  is the 3-momentum in the plane transverse to the beam. No matter what the details of the underlying model are, this variable can never exceed the mass of the parent particle. By collecting enough statistics, measuring the endpoint of the  $M_T$  distribution, and using the (excellent) approximation that the neutrino is massless, the  $W^\pm$  mass can be inferred.

In typical models, events with DM involve two parent particles and result in at least two DM particles in the final state (*e.g.* for SUSY models this is due to the presence of  $R$ -parity). Therefore, the simple definition of  $M_T$  will not suffice to extract the maximum possible information from these events. Recently a variant on the transverse mass was proposed in order to address the additional complication of events where the missing energy was due to two states. This variable, known as  $M_{T2}$ , will be discussed in Ch. VI, where we will explore a variation on its canonical use in order to determine how well the DM mass can be extracted at the LHC.

## 1.4 Outline

This thesis has been derived from five papers [78, 80, 81, 79, 77] (of eight total papers that I collaborated on as a graduate student).

In Chapter 2 we present a model where the dark matter properties which are relevant today differ from the ones which determine its relic density. The dynamics of this alteration

is governed by the dark matter couplings to a new scalar field which undergoes a late-time first order phase transition. The cosmology and collider phenomenology of this new scalar are explored.

In the next two chapters we discuss two models of asymmetric dark matter (see Sec. 1.2.3). In Chapter 3 we investigate the idea that the dark matter relic density is determined by the matter-anti-matter asymmetry in the context of a supersymmetric model with a new Abelian dark sector. The GeV scale for the dark matter is generated dynamically. Details of the cosmological history, including potential effects on big bang nucleosynthesis, direct and indirect detection constraints, and collider signatures are discussed.

In Chapter 4, motivated by the PAMELA positron excess, we present a model where the dark matter relic abundance is set by the lepton asymmetry which allows us to explain both the leptophilic nature of the dark matter and the “boosted” annihilation cross section. We explore relevant constraints and make connections with neutrino physics.

In Chapter 5 we look at some prospects for direct detection (see Sec. 1.3.1). We rely on the fact that Majorana dark matter which couples to the  $Z^0$  boson must also couple to the Higgs boson which leads to correlations between the spin-dependent and spin-independent interactions of the dark matter with nucleons. This relationship is explored in the context of upcoming direct detection experiments, under a variety of assumptions, and using the canonical example of mixed neutralinos.

In Chapter 6 we investigate the ability of the LHC to measure the DM mass (see Sec. 1.3.3). We perform a realistic collider study of a recently proposed variant on the  $M_{T2}$  kinematic variable. Our goal is to systematically analyze the error associated with making mass measurements of the parent and invisible particles utilizing single stage cascade decays.

Finally, in Chapter 7 we give our conclusions and outlook to the future of our under-

standing of dark matter.

## CHAPTER II

### Changes in Dark Matter Properties After Freeze-Out

This chapter was completed in collaboration with David Morrissey and Aaron Pierce [78].

In Sec. 1.2.1 we discussed the thermal WIMP and the role of the thermally averaged annihilation cross section,  $\langle\sigma_a v\rangle$ . With the turn-on of the Large Hadron Collider (LHC) and a host of direct and indirect detection experiments coming on-line, there is hope that the nature of the DM particle will be measured thoroughly enough that  $\langle\sigma_a v\rangle$  can be computed. Then a prediction of the thermal relic abundance,  $(\Omega_{\text{DM}} h^2)_{\text{particle}}$ , can be made. If  $(\Omega_{\text{DM}} h^2)_{\text{particle}} = (\Omega_{\text{DM}} h^2)_{\text{astro}}$ , this will be strong evidence that the universe has a standard thermal history back to the DM freeze-out temperature,  $T_{fo}$  (typically tens of GeV for weak-scale DM). This would extend the successful predictions of Big Bang Nucleosynthesis (BBN), which demonstrate a thermal history of the universe only back to temperatures of several MeV.

On the other hand, if the calculated relic density does not equal the measured one, this will be evidence for physics beyond minimal thermal DM. If  $(\Omega_{\text{DM}} h^2)_{\text{particle}} < (\Omega_{\text{DM}} h^2)_{\text{astro}}$ , it is possible that we have not identified the dominant source of DM or the DM was produced non-thermally as a decay product of another particle [166]. Conversely, if  $(\Omega_{\text{DM}} h^2)_{\text{particle}} > (\Omega_{\text{DM}} h^2)_{\text{astro}}$  the thermal relic abundance of the DM must have been diluted, perhaps by a late production of entropy [186] or a modification of the expansion



history of the universe [136, 40]. In the present chapter, we explore a novel possibility that can obtain either direction of this inequality: a change in the properties of the DM itself between  $T_{fo}$  and the present. Time-dependent DM has been considered in another context in attempts to relate DM and Dark Energy [17, 175].

Relevant changes in the attributes of the DM particle can occur if there is a field whose vacuum expectation value (VEV) changes during the crucial epoch between  $T_{fo}$  and BBN. If this field influences the mass or couplings of the DM particle, there can be a dramatic effect on the relic abundance one would calculate based on the properties of the DM particle measured today. Here we present a simple model that illustrates how this mechanism could be realized. We discuss some constraints on scenarios of this type, and we study the phenomenology that should accompany the late-time phase transitions typical of this class of models.

## 2.1 A late-time phase transition

To change the DM properties, we suppose there is a phase transition (PT) after  $T_{fo}$  [113]. In the model considered here, this PT occurs in a new sector containing a Standard Model (SM) singlet  $P$ . We couple the PT sector to a model for the DM in the next section. The PT will modify both the mass and couplings of the DM particle in this model.

Rather than introducing a new field  $P$ , one might instead try to modify the properties of the DM after freeze-out via the electroweak PT. This does not work for electroweak-mass DM using the minimal SM Higgs phase transition [87]. Unless the dynamics of this PT are modified (or the initial DM mass is very large), the temperature of the PT is typically greater than  $T_{fo}$ , and the DM properties would not be modified between  $T_{fo}$  and the present day. On the other hand, if the Higgs boson sector is non-minimal, it is possible that the electroweak transition temperature might be lowered substantially (see *e.g.* [85]).

The new singlet field  $P$  is initially stabilized at the origin in the early universe by a

thermal mass term [91, 195]. As the universe cools,  $P$  undergoes a PT at a temperature  $T_{\text{PT}} < T_{fo} \approx m_{\text{DM}}/20$ , and develops a non-zero VEV,  $\langle P \rangle \equiv v_P$ . For the PT to have a significant effect on the DM properties (perhaps by generating a large excursion in the DM mass  $\Delta_m \equiv \lambda_{\text{DM}-P} v_P$ ) typically requires  $v_P \gg T_{\text{PT}}$ <sup>1</sup>.

We take the potential for  $P$  to be

$$(II.1) \quad V_P(T=0) = -\frac{1}{2}|m_P|^2 P^2 + \frac{\lambda}{4!} P^4,$$

which induces

$$(II.2) \quad v_P(T=0) = \sqrt{6|m_P|^2/\lambda}$$

below  $T_{\text{PT}}$ . The  $\mathbb{Z}_2$  symmetry of this potential ( $P \rightarrow -P$ ) means there is a danger of forming domain walls. We can retain the form of the potential while avoiding domain walls by softly breaking the  $\mathbb{Z}_2$  with a very small cubic term, making this symmetry only approximate [5].

A large hierarchy between  $v_P$  and  $T_{\text{PT}}$  in this scenario requires that the coupling responsible for inducing a thermal mass for  $P$  be considerably larger than  $\lambda$ . This can arise if  $P$  couples to other states that are approximately massless when  $v_P = 0$ . Such states can emerge if  $P$  is part of a larger “hidden” sector, perhaps coupled to the SM only via a “Higgs portal” [170, 179]. For concreteness, we consider additional fermionic fields coupling to  $P$  according to  $\mathcal{L} \ni \lambda_{PQ_i} P \bar{Q}_i Q_i$ . Since the  $Q$ ’s have no other mass terms (which would violate the  $\mathbb{Z}_2$  of  $P$ ), these couplings contribute to the temperature-dependent mass of the  $P$  field, strongly trapping it at the origin. When  $v_P$  shifts to its non-zero value, the  $Q$ ’s acquire a mass of  $\lambda_{PQ_i} v_P$ , typically of order a few hundred GeV.

At high temperatures and near the origin of  $P$ , the potential is approximately [91, 195]

$$(II.3) \quad V_P(T) = -\frac{1}{2}(|m_P|^2 - \frac{N_Q}{6} \lambda_{PQ}^2 T^2) P^2 + \frac{1}{4!} \lambda P^4,$$

---

<sup>1</sup>Here  $\lambda_{\text{DM}-P}$  is a dimensionless coupling between the DM and  $P$ . This assumes fermionic DM. For scalar DM the VEV-dependent contribution must be even larger to make a significant change in the mass, as the new contribution should be added in quadrature.

where  $\lambda_{PQ}$  is the (universal) coupling between  $P$  and the  $Q$ 's and  $N_Q$  is the number of Dirac  $Q$  fields. This potential gives a PT temperature of

$$(II.4) \quad T_{PT} = \sqrt{\frac{6|m_P|^2}{N_Q \lambda_{PQ}^2}}.$$

Strong trapping of the  $P$  field at the origin typically leads to a brief period of thermal inflation (TI) [157, 198, 151]. The vacuum energy density during TI is  $\rho_{vac} = |m_P|^2 v_P^2/4$ . If TI ends at  $T_{PT}$  by the instantaneous decay of the  $P$  field to radiation, we can estimate the reheating temperature  $T_{RH}$  via conservation of energy:

$$(II.5) \quad T_{RH}^4 = \frac{45 |m_P|^4}{g_*^{RH} \pi^2 \lambda} + \frac{36 g_*^{PT} |m_P|^4}{g_*^{RH} N_Q^2 \lambda_{PQ}^4},$$

where  $g_*$  is the effective number of relativistic degrees of freedom. Reheating can dilute the DM abundance. Although this is not the dominant effect that we wish to explore, it can be of quantitative importance. This is also the reason why we rely on thermal corrections, rather than an additional cubic term in the tree-level potential, to trap  $P$  at the origin. With a cubic term, the trapping need not turn off as the universe supercools and could lead to a severe dilution of the DM abundance.

To estimate this dilution, we first assume there are no new sources of entropy during TI. This fixes  $n_{fo}/s_{fo} = n_{PT}/s_{PT}$ , where  $n$  and  $s$  are the number density of the DM and entropy density of the universe respectively. No DM is produced in the reheating process, implying  $n_{PT} = n_{RH}$ . Once TI ends and reheating completes, the new conserved quantity is  $n_{RH}/s_{RH} = n_{PT}/s_{RH}$ . The dilution factor,  $D$ , is

$$(II.6) \quad \frac{n_{PT}}{s_{RH}} = \frac{s_{PT} n_{fo}}{s_{RH} s_{fo}} = \left( \frac{g_*^{PT} T_{PT}^3}{g_*^{RH} T_{RH}^3} \right) \frac{n_{fo}}{s_{fo}} \equiv D \times \frac{n_{fo}}{s_{fo}}.$$

Taking into account the change in the mass of the particle, the present abundance is given by

$$(II.7) \quad (\Omega_{DM} h^2)_{astro} = D \times \left( \frac{m_{DM}^{v_P \neq 0}}{m_{DM}^{v_P = 0}} \right) \times \Omega_{DM}^{v_P = 0} h^2.$$

$ m_P $	$\lambda$	$v_P$	$\lambda_{PQ}$	$N_Q$	$T_{PT}$	$T_{RH}$	$D$
4.0 GeV	$1.5 \times 10^{-5}$	2.5 TeV	0.10	9	33 GeV	40 GeV	0.77

Table 2.1: Benchmark phase transition parameters.

This can differ dramatically from  $(\Omega_{\text{DM}} h^2)_{\text{particle}}$ , as we will see in the next section.

In Table 2.1 we exhibit a benchmark point that gives a first-order PT with a transition temperature  $T_{PT} \ll v_P$ . To obtain this feature, the value of  $\lambda$  is small. This interaction obtains additive corrections of the form  $\Delta\lambda = \sum(c_b \lambda_b^2 - c_f \lambda_f^4)/(16\pi^2)$ , where the sum runs over bosons and fermions that couple to  $P$ , and the  $c_i$  are  $\mathcal{O}(1)$  coefficients. For the benchmark couplings, the small value of  $\lambda$  is technically natural.

The value of  $T_{PT}$  for the benchmark point is also large and could exceed a typical value of  $T_{fo}$  unless the mass of the DM particle is many hundreds of GeV. Smaller values of  $T_{PT}$  can be achieved by reducing the value of  $|m_P|^2$ . This leads to light excitations of  $P$  that can be phenomenologically problematic – it is difficult to make them decay quickly enough to avoid BBN constraints while not disturbing the evolution of supernovae.

## 2.2 A Dark Matter sector

There are many possibilities for the DM sector, all of which could work with the generic phase transition module we presented in the previous section. The particular DM sector we consider is a “level-changing” model, consisting of three fermions with the same quantum numbers as the Higgsinos and Bino of the minimal supersymmetric SM: a vector-like pair of  $SU(2)_L$  doublets  $\psi_L$  and  $\psi_{\bar{L}}$  with the appropriate hypercharges, and a gauge singlet  $\psi_S$ . All fields in this DM sector are charged under an exact  $X \rightarrow -X$  symmetry (independent of the approximate  $\mathbb{Z}_2$  of  $P$ ), implying that the lightest of these particles is absolutely

$\mu$	$\mu_s$	$\lambda_s$	$\lambda_1$	$\lambda_2$
1.3 TeV	0.68 TeV	-0.070	0.020	0.010
$m_{\text{DM}}(v_P = 0)$	$m_{\text{DM}}(v_P \neq 0)$	$T_{fo}(v_P = 0)$	$T_{fo}(v_P \neq 0)$	
1.3 TeV	1.0 TeV	65 GeV	52 GeV	

Table 2.2: Benchmark parameters realizing  $(\Omega_{\text{DM}} h^2)_{\text{particle}} > (\Omega_{\text{DM}} h^2)_{\text{astro}}$ .

stable. The DM sector Lagrangian is

$$(II.8) \quad \mathcal{L} \ni \mu \psi_L \cdot \psi_{\bar{L}} + \lambda_1 H \cdot \psi_L \psi_s + \lambda_2 H^* \cdot \psi_{\bar{L}} \psi_s \\ + (\mu_s + \lambda_s P) \psi_s \psi_s + \text{h.c.},$$

where  $H = (G^+, \frac{1}{\sqrt{2}}(H^0 + iG^0))^T$  is the SM Higgs boson. The resulting “neutralino” mass matrix is

$$(II.9) \quad \mathcal{M}^0 = \begin{pmatrix} 0 & \mu & -\lambda_1 \frac{v_H}{\sqrt{2}} \\ \mu & 0 & \lambda_2 \frac{v_H}{\sqrt{2}} \\ -\lambda_1 \frac{v_H}{\sqrt{2}} & \lambda_2 \frac{v_H}{\sqrt{2}} & 2(\mu_s + \lambda_s v_P) \end{pmatrix},$$

with electroweak VEV  $\langle H^0 \rangle \equiv v_H = 246 \text{ GeV}$ <sup>2</sup>.

Within this model, it is not difficult to obtain  $(\Omega_{\text{DM}} h^2)_{\text{particle}} \gg (\Omega_{\text{DM}} h^2)_{\text{astro}}$ . As an example, we consider the benchmark parameter point given in Tables 2.1 and 2.2. At high temperatures  $v_P = 0$ . There the DM is a nearly pure combination of the doublets  $\psi_L$  and  $\psi_{\bar{L}}$ :  $X^0 \approx 1/\sqrt{2} \psi_L + 1/\sqrt{2} \psi_{\bar{L}} + \epsilon \psi_s$ , with  $\epsilon \approx (\lambda_1 - \lambda_2)v_H/(4\mu_s - 2\mu)$ . The thermal relic abundance of this state is nearly identical to that of a pure Higgsino. This is set by its annihilation to pairs of  $W$  bosons, and is given by [158]

$$(II.10) \quad \Omega_{\text{DM}}^{v_P=0} h^2 = 0.1 \left( \frac{m_{\text{DM}}}{1 \text{ TeV}} \right)^2,$$

including coannihilation with the heavier “charginos”.

<sup>2</sup>The  $\psi_s \psi_s$  coupling breaks the approximate  $\mathbb{Z}_2$  symmetry of  $P$ , and thus quantum corrections from loops of the  $\psi_s$  field would modify the  $P$  potential in Eq. (II.1). This can easily be avoided by adding a second singlet (or another pair of doublets) without significantly altering the DM story we present here. To avoid complication, we will consider only one singlet. These symmetries could also forbid a  $v_P$  dependent “Higgsino” mass which we also ignore for simplicity.

The mass and composition of the DM change after the PT. For the parameters in the Tables, the lightest of the DM-sector particles is nearly pure singlet post-PT. Using Eq. (II.7), its relic density is  $(\Omega_{\text{DM}} h^2)_{astro} = 0.1$ . This is the value measured by astrophysical probes. However, it is considerably different from the value one would reconstruct from measurements of the DM particle Lagrangian today, assuming one measured the relevant couplings but did not take into account the non-canonical cosmological effect described here <sup>3</sup>.

The dominant contribution to the *apparent* particle annihilation cross section, assuming the relevant particles and their couplings can be measured, is the  $s$ -channel exchange of a  $P$  going into  $Q\bar{Q}$ . Assuming a standard thermal history, the predicted relic density is approximately given by

$$(II.11) \quad (\Omega_{\text{DM}} h^2)_{particle} = \frac{0.02}{N_Q (\lambda_{PQ} \lambda_s)^2} \left( \frac{m_{\text{DM}}}{1 \text{ TeV}} \right)^2,$$

yielding  $(\Omega_{\text{DM}} h^2)_{particle} = 45$  for the benchmark, more than two orders of magnitude larger than  $(\Omega_{\text{DM}} h^2)_{astro}$ . Even if the PT-sector particles are not discovered at colliders, the properties of the DM today will differ from those at freeze-out. These properties can potentially still be deduced by direct and indirect detection searches for DM.

We obtained  $(\Omega_{\text{DM}} h^2)_{particle} \gg (\Omega_{\text{DM}} h^2)_{astro}$  in this example. A different choice of mass matrix (Eq. (II.9)) can lead to the opposite relationship. When this is the case, the value of  $\langle \sigma_a v \rangle$  should increase after the PT, and the DM can potentially recouple after thermal inflation. Demanding that the DM stay frozen out gives a bound on the allowed change in the relic density. Non-recoupling of the DM after reheating requires

$$(II.12) \quad n_{\text{PT}} \langle \sigma_a v \rangle^{v_P \neq 0} \leq 1.66 (g_*^{\text{RH}})^{1/2} \frac{T_{\text{RH}}^2}{M_{\text{Pl}}},$$

where  $M_{\text{Pl}}$  is the Planck mass. A similar condition holds for the initial ( $v_P = 0$ ) freeze-out cross section and temperature. Combining these expressions and accounting for redshift

---

<sup>3</sup>In practice, it is difficult to measure the couplings of this particular DM candidate. However, we see no fundamental impediment to building models with DM candidates amenable to experimental study.

from freeze-out to the PT gives

$$(II.13) \quad \frac{\langle \sigma_a v \rangle^{v_P \neq 0}}{\langle \sigma_a v \rangle^{v_P = 0}} \leq \frac{\sqrt{g_*^{\text{RH}} g_*^{v_P = 0}}}{g_*^{\text{PT}}} \left( \frac{T_{\text{RH}}^2 T_{f_o}^{v_P = 0}}{T_{\text{PT}}^3} \right).$$

Here  $g_*^{v_P = 0}$  is the effective number of relativistic degrees of freedom calculated at  $T_{f_o}^{v_P = 0}$ .

Using the standard approximate solution to the Boltzmann equation [146] to relate  $\langle \sigma_a v \rangle$  to  $\Omega_{\text{DM}} h^2$ , along with Eq. (II.7), leads to the constraint

$$(II.14) \quad \frac{(\Omega_{\text{DM}} h^2)_{\text{particle}}}{(\Omega_{\text{DM}} h^2)_{\text{astro}}} \gtrsim \sqrt{\frac{g_*^{\text{RH}}}{g_*^{v_P \neq 0}}} \frac{T_{\text{RH}}}{T_{f_o}^{v_P \neq 0}}.$$

A large change in the apparent relic density without recoupling requires a hierarchy between  $T_{\text{RH}}$  and  $T_{f_o}^{v_P \neq 0}$ . To avoid disturbing BBN,  $T_{\text{RH}}$  must be larger than about 10 MeV. Taking a typical  $T_{f_o}$  of tens of GeV, the apparent relic density can be reduced by a factor of a thousand. In practice we find it difficult to obtain such low reheating temperatures simultaneous with the large  $v_P$  needed to make a significant shift in the DM properties.

### 2.3 Phenomenology of a Late Phase Transition

For the PT to happen after DM freeze-out, the mass of the physical  $P$  excitation  $\sim |m_P|$  should be light. The existence of a light  $P$  is the most generic feature of the mechanism presented here, and so it is worth considering its phenomenology in some detail. The symmetries of the model allow the Lagrangian term  $\mathcal{L} \ni (\lambda_{PH}/2)P^2|H|^2$ , coupling  $P$  with the SM Higgs boson. The resultant mixing with the Higgs boson gives two mass eigenstates,  $p^0$  and  $h^0$ . The mixing angle is given by

$$(II.15) \quad \tan 2\theta = \frac{6 \lambda_{PH} v_P v_H}{\lambda_H v_H^2 - \lambda v_P^2},$$

where  $\mathcal{L} \ni \lambda_H (H^0)^4/4!$ <sup>4</sup>.

The relevant phenomenological constraints and signals depend on the precise mass of the  $p^0$ , which in principle could range from tens of GeV all the way down to a fraction of

<sup>4</sup>With a non-zero  $\lambda_{PH}$  term, the VEV of  $P$  modifies the potential for  $H^0$  and vice versa. Therefore, the Higgs VEV can be different when  $v_P = 0$  (changing the mass of the  $W$  boson). It is also important to check that this cross coupling still allows a well separated  $T_{\text{EW}} > T_{\text{PT}}$ .

an MeV. Mixing allows the  $p^0$  to be produced in association with a  $Z^0$ , or to appear in meson decays. For  $m_{p^0} \lesssim 100$  MeV, astrophysical constraints similar to those for axions [173] become important.

For DM masses near the weak scale, the natural value of the  $p^0$  mass is on the order of a few GeV. For the parameters in Table 2.1 and a moderate mixing angle,  $m_{p^0} \approx 6$  GeV. In this mass range, the  $p^0$  could be produced in Upsilon ( $\Upsilon$ ) decays. To lowest order [197],

$$(II.16) \quad \frac{\Gamma(\Upsilon \rightarrow p^0 \gamma)}{\Gamma(\Upsilon \rightarrow \mu^+ \mu^-)} = \frac{\sin^2 \theta m_b^2}{2 \pi v_H^2 \alpha} \left( 1 - \frac{m_{p^0}^2}{m_\Upsilon^2} \right).$$

Requiring  $\text{BR}(\Upsilon \rightarrow p^0 \gamma) \times \text{BR}(p^0 \rightarrow \tau^+ \tau^-) \lesssim 10^{-5}$  [156] gives a modest bound on the mixing angle of  $\theta \lesssim 0.3$  for  $\text{BR}(p^0 \rightarrow \tau^+ \tau^-) = 1$ . For a 6 GeV  $p^0$ , decays to charm quarks actually exceed those to  $\tau$ 's by a factor of 2 (unless a more complicated Higgs sector allows for a  $\tan \beta$  enhanced  $p^0$  couplings to down-type fermions). In this mass range, a comparable bound exists from non-observation of  $Z^0 p^0$ , which would have been seen in  $Z^0 h^0$  searches at LEP [31]. For higher masses,  $m_P > 10$  GeV, the bound on the mixing angle strengthens due to the LEP constraint:  $\theta < 0.14$ . The  $p^0$  decays are very prompt; the lifetime of  $p^0$  is  $2 \times 10^{-19}$  sec for  $\theta = 0.14$ . The  $p^0$  branching ratios are identical to a SM Higgs boson of the same mass. If the  $p^0$  mass falls below the  $B$ -meson mass, bounds on the mixing angle from  $b \rightarrow s P$  processes [15] are strong:  $\theta \lesssim 10^{-4}$ .

These considerations also provide a way to observe the  $p^0$  state at colliders. For lighter masses ( $m_{p^0} < 8$  GeV) and large mixing, searches for the rare decay  $\Upsilon \rightarrow \gamma p^0 \rightarrow \gamma \tau^+ \tau^-$  may be useful. If the  $h^0$  is not so heavy that it decays to  $W$  bosons, then  $h^0 \rightarrow p^0 p^0$  need only compete with  $h^0 \rightarrow b \bar{b}$  [71]. The ratio of the widths is given by

$$(II.17) \quad \frac{\Gamma(h^0 \rightarrow p^0 p^0)}{\Gamma(h^0 \rightarrow b \bar{b})} = \frac{3 (\xi \lambda c_\theta^2 v_P v_H)^2 (m_{h^0}^2 - 4 m_{p^0}^2)^{1/2}}{m_b^2 (m_{h^0}^2 - 4 m_b^2)^{3/2}}$$



with the effective coupling

$$(II.18) \quad \begin{aligned} \xi &= t_\theta + \frac{\lambda_H v_H}{\lambda v_P} t_\theta^2 \\ &- \frac{t_{2\theta}}{18} \left( 1 - \frac{\lambda_H v_H^2}{\lambda v_P^2} \right) \left[ 1 - 2t_\theta^2 - \frac{v_P}{v_H} (2t_\theta - t_\theta^3) \right], \end{aligned}$$

where  $t_\theta \equiv \tan \theta$  and  $c_\theta \equiv \cos \theta$ . For  $\theta$  saturating the LEP bound,  $\text{BR}(h^0 \rightarrow p^0 p^0)$  can approach 40% for  $v_P \gtrsim 750$  GeV. Then  $h^0 Z^0 \rightarrow p^0 p^0 Z^0 \rightarrow 4b Z^0$  might be observable at the LHC if  $b$ -tagging efficiencies are sufficiently high [61], though it will be challenging.

Thus far we have not mentioned the decay of the  $Q$ 's. This can proceed via higher-dimension operators. Alternately, the  $Q$ 's can decay to quarks through renormalizable operators if they are  $SU(3)_c$  triplets and are allowed a very small mixing with the quarks of the SM. For the benchmark parameters in Table 2.1,  $m_Q = 250$  GeV. Then given the latter scenario there is the possibility of producing the  $Q$ 's directly at the LHC.

## 2.4 Discussion

The DM model presented here represents an existence proof of a general mechanism: DM properties can change after freeze-out. We have focused our attention on situations where a shifting VEV causes a change in the DM mass and composition. A similar effect could occur if the coupling that sets the relic abundance of the DM is a function of a light modulus.

In another example, the DM mass might shift so that  $2m_{\text{DM}}$  is approximately resonant with some other state in the theory, such as a Higgs boson. With the DM now sitting on resonance, one would calculate a tiny thermal relic abundance. To implement this scenario using a SM Higgs boson is difficult. For a “natural” PT,  $m_{\text{DM}} \sim \text{TeV}$ . To access the Higgs resonance,  $m_{h^0} \sim 2m_{\text{DM}} \sim \mathcal{O}(\text{TeV})$ . This implies  $\Gamma_{h^0}$  will be too large to generate a strong resonant enhancement of  $\langle \sigma_a v \rangle$ . In the presence of heavy but narrow resonances, this is a viable mechanism.

Alternately, the DM itself could remain unchanged, but the properties of particles crucial for setting the thermal relic abundance are modified by the cosmology. Consider a coannihilating particle,  $C$ , nearly degenerate with the DM. If the mass of  $C$  shifts between  $T_{fo}$  and now, the importance of coannihilation would not be evident from low-temperature measurements, and the calculated  $(\Omega_{\text{DM}} h^2)_{particle}$  would differ from the true value.

If  $(\Omega_{\text{DM}} h^2)_{particle} \neq (\Omega_{\text{DM}} h^2)_{astro}$ , it is possible that the relic abundance of the DM is actually thermal, but an alternate cosmology has altered the DM properties since freeze-out. These scenarios are naturally realized if there is a light modulus that undergoes a late PT. The field responsible for the late time transition,  $P$ , could show up in future experiments. One possibility is via Higgs boson decays:  $h^0 \rightarrow p^0 p^0$ . If  $p^0$  is light enough, it could also be produced in rare meson decays. Embedding a model of this type in an extension of the minimal supersymmetric SM is a direction for future investigation.

Recent preliminary data from the PAMELA [58], ATIC [63], PPB-BETS [191], and Fermi [4] experiments report significant excesses of cosmic ray positrons and electrons above the expected astrophysical background. This excess could be the result of dark matter annihilation in our galaxy. However, such a dark matter interpretation of these results requires a DM annihilation cross-section well above the value that would generate the observed dark matter relic density [121]. The cosmology discussed here offers the possibility of explaining these indirect DM signals while maintaining a fairly standard thermal freeze-out picture. What is needed is a DM annihilation cross-section that increases significantly between freeze-out and today.

## CHAPTER III

# Asymmetric Dark Matter from a GeV Hidden Sector

This chapter was completed in collaboration with Daniel Phalen, Aaron Pierce, and Kathryn Zurek [80].

In order to have a model which realizes the asymmetric dark matter (ADM) paradigm, the symmetric component of the DM relic density must annihilate away efficiently. It is not always straightforward to achieve a sufficiently high annihilation cross section. After all, the DM is not charged under  $U(1)_{EM}$  or  $SU(3)_C$ . Furthermore, its light mass, when combined with constraints on the invisible width of the  $Z^0$  boson, precludes large interactions via the weak force. If a higher dimension operator is responsible for this annihilation, the suppression scale needs to be near or below the weak scale to achieve a large enough annihilation cross section [52]. Then one must ask the question why no hint of this new physics has been observed yet. Hence, the requirement of large symmetric annihilation cross sections implies a challenge for asymmetric dark matter (ADM) model building. One possible solution to this problem occurs when light fields couple strongly to the DM. For example, an axion from the next-to-minimal supersymmetric standard model (NMSSM) can play this role. The DM can efficiently annihilate to the singlet axion which subsequently decays; this mechanism was employed in [140]. Here, we build on this approach. Suppose the dark sector contains a new dark force, and the dark gauge boson has a mass lighter than the DM, *i.e.* roughly a GeV. Then the light gauge boson can provide the light annihilation

mode, in analogy with the NMSSM axion. The cross section for this annihilation can be large, solving the challenge of reducing the symmetric component of the DM. If the dark gauge boson has a small kinetic mixing with  $U(1)_Y$ , it can subsequently decay to SM fermions. In addition, supersymmetrizing these models can provide ways for the sub-weak scale to be generated naturally [132, 104, 29, 199, 70, 141, 167].

Large direct detection cross sections can result from the vector interaction in models where the DM annihilates to a  $U(1)_d$  gauge boson that mixes with the SM photon. DAMA [55] and the recent CoGeNT [1] results hint at a light DM candidate with a large cross section. The mass of the DM required to explain these signals is in the correct range for ADM [109, 64, 150, 16]. Whether or not these hints are borne out in future experiments, the models presented here demonstrate that the observation of light DM at direct detection experiments might point towards a model of GeV hidden sector ADM.

In the next section we present a toy model that illustrates the main features of ADM models with dark photons. In Sec. 3.2 we give a realistic supersymmetric (SUSY) model which realizes this paradigm. In Sec. 3.3 we discuss the cosmological history of this simple SUSY model. In Sec. 5.1 we discuss the direct detection cross section and then turn in Sec. 3.5 to exploring the collider implications of this model. Then we conclude.

### 3.1 Ingredients

In models of ADM, there are two key ingredients: an operator that transfers the asymmetry from the SM to the DM and a large annihilation mode that effectively suppresses the symmetric component of the relic density. In this section we present a simple non-SUSY model that demonstrates the broad features of ADM models with a dark Abelian gauge group.

The Lagrangian for the dark sector is

$$(III.1) \quad \begin{aligned} \mathcal{L} = & \bar{\chi}(i\not{D} - m_\chi)\chi + |D_\mu H'|^2 - V(H') \\ & - \frac{1}{4}b_{\mu\nu}b^{\mu\nu} + \frac{\epsilon}{2}b_{\mu\nu}B^{\mu\nu} + \mathcal{O}_{\text{asym}}. \end{aligned}$$

Here  $b_{\mu\nu}$  and  $B_{\mu\nu}$  are the dark gauge boson and hypercharge field strengths, respectively.  $\chi$  is a Dirac fermion with charge  $Q$  under  $U(1)_d$  – it is the DM, and  $H'$  is the dark Higgs with charge  $-1$  under  $U(1)_d$ . The operator  $\mathcal{O}_{\text{asym}}$  transfers the  $B - L$  asymmetry from the SM sector to the dark sector.  $\epsilon$  parametrizes a kinetic mixing between the dark photon and the hypercharge boson. It is naturally generated by integrating out matter charged under both symmetries; the result is an  $\epsilon$  of the size [131]:

$$(III.2) \quad \epsilon \sim \frac{g_Y g_d}{16\pi^2} \log \frac{M'}{M},$$

where  $g_Y$  is the hypercharge coupling constant;  $g_d$  is the  $U(1)_d$  coupling constant, and the logarithm of scales results from splittings between fields charged under both symmetries. Due to the loop factor suppression,  $\epsilon \sim 10^{-3}$ , at least in the absence of large logarithmic enhancements. When  $H'$  acquires a non-zero vacuum expectation value (vev), the dark  $U(1)$  is broken and the dark photon becomes massive. The dominant symmetric annihilation mode for the DM is  $\bar{\chi}\chi \rightarrow \gamma_d\gamma_d$ .

The asymmetry transfer operator must conserve dark charge, and so is of the form

$$(III.3) \quad \mathcal{O}_{\text{asym}} = \frac{(H'^n \chi^p) \mathcal{O}_{B-L}}{\Lambda^r}$$

where  $\Lambda$  is the mass suppression scale,  $p = n/Q$ , and  $\mathcal{O}_{B-L}$  is an operator with a non-zero  $B - L$  number that involves only SM fields.  $p > 1$  is a necessary condition for ensuring the stability of the DM. Using the equilibrium methods outlined in [127], one can solve for the DM asymmetry in terms of the  $B - L$  asymmetry. If this asymmetric component dominates, the measured value of the DM relic density determines the mass of the DM.

We discuss how the choice of transfer operator and corresponding  $\Lambda$  singles out a DM mass in Sec. 3.3. Here, we note only that this operator need be in equilibrium after the baryon asymmetry is generated, but must go out of equilibrium before  $T \sim m_\chi$ , or the DM asymmetry will be Boltzmann suppressed.

### 3.2 A Supersymmetric Model

Supersymmetry will stabilize both the electroweak scale as well as the dark scale. While in the above model the DM mass is put in by hand, here we can generate it dynamically. We propose the following model:

$$(III.4) \quad \mathcal{L}_d \supset \int d^2\theta \left( \lambda S T H' + \frac{\epsilon}{2} \mathcal{W}_d \mathcal{W}_Y \right).$$

Here  $S$  is a singlet, while  $T$  has charge  $+1$  under  $U(1)_d$ . The dark Higgs,  $H'$ , has charge  $-1$  under  $U(1)_d$ .  $\mathcal{W}_d$  and  $\mathcal{W}_Y$  represent the gauge field strength superfields for the dark photon and hypercharge, respectively, with kinetic mixing  $\epsilon$ . In the absence of large soft terms in the hidden sector, this model gives rise to a symmetry breaking pattern where  $\langle S \rangle = \langle T \rangle = 0$  and  $\langle H' \rangle \neq 0$  [70, 167].<sup>1</sup> There is an accidental global symmetry under which  $S = +1$  and  $T = -1$ , leading to a stable state. The lightest component of the  $S$  and  $T$  chiral superfields constitutes the DM.

We suppose SUSY breaking is communicated to the MSSM by gauge mediation, while the  $U(1)_d$  does not couple directly to the messengers. Then the hidden sector is shielded from SUSY breaking in the MSSM and only receives soft-terms via the small kinetic mixing parameter. Once electroweak symmetry is broken, the kinetic mixing induces an effective Fayet-Iliopoulos (FI)  $D$ -term for the  $U(1)_d$ ,  $\epsilon \langle D_Y \rangle$ , as in [70]. Ignoring the small supersymmetry breaking effects, the potential is

$$(III.5) \quad V = \frac{1}{2} (g_d (|T|^2 - |H'|^2) + \epsilon \langle D_Y \rangle)^2 + |\lambda|^2 (|S|^2 |H'|^2 + |S|^2 |T|^2 + |T|^2 |H'|^2),$$

<sup>1</sup>Note this superpotential was also recently considered in an attempt to explain the CoGeNT excess in [99], in a symmetric DM model and with different assumptions about supersymmetry breaking.

where  $\langle D_Y \rangle = \frac{g_Y v^2 c_{2\beta}}{4} + \xi_Y$ . Here,  $v = 246$  GeV is the effective MSSM Higgs vev,  $\tan \beta = v_u/v_d$ .  $\xi_Y$  is a “fundamental” FI term for hypercharge whose existence is more model dependent. For example, a weak scale  $\xi_Y$  can be naturally generated in  $U(1)$  messenger models of gauge mediation [89]. For  $c_{2\beta} = -1$  and  $\xi_Y = 0$ ,  $\sqrt{|D_Y|} \simeq 72$  GeV. Then for  $\epsilon = 10^{-3}$  and  $\epsilon \langle D_Y \rangle \simeq 5$  GeV<sup>2</sup>, the GeV scale has been generated from the weak scale. The dark Higgs,  $H'$ , obtains a vev to cancel the  $D$ -term

$$(III.6) \quad \langle H' \rangle = \sqrt{\frac{\epsilon \langle D_Y \rangle}{g_d}},$$

from which the scalars obtain masses

$$(III.7) \quad m_{H'}^2 = 2g_d^2 \langle H' \rangle^2; \quad m_S^2 = m_T^2 = \lambda^2 \langle H' \rangle^2.$$

The mass of the dark photon is

$$(III.8) \quad m_{\tilde{\gamma}_d} = \sqrt{2}g_d \langle H' \rangle.$$

At this point, the vacuum is supersymmetric. The mass matrix in the fermion sector (in the  $(\tilde{\lambda}_d, \tilde{H}', \tilde{S}, \tilde{T})$  basis) is given by

$$(III.9) \quad \mathcal{M} = \begin{pmatrix} 0 & \sqrt{2}g_d \langle H' \rangle & 0 & 0 \\ \sqrt{2}g_d \langle H' \rangle & 0 & 0 & 0 \\ 0 & 0 & 0 & \lambda \langle H' \rangle \\ 0 & 0 & \lambda \langle H' \rangle & 0 \end{pmatrix}.$$

The dark Higgsino-photino mass eigenstate,  $\tilde{\gamma}_d$ , is degenerate with the gauge boson, and the  $S - T$  fermions,  $\psi$  and  $\bar{\psi}$ , are degenerate with their scalar superpartners.

We now address how the small SUSY breaking effects leak into this sector. In particular, two loop gauge mediated diagrams contribute positive mass squareds to the  $T$  and  $H'$  scalars via the kinetic mixing. We normalize the size of this contribution to right handed selectron mass,  $\tilde{m}_{E^c}$ , as

$$(III.10) \quad \Delta \tilde{m}_{T, H'}^2 = \epsilon^2 \left( \frac{g_d}{g_Y} \right)^2 \tilde{m}_{E^c}^2.$$

This equation is valid at the messenger scale; renormalization group running to the hidden sector scale is a 10% effect. This soft mass affects the cosmology of this model since it raises the  $T$  scalar above  $\psi$ .

Because it is a singlet, the  $S$  scalar does not receive a positive (mass)<sup>2</sup> from gauge mediation. Rather, it has a negative soft mass squared at one loop due to the presence of the  $T$  and  $H'$  soft masses. This lowers the  $S$  scalar just below  $\psi$  by an amount

$$(III.11) \quad \Delta\tilde{m}_S^2 = -\frac{2\lambda^2}{16\pi^2}(\Delta\tilde{m}_{H'}^2 + \Delta\tilde{m}_T^2) \log\left(\frac{M_{\text{mess}}}{m_S}\right).$$

Here  $M_{\text{mess}}$  is the messenger scale where the soft masses are generated. Thus the lightest state charged under the  $S/T$  parity is the  $S$  scalar. It is this state which constitutes the DM.

While the splittings of Eqs. (III.10) and (III.11) will be most important for cosmology, for completeness we note the leading splitting in the gauge multiplet. The dark photino gets a small correction from mixing with the MSSM gauge sector that splits the fermion into two Majorana states around the dark gauge boson. Including the leading corrections to the dark photino mass,

$$(III.12) \quad m_{\tilde{\gamma}_d}^{(1,2)} = \sqrt{2}g_d\langle H' \rangle \pm \epsilon^2 \left( \frac{m_Z^2 s_W^2 s_{2\beta}}{\mu} + \frac{m_{\tilde{\gamma}_d}^2}{M_1} \right).$$

There are two contributions to the mass of the dark Higgs radial mode,  $h'$ , which take it away from the SUSY limit: the small correction from mixing with the Higgs boson via the  $D$ -term and a 1-loop radiative correction which contributes to its quartic. The correction to the quartic is the larger of the two. It shifts the physical dark Higgs boson mass by an amount

$$(III.13) \quad \Delta m_{h'}^2 = \frac{\lambda^4 \langle H' \rangle^2}{16\pi^2} \log \frac{m_T^2}{m_\psi^2} \simeq \frac{\lambda^2}{8\pi^2} \Delta\tilde{m}_T^2.$$

To allow efficient annihilation of the  $S/T$  sector to gauge bosons, we choose  $\sqrt{2}g_d < \lambda$ . The spectrum is shown schematically in Fig. 3.1. Aside from the gravitino,  $\tilde{\gamma}_d$  is the



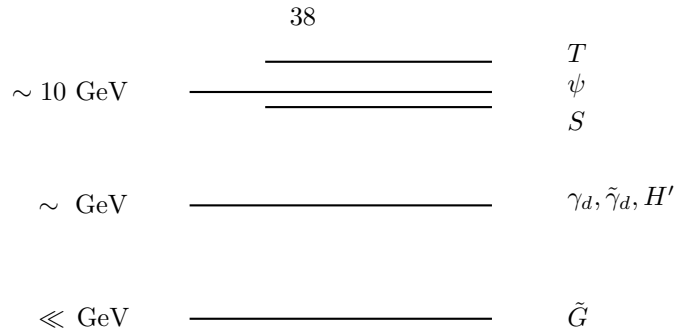


Figure 3.1: The spectrum of the SUSY model. We have illustrated the mass pattern of the  $S/T$  multiplet (not to scale) since this splitting determines the identity of the DM. The splittings within the dark photon multiplet have been suppressed.

lightest R-odd particle. Although the dark gaugino is slightly lighter than the gauge bosons, thermal effects allow it to annihilate to the gauge bosons which subsequently decay. We describe this process in detail in Sec. 3.3.

There are phenomenological constraints on an Abelian GeV hidden sector. If the dark photon mass is smaller than the mass of the  $\Upsilon(3s)$ , the lack of observation of dark photons at  $B$ -factories constrains the  $m_{\gamma_d} - \epsilon$  parameter space [100], yielding  $\epsilon \lesssim 4 \times 10^{-3}$ . For larger dark photon masses, the strongest constraints are  $\epsilon \lesssim 10^{-2}$  coming from precision electroweak measurements – there are  $\epsilon$  suppressed couplings to the  $Z^0$  which can lead to changes in these observables [120]. Finally, avoiding Landau poles for  $\lambda$  before the GUT scale enforces  $\lambda \lesssim 1.5$  which (due to the requirement that  $\sqrt{2}g_d < \lambda$  in our model) constrains  $g_d \lesssim 1.1$ . If one only requires no Landau poles appear before  $\mathcal{O}(10 \text{ TeV})$ , this constraint is  $\lambda \lesssim 2.5$  and  $g_d \lesssim 1.8$ . Stronger constraints on  $\epsilon/g_d$  from the Landau pole are dependent upon the DM mass (see Sec. 3.3 below). We plot the excluded region due to all of these constraints in Fig. 3.2.

### 3.3 Cosmology

The proposed SUSY model of ADM with a dark photon has a non-trivial cosmological history. In particular, the near degeneracy of the states which comprise the DM and

massive dark photon superfields imply the potential for late decays. In the analysis that follows, we demonstrate that we maintain the success of Big Bang Nucleosynthesis (BBN). In addition, the presence of the global symmetry on  $S/T$  and R-parity results in two stable states,  $S$  and the gravitino. We must check that  $\Omega_{\text{DM}}$  is dominated by the asymmetric part of the  $S$  density.

We present two different asymmetry transfer operators. One of these operators has processes that re-symmetrize the DM and anti-DM at late times. The model with a symmetric DM density today is subject to additional constraints. For this reason, this transfer operator must be discussed separately.

In all cases, we assume that the gravitino mass is  $\leq 16$  eV, consistent with low-energy gauge mediation, in order to evade constraints from measurements of the Lyman- $\alpha$  forest without restricting the reheat temperature after inflation [193]. We will conclude this section with some variations on our canonical cosmology.

One key component of ADM models is the requirement of an asymmetry transfer mechanism. We assume that the transfer occurs via some higher dimensional operator,  $\mathcal{O}_{\text{asym}}$ , generated by integrating out physics at a scale,  $M$ . The states integrated out to generate  $\mathcal{O}_{\text{asym}}$  can be charged under both  $U(1)_d$  and  $U(1)_Y$ , and in principle could also be responsible for generating  $\epsilon$ . We are agnostic about the source of the  $(B - L)$  asymmetry - we only require that it is generated before  $\mathcal{O}_{\text{asym}}$  falls out of equilibrium.

Since the  $S$  field is a gauge singlet,<sup>2</sup> asymmetry transfer operators will have the following generic form [140]:

$$(III.14) \quad \mathcal{O}_{\text{asym}} = \frac{S^p \mathcal{O}_{B-L}}{M^r},$$

where  $\mathcal{O}_{B-L}$  is a SM gauge singlet operator involving only MSSM fields with a non-zero  $B - L$  number  $q$ . This operator transfers the  $B - L$  into the  $S/T$  global symmetry. The

---

<sup>2</sup>One is also free to use the combination  $(TH')$  in constructing these operators.

four lowest dimension MSSM superpotential operators with  $|q| = 1$  are  $LH_u$ ,  $U^c D^c D^c$ ,  $LLE^c$ , or  $LQD^c$ . Higher  $q$  operators can be built from combinations of these. The size of the asymmetry produced only depends on  $q$  [65, 103].

Assuming the symmetric component of the DM abundance is negligible (we verify this in specific cases below), we can compute the  $S - S^\dagger$  asymmetry using standard equilibrium methods [127]. Above the  $\langle H' \rangle \neq 0$  phase transition there is the additional requirement that the net  $U(1)_d$  charge is zero. If  $\mathcal{O}_{\text{asym}}$  decouples before the electroweak phase transition (EWPT), the mass for the DM in the SUSY model is given by

$$(III.15) \quad m_{\text{DM}} = \frac{158}{33} \frac{p}{|q|} \frac{\Omega_{\text{DM}}}{\Omega_B} \frac{B}{B-L} m_p \simeq (7.1 \text{ GeV}) \frac{p}{|q|},$$

where  $m_p$  is the proton mass.  $\Omega_{\text{DM}}$  is the DM relic abundance, and  $\Omega_B$  is the abundance of baryonic matter.  $B/(B-L) \simeq 0.35$  with an uncertainty of  $\mathcal{O}(10\%)$  due to the details of the sphalerons and the EWPT [127]. If the asymmetry transfer operator decouples after the EWPT but before the dark sector phase transition (which occurs at  $T \sim m_{\text{DM}}$ ), the effective  $B - L$  transferred is different, and

$$(III.16) \quad m_{\text{DM}} = \frac{197}{87} \frac{p}{|q|} \frac{\Omega_{\text{DM}}}{\Omega_B} \frac{B}{B-L} m_p \simeq (3.3 \text{ GeV}) \frac{p}{|q|}.$$

In the main body of the text, we will focus on the operators:

$$(III.17) \quad \mathcal{O}_{\text{asym}}^{(1)} = \frac{S^2 U^c D^c D^c}{M_{(1)}^2} \left( \text{or } \frac{S^2 L L E^c}{M_{(-1)}^2}, \text{ etc.} \right);$$

$$(III.18) \quad \mathcal{O}_{\text{asym}}^{(-2)} = \frac{S^2 (LH_u)^2}{M_{(-2)}^3},$$

where the superscript refers to the  $B - L$  number,  $q$ , for the MSSM operator. We will show in an appendix that  $\mathcal{O}_{\text{asym}}^{(-1)} = (S^2 LH_u)/M_{(-1)}$  does not give rise to a viable cosmology when all constraints are analyzed. If they decouple above the EWPT, these operators imply a

DM mass:

$$(III.19) \quad m_{\text{DM}}^{(1)} = 14.2 \text{ GeV} \Rightarrow \lambda \sqrt{\frac{\epsilon/g_d}{10^{-1}}} \left( \frac{\sqrt{\langle D_Y \rangle}}{72 \text{ GeV}} \right) = 0.62;$$

$$(III.20) \quad m_{\text{DM}}^{(-2)} = 7.1 \text{ GeV} \Rightarrow \lambda \sqrt{\frac{\epsilon/g_d}{10^{-2}}} \left( \frac{\sqrt{\langle D_Y \rangle}}{72 \text{ GeV}} \right) = 1.0.$$

Hence, the choice of operator implies a relationship among the parameters in the dark sector. One can use the upper bounds on  $\lambda$  arising from the absence of a Landau pole to constrain the minimum allowed  $\epsilon/g_d$ , see Fig. 3.2.

### 3.3.1 After Decoupling of Asymmetry Transfer

After  $U(1)_d$  is broken, the asymmetric DM abundance is spread across  $S, T$ , and  $\psi$  in the ratios  $\frac{1}{3}$ ,  $\frac{1}{3}$ , and  $\frac{1}{3}$ . However, the  $\psi$  and  $T$  are unstable. Since we are working in the context of low scale gauge mediation, the decays  $T \rightarrow \tilde{G}\psi$  and  $\psi \rightarrow \tilde{G}S$  are allowed. Decays to gauginos are kinematically forbidden due to the small mass splitting between the  $S, T$  scalars and  $\psi$  fermion. The decay width for these processes are:

$$(III.21) \quad \Gamma(T \rightarrow \psi\tilde{G}) = \frac{1}{8\pi} \frac{(m_T^2 - m_\psi^2)^4}{F^2 m_T^3};$$

$$(III.22) \quad \Gamma(\psi \rightarrow S\tilde{G}) = \frac{1}{16\pi} \frac{(m_\psi^2 - m_S^2)^4}{F^2 m_\psi^3},$$

where we have assumed a massless gravitino. Since the decays are invisible to the SM, these processes will not interfere with BBN predictions. In any case, for the parameters we consider, they occur on time scales less than a second. These mass splittings are calculable in terms of the underlying parameters and are given by (see Eqs. (III.10) and (III.11)):

$$(III.23) \quad m_T^2 - m_\psi^2 \simeq 3 \times 10^{-3} \left( \frac{g_d \epsilon}{10^{-4}} \right)^2 \left( \frac{\tilde{m}_{E^c}}{200 \text{ GeV}} \right)^2 \text{ GeV}^2;$$

$$(III.24) \quad m_\psi^2 - m_S^2 \simeq 6 \times 10^{-4} \lambda^2 \left( \frac{g_d \epsilon}{10^{-4}} \right)^2 \left( \frac{\tilde{m}_{E^c}}{200 \text{ GeV}} \right)^2 \text{ GeV}^2.$$

Depending upon the asymmetry transfer operator, decays that change the DM asymmetry number by two units could also be allowed. This ‘re-symmetrization’ of the DM

must occur when the DM number density is sufficiently low to prevent annihilations from turning back on, re-coupling the DM and reducing the relic density. Since the cross section for annihilation of DM is large in these models, the operators that allow re-symmetrization of the DM abundance are also tightly constrained by indirect signals. We will discuss this further when we consider specific asymmetry transferring operators.

The symmetric abundance of  $S$  should be subdominant to the asymmetric density, so that the DM density is truly set by the baryon asymmetry and not thermal freeze-out. The  $S$  annihilations are dominated by the process  $SS^\dagger \rightarrow \tilde{\gamma}_d \tilde{\gamma}_d^\dagger$ , which comes from the  $t$ -channel exchange of a  $T$  fermion. This annihilation cross section is approximately

$$(III.25) \quad \langle \sigma_{\text{sym}} v \rangle \simeq (2 \times 10^{-20} \text{ cm}^3/\text{s}) \lambda^4 \left( \frac{7 \text{ GeV}}{m_S} \right)^2,$$

where we have assumed that the gauge sector is much lighter than the ADM sector. This yields a *symmetric* relic density of

$$(III.26) \quad \Omega_S^{\text{sym}} h^2 \simeq 2 \times 10^{-8} \lambda^{-4} \left( \frac{m_S}{7 \text{ GeV}} \right)^2 \ll 0.1,$$

which is clearly subdominant to the measured abundance of DM.

The cosmology of  $\gamma_d$  and  $h'$  is straightforward since they both decay to the SM via  $\epsilon$  suppressed couplings long before BBN. The story is not so simple for the dark photino. The presence of R-parity stabilizes the lightest of the superpartners, which for this scenario (low energy SUSY breaking), is the gravitino. The dark photino is the second lightest R-odd state, and decays via  $1/F$  suppressed couplings. Due to the dark photino's near degeneracy with the dark photon, the dominant decay channel is  $\tilde{\gamma}_d \rightarrow \gamma \tilde{G}$ , which is suppressed both by the scale SUSY breaking and the kinetic mixing  $\epsilon$ . This decay time is [70]

$$(III.27) \quad \tau(\tilde{\gamma}_d \rightarrow \gamma \tilde{G}) = 190 \text{ s} \left( \frac{10^{-3}}{\epsilon} \right)^2 \left( \frac{\text{GeV}}{m_{\tilde{\gamma}_d}} \right)^5 \left( \frac{\sqrt{F}}{50 \text{ TeV}} \right)^4.$$

This late production of photons could, in principle, alter the predictions of BBN. This depends on the destructive power of the dark photinos, which is given by  $m_{\tilde{\gamma}_d} n_{\tilde{\gamma}_d}/s \equiv m_{\tilde{\gamma}_d} Y_{\tilde{\gamma}_d}$ ,

where  $n_{\tilde{\gamma}_d}$  is the number density of photinos and  $s$  is the entropy density of the universe. Since the Higgsino component of the dark photino induces an interaction between the dark photino and the dark photon, the number density is set by these interactions. Though the dark photino and photon masses are degenerate, the thermal tail of the Boltzmann distribution allows efficient annihilation of the dark photinos. To good approximation, the annihilation cross-section for this process is given by [167]:

$$(III.28) \quad \langle \sigma_{\tilde{\gamma}_d} v \rangle \simeq \frac{g_d^4}{16\pi m_{\tilde{\gamma}_d}^2} v_{f.o.} \simeq 7 \times 10^{-24} \text{cm}^3/\text{s} \left( \frac{g_d}{0.1} \right)^4 \left( \frac{1 \text{ GeV}}{m_{\tilde{\gamma}_d}} \right)^2 \left( \frac{v_{f.o.}}{0.3} \right),$$

where  $v_{f.o.}$  is the velocity when the dark photinos freeze out. Hence, the dark photinos can have a small relic abundance when they decay to a gravitino and a photon. In Fig. 3.2 we show the regions in the  $g_d - \epsilon$  plane which do not alter the predictions of BBN and satisfy constraints from  $B$ -factories and from precision electroweak (PEW) measurements. In generating this figure we have done the full calculation of the thermally averaged cross section to capture the effects of the degeneracy between the initial and final states. We also show the region of specific choices of  $\epsilon$  and  $g_d$  which can modify the abundance of Li-7, alleviating the tension with the current measurements [134].

Next we explore the cosmology associated with transferring the asymmetry to the DM. We pay particular attention to the requirement that the transfer operator not imply a Boltzmann suppression for the asymmetry by remaining in equilibrium to very low scales,  $T < m_{\text{DM}}$ . This requirement constrains the asymmetry transfer scale,  $M$ . The physics involved in the determination of this scale is sensitive to the choice of the transfer operator, so we discuss each operator in turn.

### 3.3.2 Cosmology of Models with $\mathcal{O}_{\text{asym}} \sim S^2 U^c D^c D^c$

The cosmology associated with the  $q = 1$  operator is the most straightforward. Comments similar to those below also apply to operators where  $U^c D^c D^c$  is replaced by either  $LLE^c$  or  $LQD^c$ . Since there are three MSSM fields involved which do not obtain vevs, at

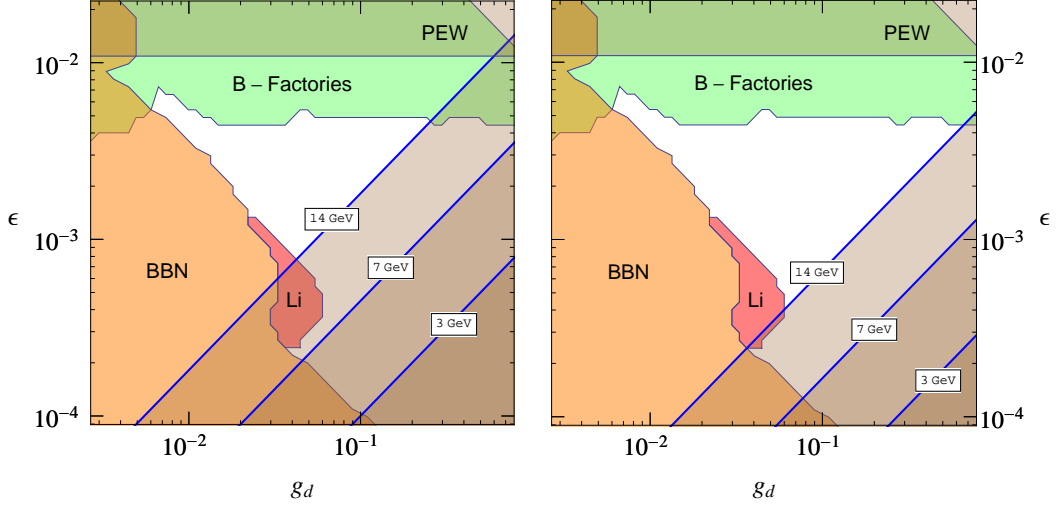


Figure 3.2: Constraints in the  $\epsilon - g_d$  plane. We have shown the regions which are excluded by BBN constraints due to  $\tilde{\gamma}_d \rightarrow \gamma \tilde{G}$  [134] (orange),  $B$ -factories due to direct searches for  $\gamma_d$  [99] (green), and precision electroweak measurements due to  $\gamma_d - Z^0$  mixing [120] (brown). The red region corresponds to parameters which solve the lithium-7 problem [134]. On the left (right) we show contours where  $\lambda$  is constrained so as not to reach Landau pole before  $M_{\text{GUT}}$  (10 TeV) for  $m_{\text{DM}} = 14.2$  GeV,  $m_{\text{DM}} = 7.1$  GeV and  $m_{\text{DM}} = 3.3$  GeV, assuming  $\langle D_Y \rangle = 72$  GeV. The region below these contours is excluded.

tree level all asymmetry transfer interactions will involve at least one SM superpartner. For these processes the transfer rate will be Boltzmann suppressed for temperatures below the superpartner scale, and will be strongly suppressed when  $T \sim m_{\text{DM}}$ . So, for low temperatures (below the SUSY scale), the dominant process arises from a one-loop diagram where a gluino is exchanged. This converts two squarks to quarks and generates an effective dimension-7 operator  $(S\psi_S\psi_d^c\psi_{d^c}\psi_{u^c}/M_{eff}^3)$ . Taking a superpartner scale of 1 TeV, the requirement that this effective operator be out of equilibrium before  $T \sim m_{\text{DM}}$  enforces the mild constraint  $M_{(1)} > 2$  TeV.

If one imposes the stronger bound that the transfer operator decouples before the EWPT, a stronger bound on  $M_{(1)}$  is present. Depending on the precise spectrum of the superpartner masses, either the tree-level or loop induced process can be the most important. However, both give bounds of  $M_{(1)} \sim \mathcal{O}(100 \text{ TeV})$ . If this stronger condition holds, then the DM mass is as given in Eq. (III.19), otherwise Eq. (III.16) applies.

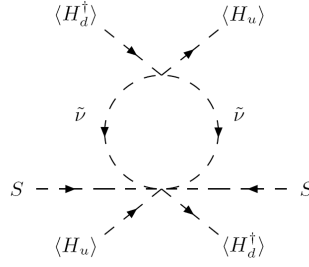


Figure 3.3: The one-loop diagram which generates the  $S$  number violating mass  $b_S$ .

### 3.3.3 Cosmology of Models with $\mathcal{O}_{\text{asym}} \sim S^2(LH_u)^2$

For the  $q = -2$  operator, the story is different: the process  $SS \rightarrow \nu^\dagger \nu^\dagger$  has the potential to wash-out the asymmetry. Requiring that this process be out of equilibrium at temperatures of order the DM mass yields:

$$(III.29) \quad M_{(-2)} \gtrsim 20 \text{ TeV} \left( \frac{m_S}{7 \text{ GeV}} \right)^{1/6}.$$

The mass estimate of  $m_{\text{DM}}$  in Eq. (III.15) requires the stronger condition that the asymmetry transfer operator decouples at temperatures above the EWPT (and does not recouple once  $\langle H_u \rangle \neq 0$ ). This implies that  $M_{(-2)} \gtrsim 30 \text{ TeV}$ .

The origin of neutrino masses has a strong impact on the cosmology for this transfer operator. If neutrinos are Majorana, then the superpotential operator  $(LH_u)^2/M_{\nu_R}$  is non-vanishing, where  $M_{\nu_R}$  is the right handed neutrino mass scale. The operator  $S^2(LH_u)^2$  equates  $L$  number with  $S$  number. Therefore, the neutrino mass operator violates  $S$  number and generates a mass term via the one-loop diagram in Fig. 3.3 that breaks  $S$  number by two units,  $b_S SS + \text{h.c.}$ . This splits the real and imaginary components of the  $S$  scalar by

$$(III.30) \quad \begin{aligned} \Delta m_S &= \frac{b_S}{m_S} \simeq \frac{1}{16\pi^2} \frac{v^2 c_\beta^2 \mu^2}{M_{(-2)}^3} \frac{m_\nu}{m_S} \log \left( \frac{\tilde{m}_{\nu_L}}{M_{\text{mess}}} \right) \\ &\simeq 4 \times 10^{-22} \text{ GeV} \left( \frac{7 \text{ GeV}}{m_S} \right) \left( \frac{\mu}{100 \text{ GeV}} \right)^2 \left( \frac{10^5 \text{ GeV}}{M_{(-2)}} \right)^3. \end{aligned}$$

Here  $\mu$  is the supersymmetric Higgs mass parameter;  $\tilde{m}_{\nu_L}$  is the sneutrino soft mass,



and  $m_\nu$  is the neutrino mass. This splitting will induce  $S - S^\dagger$  oscillations when  $H \sim \Delta m_S$  similar to [81].

When these oscillations begin, one must check that the now symmetric relic density does not recouple and annihilate away. This condition is given by  $H(T_r) > \Delta m_S$ , where the recoupling temperature ( $T_r \sim m_S^3/\lambda^4$ ) is in the range 0.1 – 100 keV. This constraint implies a limit on  $M_{(-2)} \gtrsim 10^5$  GeV which is more restrictive than the decoupling constraints described above in Eq. (III.29). Hence, the asymmetry operator decouples before the EWPT, and the DM mass is 7.1 GeV, from Eq. (III.15).

Even if the oscillations do not occur so early as to affect the relic density, they could lead to residual annihilation which could give additional constraints. The annihilation mode  $SS^\dagger \rightarrow \tilde{\gamma}_d^\dagger \tilde{\gamma}_d \rightarrow \gamma\gamma\tilde{G}\tilde{G}$  could produce photons which can effect the reionization depth of the CMB, see [185] for a recent analysis. The quantity constrained is the annihilation cross section times the ionization fraction,  $f$ . For DM in the 10 GeV range,

$$(III.31) \quad f\langle\sigma v\rangle \left(\frac{\rho_S}{\rho_{DM}}\right) \left(\frac{\rho_{S^\dagger}}{\rho_{DM}}\right) = \frac{1}{4}f\langle\sigma v\rangle \lesssim \text{few} \times 10^{-26} \text{ cm}^3/\text{s}.$$

We expect that  $f$  will be in the range 0.1 – 0.5. Hence, if oscillations occur before recombination, the requirement  $\langle\sigma v\rangle \lesssim 10^{-24}$  translates to  $\lambda \lesssim 0.1$ .

After fixing  $\lambda \sim 0.1$ , one must check that  $m_S = 7.1$  GeV can be achieved in this model. To obtain a DM mass of this size, one must maximize the ratio  $\epsilon/g_d$ . From Fig. 3.2, the maximum this ratio can be is  $(\epsilon/g_d)_{\text{max}} \sim (7 \times 10^{-3}/7 \times 10^{-3})$ , which, when combined with  $\lambda \sim 0.1$ , implies  $m_S = 7.2$  GeV. Hence, this scenario is marginally feasible. Including a bare FI term for hypercharge could mitigate this tension. Note that this point in parameter space should be probed by the existing but as yet unanalyzed data from the  $B$ -factories.

Alternatively, if  $M_{(-2)} \gtrsim 10^{10}$  GeV, the oscillations occur at temperatures below an eV. Hence there are no DM annihilations during recombination. In this case, the strongest constraints come from considering the effect of DM annihilation on reionizing the universe.

Since the high energy photons which result from the  $SS^\dagger \rightarrow \tilde{\gamma}_d^\dagger \tilde{\gamma}_d \rightarrow \gamma\gamma\tilde{G}\tilde{G}$  annihilations are poor ionizers [51], the strongest constraint comes from (for example) the annihilation channel  $SS^\dagger \rightarrow \gamma_d\gamma_d \rightarrow e^+e^-e^+e^-$  where the electrons subsequently upscatter CMB photons. This cross section is roughly two orders of magnitude smaller than the one quoted in Eq. (III.25). This translates into a bound<sup>3</sup>  $\lambda \lesssim 0.3$  [51]. Note that this larger value of  $\lambda$  will alleviate some of the tension with achieving the correct size for  $m_S$ .

If  $M_{-2} \gtrsim 10^{12}$  GeV, then DM has not begun oscillating yet. Alternately, since the mass splitting is proportional to the Majorana neutrino mass, if the neutrinos have Dirac masses no oscillation occurs. In these cases, the DM abundance would still be asymmetric today and the above constraints do not apply.

### 3.3.4 Variations on the Cosmological History

In this section we will explore various other allowed cosmological histories beyond the simplest story we have presented above. For example, one could imagine a scenario with a heavier gravitino. The dark sector will generically feel anomaly mediated supersymmetry breaking contributions, which for too large a gravitino mass could potentially raise the DM above the GeV scale or destabilize the  $H'$  vev. This implies

$$(III.32) \quad \frac{\alpha}{4\pi} m_{3/2} = \frac{\alpha}{4\pi} \frac{F}{\sqrt{3}m_{\text{Pl}}} \lesssim \text{GeV} \Rightarrow \sqrt{F} \lesssim 2 \times 10^{10} \text{ GeV},$$

which implies a bound of  $m_{3/2} \lesssim 130$  GeV. Thus, the gravitino can be heavier than the dark photino. In this case, the photino cannot decay, so one should ensure that the abundance of dark photinos is small enough to only constitute a subdominant portion of the DM:

$$(III.33) \quad \Omega_{\tilde{\gamma}_d} h^2 \simeq 3.5 \times 10^{-2} \left( \frac{0.02}{g_d} \right)^4 \left( \frac{m_{\tilde{\gamma}_d}}{1 \text{ GeV}} \right)^2 \left( \frac{0.3}{v_{f.o.}} \right).$$

---

<sup>3</sup>In [51] the DM mass is 100 GeV. Since our DM is 7.1 GeV in this model the constraint will be slightly stronger than what they quote.

This implies a lower bound on  $g_d \gtrsim 0.02$ . Alternately, a small amount of R-parity violation (RPV) in the MSSM could allow dark photino decays without spoiling BBN. If this RPV is provided by a  $LLE^c$  or  $LQD^c$  operator, assuming no non-trivial textures, this implies a value for the coefficient near the limits from  $\mu \rightarrow e\gamma$ .

In this scenario, the gravitino would decay to dark photinos as well. Again, constraints from BBN would limit the abundance of gravitinos produced in the early universe, which translates into a constraint on the reheat temperature of the universe of  $\mathcal{O}(10^5 \text{ GeV})$  [142]. This could pose a problem for asymmetry transfer operators which require higher reheat temperatures to ensure the transfer is ever in equilibrium.

Another way to avoid a gravitino overabundance is to imagine a too-large baryon asymmetry was generated via the Affleck-Dine mechanism [8], which was subsequently diluted by a period of late-time inflation to the measured value while simultaneously diluting the gravitinos. Since the DM is set by the same large asymmetry, it would be diluted by the same fraction and would maintain the correct ratio between the relic density of baryons and DM.

### 3.4 Direct Detection

Since  $S$  is neutral under the dark gauge force, tree-level direct detection proceeds either by the exchange of  $h'$  via mixing with the MSSM Higgs, which is suppressed by  $\epsilon$ , or by mixing with the  $T$  via the  $A_\lambda$  term to exchange a dark photon. However, since we have assumed that the only SUSY breaking is communicated to the dark sector through kinetic mixing, this  $A$ -term is suppressed by  $\epsilon^2$ . So, these tree-level diagrams are small. However, once  $H'$  acquires a vev the  $S$  scalar receives a coupling to the dark photon at the one-loop level:

$$(III.34) \quad \frac{\lambda^2 g_d}{16\pi^2} \left( \frac{4g_d^4 - \lambda^4 + 4\lambda^2 g_d^2 \log\left(\frac{\lambda^2}{2g_d^2}\right)}{2(2g_d^2 - \lambda^2)^2} \right) S^\dagger \overleftrightarrow{\partial}_\mu S \gamma_d^\mu \equiv g_d q_{\text{eff}} S^\dagger \overleftrightarrow{\partial}_\mu S \gamma_d^\mu.$$

This coupling is analogous to the one-loop  $Z^0 b\bar{b}$  vertex corrections from a charged Higgs and a top quark [124].

Since the dark photon only couples to the atomic number of the nucleus, the effective cross section per proton is

$$(III.35) \quad \sigma_p = \frac{4 g_W^4 c_W^4 \mu_{S,p}^2}{\pi c_{2\beta}^2 m_W^4} q_{\text{eff}}^2,$$

where  $g_W$  is the weak coupling constant,  $c_W$  is the cosine of the weak mixing angle, and  $\mu_{S,p}$  is the reduced mass of  $S$  and a proton. Due to the  $g_d$  and  $\epsilon$  dependence in  $m_{\gamma_d}$  (see Eq. (III.8)), this cross section is approximately independent of both parameters [70]. This is

$$(III.36) \quad \sigma_p \simeq (9.1 \times 10^{-42} \text{cm}^2) \lambda^4,$$

where we have taken the limit  $\lambda \gg g_d$ . This is not large enough to give rise to the signal observed by CoGeNT, but it will be probed by a variety of upcoming experiments.

In Fig. 3.4, we have plotted the predicted range of direct detection cross sections, appropriate to  $m_{\text{DM}} = 14.2$  GeV, 7.1 GeV and 3.3 GeV where these mass choices are relevant for the operators and decoupling temperatures described above (see Eqs. (III.15) and (III.16)). The upper bound is due to the assumption that there is no Landau pole for  $\lambda$  before the GUT scale, and the lower bound occurs for the smallest allowed value of  $\lambda$  consistent with the correct DM mass (using  $(\epsilon/g_d)_{\text{max}} \simeq 1$  as described in Sec. 3.3.3). We also show the current Xenon-10 bound (solid black line), the projected Xenon-100 bound, assuming 6000 kg-days (dashed green line), the projected Xenon-1T bound (dotted blue line) [133], and the projected limit from the Majorana experiment (dot-dashed purple line) [83]. We have normalized these bounds by the factor  $(Z/A)^2$  which is appropriate for our model where scattering is only off of protons ( $\sigma_p$ ). For  $m_{\text{DM}} = 14.2$  GeV, the largest values of  $\lambda$  are already excluded by Xenon-10 [18]. At 14 GeV, the bound from

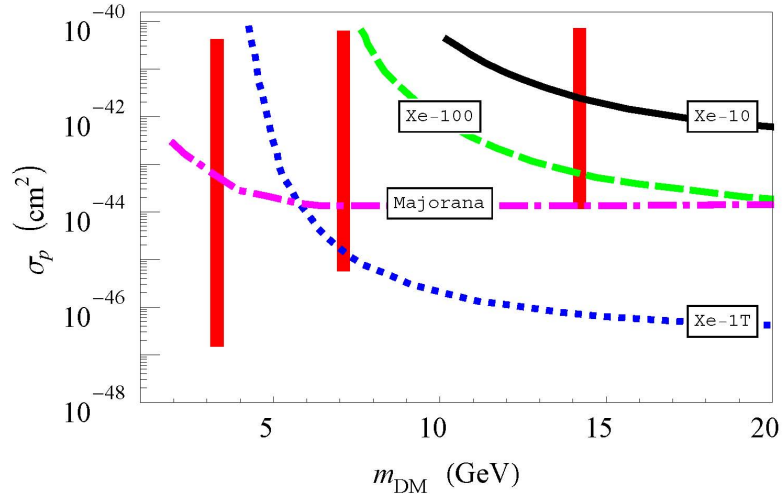


Figure 3.4: The predictions for the direct detection scattering cross sections normalized per proton ( $\sigma_p$ ) for  $m_{\text{DM}} = 14.2$  GeV, 7.1 GeV and 3.3 GeV. We have plotted current/projected limits (also normalized per proton) from Xenon-10 (solid black line), Xenon-100 with 6,000 kg-days (dashed green line), Xenon-1T (dotted blue line) [133], and Majorana (dot-dashed purple line) [83].

Xenon-10 is approximately  $3 \times 10^{-43} \text{ cm}^2$ , which translates to  $\lambda < 0.7$ . Nearly the entire parameter space for  $m_{\text{DM}} = 14.2$  GeV can be probed by Xenon-100 with 6,000 kg-days. For  $m_{\text{DM}} = 7.1$  GeV, Xenon-1T will cover the allowed region, and for  $m_{\text{DM}} = 3.3$  GeV, Majorana will probe much of the allowed range. Hence, a combination of current and proposed experiments will have the potential to cover most of the interesting parameter space for this model.

### 3.5 Colliders

Finally, we discuss some collider implications of this class of models. There are three portals into the dark sector which could potentially be probed: photon kinetic mixing, Higgs boson mixing, and the asymmetry transfer operator.

The MSSM LSP ( $\text{LSP}_{\text{MSSM}}$ ) is unstable to decay to the low mass hidden sector [188, 187]. One mediation mechanism for decay to the hidden sector is through kinetic mixing, as discussed in [132, 27]. The collider phenomenology of such scenarios has been studied

extensively recently; see for example [2, 101, 180, 57, 100, 44, 43, 42].

Photon kinetic mixing may also be probed via the decays of the  $\text{LSP}_{\text{MSSM}}$  to the dark sector [132, 29]. If the  $\text{LSP}_{\text{MSSM}}$  has electroweak quantum numbers, then it will decay promptly to its SM partner and a dark gaugino via an  $\epsilon$ -suppressed interaction. This dark gaugino is stable on detector time scales, and so will manifest as missing energy. More interesting is if  $\text{LSP}_{\text{MSSM}}$  is a neutralino, since it will decay to a dark gaugino and dark Higgs via  $\epsilon$  mixing in the neutralino mass matrix. The dark gaugino will again result in missing energy. However, the dark Higgs will promptly decay back to SM fermions via mixing with the MSSM Higgs boson. These could produce “lepton jets” [29].

The  $T$  and  $\psi$  fields couple to the  $Z^0$  and the MSSM Higgs boson via  $\epsilon$  suppressed couplings, so it will be difficult to produce these particles directly. Furthermore, the DM state  $S$  only interacts through couplings which are both  $\epsilon$  and loop suppressed. Hence, the LHC study of the DM will be indirect. There will be rare decay of the Higgs boson either to a pair of dark photinos (invisible) or dark Higgs bosons (multijet). For the largest values of  $\epsilon$  these branching ratios will be  $\mathcal{O}(10\%)$ .

Finally, if the  $\mathcal{O}_{B-L} \sim U^c D^c D^c$ , then the UV completion will necessarily involve colored objects, some of which could have the quantum numbers of diquarks. If this asymmetry operator decouples after the EWPT (which would imply a DM mass quoted in Eq. (III.16)), then this UV completion is a candidate for early discovery at the LHC [45, 138].

### 3.6 Discussion and Conclusions

In this chapter we have presented a supersymmetric model of Asymmetric Dark Matter, where the GeV scale for the DM mass is naturally generated by loop suppressed gauge kinetic mixing between the hypercharge and dark gauge bosons. This scenario allows the symmetric component of the DM to annihilate efficiently into the dark photons. Direct detection signals proceed via interactions with the dark photon.

This model also provides a solution to the DM problem in models of low scale gauge mediation where the very light gravitino is the LSP and cannot account for the DM. Since gauge mediation is a key component for achieving the appropriate spectrum in this model, the connection is robust. Hence, we have shown that this ADM module can provide the DM for gauge mediated SUSY breaking models.

While we chose to focus on a simple model, this paradigm encompasses a large class of theories which connect the ADM mass scale with the weak scale via a one loop suppression. We note two interesting mechanisms for achieving this goal. The first was proposed in [199, 167] and was coined “singlet mediation” by these authors. The idea is to mediate a weak scale soft mass to a hidden sector singlet field which is then transferred to the rest of the dark sector at one loop via Yukawa couplings. Another choice uses the ideas of [141], where the soft spectrum of the MSSM is due to gaugino (or gravity) mediation while the dark sector only receives contributions from anomaly mediation, again resulting in a one loop suppression. Both of these ideas can be convolved with the ADM paradigm in straightforward – if not minimal – ways, resulting in an explanation for the GeV scale DM mass.

Finally we note that the model presented here provides another example of GeV scale DM with an observable direct detection cross section. The DM mass in models of this type are typically  $\sim 10$  GeV, so direct detection experiments with low energy thresholds are best suited to discover DM of this type.

## CHAPTER IV

### Leptophilic Dark Matter from the Lepton Asymmetry

This chapter was completed in collaboration with Kathryn Zurek [81].

Next we will explore an ADM model which is motivated by the excess in cosmic ray positron and electron signals over the expected background as observed by AMS-01 [10], HEAT [41, 46], PPB-BETS [191], PAMELA [7], Fermi [4] and ATIC [82] which may be a signal of annihilating DM (see Sec. 1.3.2). The annihilation cross-section needed to produce these signals is non-thermal, a factor  $\sim 10-1000$  (depending on DM mass and astrophysical boost factor) larger than the thermal annihilation cross-section [74, 165]. Annihilation predominantly to leptons is preferred both by the shape of the PAMELA signal and the lack of excess in the anti-proton data [92]. These facts appear to disfavor an explanation utilizing a canonical neutralino (though when combined with an astrophysical flux, it may be obtained [137]). One possibility is to introduce new GeV scale particles [27]. These light states mediate a Sommerfeld enhancement [129, 75], implying boosted annihilation in the halo today, while also acting as intermediate final states, thereby providing kinematic constraints on the allowed SM particles produced from DM annihilations.

In this chapter we provide a simple paradigm which gives rise to both boosted and leptophilic annihilation of DM, involving neither Sommerfeld enhancements nor new GeV mass states. When the DM relic density is set by the lepton asymmetry, the annihilation modes are naturally leptophilic. Additionally, this density is derived using lepton number



( $L$ ) violating operators that transfer the asymmetry, and not the  $L$ -preserving operators which lead to a signal for indirect detection experiments (such as PAMELA and Fermi) at low temperatures<sup>1</sup>. Though these models can provide a unique explanation for the cosmic ray excesses, their interest extends beyond this application.

## 4.1 Ingredients

We begin by outlining the general features of this class of models and then turn to constructing a simple model for illustration. An initial lepton asymmetry is generated at temperatures well above the electroweak scale. We are agnostic about the source of this asymmetry for the purposes of this paper. Lepton number violating operators, which connect the SM leptons to dark sector fields, transfer the lepton asymmetry to the dark sector. As in all models of ADM, these operators relate the DM number density to the lepton, and therefore baryon, density,

$$(IV.1) \quad (n_X - n_{\bar{X}}) \sim (n_\ell - n_{\bar{\ell}}) \sim (n_b - n_{\bar{b}}),$$

where the exact proportions are  $\mathcal{O}(1)$  and are determined by the particular operator transferring the asymmetries, and  $(n_X - n_{\bar{X}})$ ,  $(n_\ell - n_{\bar{\ell}})$  and  $(n_b - n_{\bar{b}})$  are the asymmetries in the DM ( $X$ ), leptons and baryons respectively. As a result  $m_X \sim \frac{\Omega_{\text{DM}}}{\Omega_b} m_p$ , where  $m_X$  is the DM mass,  $m_p$  is the proton mass,  $\Omega_{\text{DM}}$  is the DM relic density and  $\Omega_b$  is the baryon density of the universe. This relation implies a DM mass  $m_X \simeq 5$  GeV. Though the size of this mass is phenomenologically viable, it does not directly link the DM sector to the new physics which stabilizes the weak scale.

If the  $L$ -violating operators which transfer the asymmetry have not decoupled as the DM becomes non-relativistic, there is a Boltzmann suppression of the DM asymmetry (see

---

<sup>1</sup>Previous works considered DM from the lepton asymmetry as an explanation of the cosmic ray positron excesses, but utilized decaying DM with a lifetime tuned to the age of the universe [114, 67]. There have also been other models of leptophilic DM unrelated to the lepton asymmetry that have utilized a Sommerfeld enhancement to generate the boost [110, 199, 60]

[39, 127] for a more detailed discussion)

$$(IV.2) \quad (n_X - n_{\bar{X}}) \sim (n_\ell - n_{\bar{\ell}}) e^{-m_X/T_d},$$

where  $T_d$  is the temperature at which the  $L$ -violating operators decouple. This implies that the DM mass can be much larger <sup>2</sup>

$$(IV.3) \quad m_X = \frac{45}{29} \frac{1}{N_X} \frac{f(0)}{f(m_X/T_d)} \frac{\Omega_{\text{DM}}}{\Omega_b} m_p,$$

where  $N_X$  is the number of DM families and  $f(x)$  is the Boltzmann suppression factor given by [39]

$$(IV.4) \quad f(x) = \frac{1}{4\pi^2} \int_0^\infty \frac{y^2 dy}{\cosh^2(\frac{1}{2}\sqrt{y^2 + x^2})}.$$

The decoupling temperature,  $T_d$ , is naturally at the electroweak scale if the corresponding higher dimensional operators are TeV scale suppressed. Once these  $L$ -violating operators decouple, the asymmetric DM density is frozen in.

Although the  $L$ -violating interactions have frozen out,  $L$ -preserving interactions are expected to remain in thermal equilibrium to lower temperatures. This is particularly natural if the  $L$ -violating operators are generated by a combination of the  $L$ -preserving interactions and an operator which introduces a small amount of  $L$ -violation into the theory. While the  $L$ -preserving operators may be in thermal equilibrium longer than the resulting  $L$ -violating interactions, they do not change the *relic* DM density, which will be dominantly composed of  $\bar{X}$ s with essentially no  $X$ s.

If the asymmetry in the DM persisted until today, there would be no indirect detection signal from  $X - \bar{X}$  annihilation. If, however, there is a small violation of DM number in the dark sector, as may result from a small DM Majorana mass,  $X - \bar{X}$  oscillations

---

<sup>2</sup>In deriving this relation we have assumed that the universe reheated high enough for the electroweak sphalerons to be active and that they remain in equilibrium at temperatures below the electroweak phase transition. Hence, at the sphaleron decoupling temperature we assume that the top quark and  $H'$  particles do not contribute to the relevant number densities.

will erase the asymmetry without reducing the relic density, giving rise to a signal for indirect detection experiments from  $\bar{X} X \rightarrow \ell^+ \ell^-$ . In some cases the hidden sector may be more complicated, and four lepton final states may also result, *e.g.*  $\bar{X} X \rightarrow \ell^+ \ell^- \ell^+ \ell^-$ . Since this  $L$ -preserving interaction is expected to be stronger than the  $L$ -violating operator which set the asymmetry, the associated annihilation cross-section may be large enough to generate the cosmic ray positron excesses.

## 4.2 An Explicit Model

There are many models which exhibit the generic features described above. The rest of the chapter is devoted to an illustrative toy model which reproduces this scenario. Consider the  $L$ -violating interaction (from [140])

$$(IV.5) \quad \mathcal{L}_{\text{asym}} = \frac{1}{M'^4_{ij}} \bar{X}^2 (L_i H)(L_j H) + \text{h.c.},$$

where  $L$  is the lepton doublet,  $H$  is the SM Higgs doublet and  $M'$  is a new  $L$ -violating mass scale. This term mediates  $\bar{X} \bar{X} \leftrightarrow \bar{\nu} \bar{\nu}$ , thereby transferring the lepton asymmetry to an  $X - \bar{X}$  asymmetry. Consider in addition the  $L$ -preserving interaction

$$(IV.6) \quad \mathcal{L}_{\text{sym}} = \frac{1}{M^2_{ij}} \bar{X} X \bar{L}_i L_j + \text{h.c.},$$

where  $M$  is a new  $L$ -preserving mass scale, which mediates  $\bar{X} X \leftrightarrow \ell^+ \ell^-, \bar{\nu} \nu$ . A UV completion of these operators is

$$(IV.7) \quad \mathcal{L} \ni y_i L_i H' \bar{X} - \frac{\lambda'}{2} (H^\dagger H')^2 + \text{h.c.},$$

where  $H'$  is a new Higgs doublet. There is a  $\mathbb{Z}_2$  symmetry under which  $X$ ,  $\bar{X}$  and  $H'$  are charged, which is unbroken for  $\langle H' \rangle = 0$ . This symmetry ensures that the lightest  $\mathbb{Z}_2$  odd state, which we take to be  $\bar{X}$ , is stable. Upon integrating out  $H'$ , the effective scale of  $L$ -violation (Eq. (IV.5)) is  $M'^4_{ij} = m^4_{H'}/(y_i y_j \lambda')$ , and the scale of the  $L$ -preserving operator (Eq. (IV.6)) is  $M^2_{ij} = m^2_{H'}/(y_i y_j)$ . Also note that while the model with  $N_X = 1$  does

not violate  $L$ , it does violate any two of electron number, muon number and tau number due to the first interaction in Eq. (IV.7). For weak scale parameters and assuming that  $y_i = y \simeq 1$ , the rate for  $\mu \rightarrow e \gamma$  is  $\sim 15$  orders of magnitude above the current bound. One way to avoid this bound is to assume a hierarchy of  $\mathcal{O}(10^{-8})$  between the first two generations of  $y_i$  couplings. For  $N_X = 3$  the interactions are expanded to

$$(IV.8) \quad \mathcal{L} = y_{ij} L_i H' \bar{X}_j + m_X^i \bar{X}_i X_i.$$

For a generic  $y_{ij}$  matrix, the same large rates for  $\mu \rightarrow e \gamma$  are present as describe above for  $N_X = 1$ . If  $y_{ij} = \text{diag}(y_1, y_2, y_3)$  in this basis (where  $m_X$  is diagonal), contributions to  $\mu \rightarrow e \gamma$  vanish.

The  $\lambda'$  term is present in Eq. (IV.7) to break a global  $U(1)_X$ , under which  $X$ ,  $\bar{X}$  and  $H'$  are charged so that an  $X$  asymmetric operator such as Eq. (IV.5) can arise. For  $M$  and  $M'$  at or above the electroweak scale and  $\lambda' < 1$ ,  $(M'_{ij})^2 \gtrsim (v M_{ij})$ , implying that the  $L$ -violating operators decouple first ( $v \equiv \langle H \rangle$ ). The annihilations through the operator in Eq. (IV.6) (and Eq. (IV.12) below) give rise to larger cross-sections than through Eq. (IV.5). The smaller cross-section from the  $L$ -violating operators set the DM asymmetry, and hence its relic density.

From Eq. (IV.3),  $m_X/T_d \approx 5 - 8$  for  $m_X \approx 100 - 1000$  GeV (note there is only logarithmic sensitivity to  $m_X$ ). Then using  $H(T_d) = n_{\bar{X}} \langle \sigma_{\text{asym}} v \rangle$  to set the  $L$ -violating cross-section yields  $\lambda' = 2 \times 10^{-4}$  for  $m_X = 500$  GeV,  $N_X = 1$  and  $y = 1$ , or equivalently  $M' \simeq 5 \text{ TeV} (m_X/500 \text{ GeV})^{3/8} N_X^{1/8}$ . For reference we include the zero temperature result for the asymmetric annihilation  $\bar{X} \bar{X} \leftrightarrow \bar{\nu} \bar{\nu}$

$$(IV.9) \quad \langle \sigma_{\text{asym}} v \rangle = \frac{1}{16 \pi} \frac{v^4 m_X^2}{M'^8},$$

which results in an  $\mathcal{O}(20\%)$  error when calculating  $M'$ .

The symmetric annihilation  $\bar{X} X \leftrightarrow \ell^+ \ell^-$ ,  $\bar{\nu} \nu$  through Eq. (IV.6) with cross-section

$$(IV.10) \quad \langle \sigma_{\text{sym}} v \rangle = \frac{1}{8\pi} \frac{m_X^2}{M_{ij}^4},$$

will typically freeze-out at a temperature lower than  $T_d$ . These annihilations do not affect the relic density, which is set by the DM asymmetry.

### 4.3 Indirect Detection Signals and Neutrino Masses

As long as the DM density is asymmetric, there will be no indirect signals for DM in the universe today. However, a small Majorana mass  $m_M$  term,

$$(IV.11) \quad \mathcal{L}_M = m_M \bar{X} \bar{X},$$

will induce  $X - \bar{X}$  oscillations which erase the DM asymmetry and give rise to  $X - \bar{X}$  annihilation signals in the universe today. For  $m_X = 500$  GeV and  $M = 300 - 600$  GeV (corresponding to  $y = 2 - 1$  and  $m_{H'} = 600$  GeV),  $\langle \sigma_{\text{sym}} v \rangle = 10^{-23} - 10^{-24}$  cm<sup>3</sup>/s which is the size required to generate the PAMELA and Fermi signals.

One can also generate four lepton final states in this model with only a minor modification. For example the Dirac mass term,  $m_X \bar{X} X$ , could result from the vev of a new singlet scalar ( $\Phi$ ) and the interaction

$$(IV.12) \quad \mathcal{L}_X = \lambda_X \Phi \bar{X} X,$$

where  $m_X \equiv \lambda_X \langle \Phi \rangle$ . Assuming  $\Phi$  has no direct couplings to the SM, its decays will occur exclusively to leptonic final states through a one-loop diagram. Then the interactions in Eq. (IV.12) mediate annihilations to  $\bar{X} X \rightarrow \Phi \Phi \rightarrow \ell^+ \ell^- \ell^+ \ell^-$ . Note that we do not require kinematic restrictions to force  $\Phi$  to decay to leptonic final states.

There is a cosmological restriction on the  $X$  Majorana mass – to preserve the relic density, we require that no annihilations recouple when the  $X - \bar{X}$  oscillations commence. Otherwise the relic density would be reduced to the (small) thermal value set by the

symmetric processes. Quantitatively, the symmetric “no-recoupling” temperature ( $T_{\text{nr}}$ ), defined by

$$(IV.13) \quad \frac{n_{\text{asym}}(T_{\text{nr}})}{2} \langle \sigma_{\text{sym}} v \rangle = H(T_{\text{nr}}),$$

must be greater than the temperature when oscillations begin ( $T_{\text{osc}}$ ):

$$(IV.14) \quad H(T_{\text{nr}}) \gtrsim H(T_{\text{osc}}) \sim m_M.$$

For the no-recoupling relation, we have taken equal parts  $\bar{X}$  and  $X$  from oscillations at  $T_{\text{nr}}$ , and  $n_{\text{asym}}$  is the relic DM density set by asymmetric annihilations. Using Eq. (IV.3) to find  $n_{\text{asym}}(T_{\text{nr}})$  and Eq. (IV.10) we find  $T_{\text{nr}} \simeq 0.8 \text{ GeV } g_*^{-1/2} (10^{-23} \text{ cm}^3/\text{s}/\langle \sigma_a v \rangle)$  for  $m_X = 500 \text{ GeV}$ . Then Eq. (IV.14) implies  $m_M \lesssim \mathcal{O}(10^{-14} - 10^{-20} \text{ GeV})$  for  $\langle \sigma_{\text{sym}} v \rangle \sim \mathcal{O}(10^{-26} - 10^{-23} \text{ cm}^3/\text{s})$ . This very small mass is natural since  $X$  effectively carries lepton number, an unbroken global symmetry in the absence of Majorana neutrino masses. Then the presence of Majorana neutrino masses induces an  $X$  Majorana mass:

$$(IV.15) \quad m_M \sim \frac{1}{16 \pi^2} y^2 \lambda' v^2 \frac{m_\nu}{m_{H^0}^2} \sim \mathcal{O}(10^{-18} \text{ GeV}),$$

where the last relation is for the parameters described above Eq. (IV.9). This is a small enough Majorana mass that no wash out occurs for  $\langle \sigma_{\text{sym}} v \rangle \lesssim 10^{-24} \text{ cm}^3/\text{s}$ . Also note that since we are assuming instantaneous oscillations, even when  $m_M$  is at the upper bound of the constraint implied by Eq. (IV.14) there will only be an  $\mathcal{O}(1)$  change in the DM relic density. Thus for the symmetric annihilation cross-sections of interest here, Majorana neutrino masses are often consistent with the no-recoupling condition. Models with mass varying neutrinos [102] or where the neutrinos are Dirac will weaken this or eliminate this constraint.

The constraints from neutrino masses also do not apply if the  $X$  Majorana mass *induces* Majorana neutrino masses. If the  $X$  Majorana mass results from the vev of a sub-GeV

scalar field ( $S$ ), from the interaction

$$(IV.16) \quad \mathcal{L}_M = \kappa_{\alpha\beta} S \bar{X}_\alpha \bar{X}_\beta,$$

and the scalar field only obtains a vev at  $T < T_{\text{nr}}$ , the Majorana mass  $((m_M)_{\alpha\beta} \equiv \kappa_{\alpha\beta} \langle S \rangle)$  can be arbitrarily large without reducing the DM number density. In this case, the neutrino mass is generated at one-loop [107]:

$$(IV.17) \quad (m_\nu)_{ij} = y_{i\alpha} y_{j\beta} \frac{\lambda'}{16\pi^2} v^2 \frac{(m_M)_{\alpha\beta}}{m_{H^0}^2},$$

where we have taken  $N_X = 3$ . Since one must assume that  $y_{ij}$  is flavor diagonal to avoid lepton flavor violating decays, the flavor and CP violation in the neutrino sector result from the structure of the  $X$  Majorana mass matrix. The parameters  $y \sim \mathcal{O}(1)$ ,  $\lambda' \sim \mathcal{O}(10^{-4})$  and  $m_{H^0} \sim \mathcal{O}(600 \text{ GeV})$  require  $m_M \sim \mathcal{O}(10^{-5} \text{ GeV})$  to achieve  $m_\nu \sim \mathcal{O}(10^{-2} \text{ eV})$ . The off-diagonal entries in  $m_M$  lead to  $\mu \rightarrow e\gamma$  but for these parameters the constraint is satisfied.

One might worry that the interaction in Eq. (IV.16) could wash out the  $X$  asymmetry through, *e.g.*,  $\bar{X} \bar{X} \leftrightarrow S S$  processes. The  $X$  asymmetry is safe from wash out provided this process decouples above  $T_d$ , which happens for small  $U(1)_X$  violation,  $\kappa \lesssim \mathcal{O}(10^{-3})$ . The phase transition to the vacuum with a non-zero vev for  $S$  obtains if either the temperature drops below the critical temperature associated with the  $S$  potential or the  $S$  particles decay.  $S$  decays to two neutrinos via a one-loop diagram with rate  $\Gamma_{S\text{-decay}} \sim \mathcal{O}(10^{-22} \text{ GeV})$  for the parameters discussed above and  $m_S \simeq 10 \text{ MeV}$ . The decay happens just after  $S$  becomes non-relativistic but before big bang nucleosynthesis, avoiding any cosmological problems.

#### 4.4 Direct Detection

This model does not possess any DM-nucleon couplings at tree-level. However, the operator in Eq. (IV.6) induces an effective magnetic dipole moment for the DM when

coupling a photon to the lepton loop. This leads to a direct detection cross-section for  $X$  scattering off of a nucleon (see [140] and the references therein for details)

$$(IV.18) \quad \sigma_{dd} \simeq 2 \times 10^{-46} \text{ cm}^2 \left( \frac{Z/A}{0.4} \right)^2 \left( \frac{600 \text{ GeV}}{m_{H'^{\pm}}/y} \right)^4.$$

This will be a signal for the next generation of experiments.

## 4.5 Discussion

To conclude this chapter, relating the lepton asymmetry to the DM density implies a novel mechanism for obtaining both leptophilic DM and a separation between the freeze-out and present day annihilation cross-sections. In these models,  $L$ -violating operators which transfer the lepton asymmetry set the DM density, while related  $L$ -preserving operators set the rates for annihilation in indirect detection experiments (such as PAMELA and Fermi). The smaller  $L$ -violating cross-sections set the relic density, while allowing for large cross-sections for indirect detection experiments through the  $L$ -preserving operators. If DM of this type is responsible for the cosmic ray anomalies, then it will be observed in the next generation of direct detection experiments. Non-minimal versions of the model can generate the SM neutrino masses and mixings at one-loop. Asymmetric Dark Matter will continue to be important for both model building and experimental searches for DM in the galaxy today.



## CHAPTER V

### On the Correlation Between the Spin-Independent and Spin-Dependent Direct Detection of Dark Matter

This chapter was completed in collaboration with Daniel Phalen and Aaron Pierce [79].

One DM candidate worthy of special attention is the Weakly Interacting Massive Particle (WIMP). However, the naive WIMP paradigm turns out to be an over-simplification. Not just any weak scale stable particle will do. If the DM is weakly interacting in the strictest sense – *i.e.* has full-strength  $SU(2)_L \times U(1)_Y$  gauge interactions – then DM may be excluded by existing direct detection (DD) experiments. In particular, a weak-scale Dirac (vector-like) fermion,  $\chi_D$ , with  $SU(2)$  interactions (which encompasses the simplest DM model of all, a Dirac neutrino), feels the weak force via the operator:

$$(V.1) \quad \mathcal{O}_{\text{vector}} = (\bar{\chi}_D \gamma^\mu \chi_D) Z_\mu^0.$$

When the coefficient of this operator is typical in size, namely  $\mathcal{O}(g/\cos\theta_w)$ , where  $g$  is the  $SU(2)$  coupling constant and  $\theta_w$  is the weak mixing angle, it leads to a huge DD signal – experiments constrain the DM mass to be greater than 50 TeV [181]. Furthermore, the thermal relic density for a 50 TeV Dirac neutrino will be far too large to explain the WMAP measurement. Thus, DM at the weak scale requires a strong suppression of this operator. In fact, it is straightforward to eliminate it entirely. If  $\chi$  is a Majorana spinor, the operator  $(\bar{\chi} \gamma^\mu \chi) Z_\mu^0$  identically vanishes due to the properties of Majorana bilinears. The DM may

be Majorana if an  $SU(2)$  singlet Majorana fermion mixes with a Dirac state. This mixing can only be accomplished via  $SU(2)$  breaking in the WIMP sector, *i.e.* through a Higgs boson vacuum expectation value (vev). Then the resultant DM particle has a non-zero coupling to a Higgs boson,  $h$ , and the dominant scattering process is due to the following operators:

$$(V.2) \quad \mathcal{O}_{\text{Higgs}} = (\bar{\chi} \chi) h,$$

$$(V.3) \quad \mathcal{O}_{Z^0} = (\bar{\chi} \gamma^\mu \gamma^5 \chi) Z_\mu^0.$$

In a multi-Higgs boson theory,  $h$  need not be *the* Higgs boson of the Standard Model (SM), but even in these theories, there often is a Higgs boson that has SM-like properties. We will explore the impact of these operators on Spin-Independent (SI) and Spin-Dependent (SD) scattering off of nuclei, paying particular attention to the expected correlation between the rates at these two types of experiments.

While we perform most of our analysis in the context of the Minimal Supersymmetric Standard Model (MSSM) (for a review of the MSSM, see [162]), we reference other models where appropriate to emphasize the generality of our arguments. We will review the assertion that post-LEP (largely due to the constraints on the chargino and slepton masses), one may consider a mixed or “well-tempered” neutralino as a likely DM candidate, if it is thermally produced [24]. We will show that in this case, light Higgs boson and  $Z^0$  exchange will generically lead to a signal in the next generation of SI and SD experiments.

A thermal history for the WIMP is not the only possibility. As described in Sec. 1.2.2, non-thermal mechanisms may populate the DM (*e.g.* through the decay of a modulus or gravitino [166]), or the DM can be overabundant and subsequently diluted by extra sources of entropy. These options allow a WIMP with a wider range of properties, since the annihilation rate is not fixed by the thermal history. In what follows, we do not rescale DD signals to the (too-low/too-high) thermal relic density. *In all cases, we assume that the*

WIMP constitutes the total DM density, determined from astrophysical measurements to be  $\rho_{\text{DM}} \approx 0.3 \text{ GeV}/\text{cm}^3$ . We will be clear when we are making the assumption of a thermal history. For the purposes of this study, a “thermal” WIMP is one whose thermal relic density is within the generous range  $\pm 3\sigma$  of the WMAP measurement given in Eq. (I.1). We also note that more recent determinations favor a slightly larger value:  $\rho_{\text{DM}} = 0.39 - 0.43 \text{ GeV}/\text{cm}^3$  [62, 178]. This would extend the reach of the direct detection experiments by a factor of  $\approx 4/3$  and probe more parameter space. An accurate determination of the local DM density is important for an accurate measurement of the DM DD cross section.

Related results already exist in the literature, including some comprehensive numerical scans. However, we find that often the (simple) underlying physics is left obscure. We hope to make clear the expected size of various contributions to DD and the relationship to the assumption of a thermal relic abundance. Assuming there are no conspiratorial cancellations, these typical sizes represent important targets for DD experiments.

There is an overwhelming literature in existence on the subject of DD, see reviews [115, 135] and references therein. Of particular interest to us is the relationship between the size of the SD and SI signals, which has recently been explored in [33, 50, 56, 53].

In the next section, we begin by discussing the current experimental status and then make naive estimates for the SI and SD DD cross sections from  $h$  and  $Z^0$  exchange respectively. In Sec. 5.2 we lay out the specific structure of the SI and SD operators in the MSSM and estimate the naive size of the SI and SD cross sections. Then in Sec. 5.3 we review the argument for a well-tempered neutralino and discuss some alternatives. Sec. 5.4 concentrates on illuminating the expected size of the SD cross section for mixed DM models with various restrictions. In Sec. 5.5 we describe the conditions under which SI and SD signals in the MSSM are expected to be correlated. Technical results are relegated to three appendices.

## 5.1 Direct Detection Preliminaries

The interactions in Eqs. (V.2) and (V.3) lead to SI and SD elastic signals in DD experiments, respectively. In Fig. 5.1 we have plotted the current experimental limits for SI and SD DD. Currently, the state of the art SI experiments are CDMS [12] and XENON [19]. XENON constrains  $\sigma_{\text{SI}}^{\chi p} < 4.5 \times 10^{-8}$  pb for  $m_\chi = 30$  GeV. After combining their most recent run with previous data, CDMS-II has a 90% CL bound of  $3.8 \times 10^{-8}$  pb for a WIMP with a mass of 70 GeV [11]. In the most recent data set, two tantalizing events were seen, but it is premature to attribute these to signal. In any case, XENON100 expects to place a limit on the order of  $\sigma_{\text{SI}}^{\chi p} \approx \text{few} \times 10^{-9}$  pb by early 2010. Thus, we will consider SI cross sections greater than  $5 \times 10^{-9}$  pb as potentially probeable in the short-term, and hence “large.”

There are two ways the SD cross sections are constrained. The first is via DD experiments. The current best bound on the SD DM-proton interaction comes from the KIMS experiment [152],  $\sigma_{\text{SD}}^{\chi p} < 1.6 \times 10^{-1}$  pb for  $m_\chi = 70$  GeV; the best bound on the SD DM-neutron interaction coming from the XENON experiment,  $\sigma_{\text{SD}}^{\chi n} < 6 \times 10^{-3}$  pb for  $m_\chi = 20$  GeV, with the strongest bounds for masses of  $\mathcal{O}(10)$  GeV coming from PICASSO [22]. There are also bounds from DM capture in the sun, assuming (as is the case in the MSSM) that the DM has annihilation products which give rise to relatively hard neutrinos. Assuming annihilation of the DM to  $W^\pm$  bosons is appreciable (as is appropriate for much of the parameter space considered here, see Sec. 5.3), IceCube [3] places very strong bounds for masses above 250 GeV with the strongest bounds coming at 250 GeV,  $\sigma_{\text{SD}}^{\chi p} < 3 \times 10^{-4}$  pb. At present, no limits exist from IceCube below this mass. For smaller masses, the best limits of this type come from SuperK [86],  $\sigma_{\text{SD}}^{\chi p} < 10^{-2}$  pb above  $m_\chi > 20$  GeV.

Perhaps within the next two years [155], the COUPP [49] and PICASSO [34] experiments will take data with a projected sensitivity to SD scattering of  $\sigma_{\text{SD}}^{\chi p} \approx 10^{-4}$  pb. They

will also have sensitivity down to much lower masses than the neutrino experiments. The XENON data will probe  $\sigma_{\text{SD}}^{\chi p} \approx 4 \times 10^{-3}$  pb for a 30 GeV WIMP. A 1 ton COUPP-like proposed experiment [56], might ultimately probe values as low as  $10^{-7}$  pb. The DeepCore extension to the IceCube detector should be able to extend down to the  $10^{-5}$  pb level with 5 years of data [196]. Bounds from neutrino experiments can be avoided if particular final states dominate WIMP annihilation, *e.g.* 1<sup>st</sup> generation quarks, though this does not happen in the MSSM. We consider SD cross sections greater than  $10^{-4}$  pb as potentially achievable in the short-term, and hence “large.”

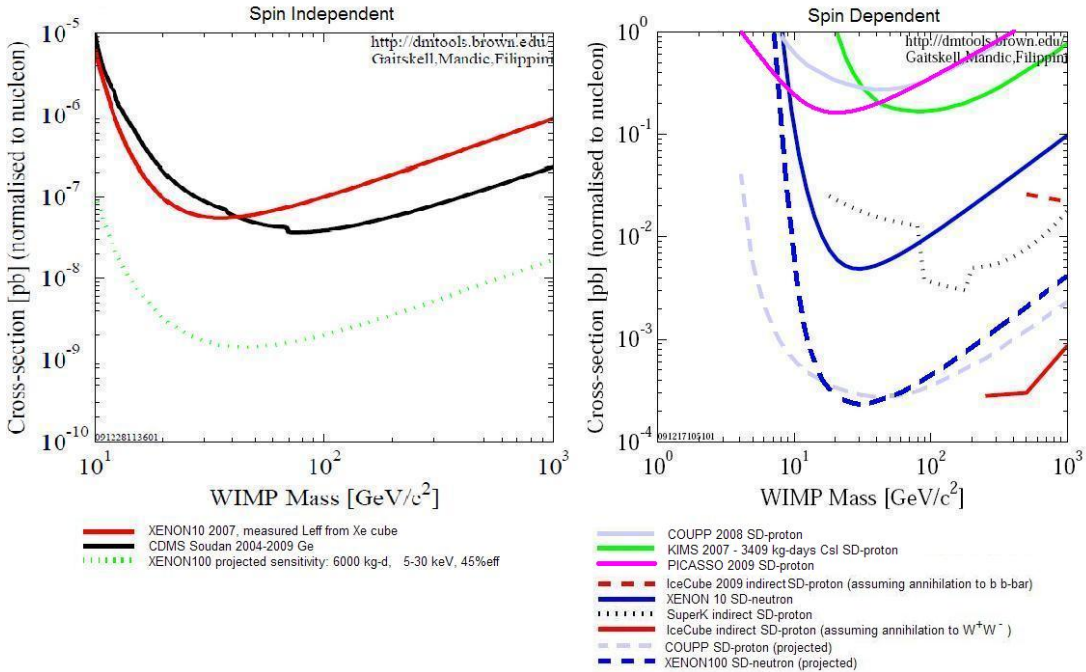


Figure 5.1: Current bounds on SI (left) and SD (right) DM-nucleon cross sections. The COUPP and XENON100 projected SD bounds are only estimates – we have scaled the current exclusion curve of COUPP by a factor of  $10^{-3}$  [154] and the current SD exclusion curve of XENON10 by the factor which scales the XENON10 SI limit to the XENON100 SI limit.

### 5.1.1 Spin Independent

The operator responsible for SI DM-nucleus interactions is

$$(V.4) \quad \mathcal{O}_q^{\text{SI}} = c_q (\bar{\chi} \chi) (\bar{q} q),$$

where  $\chi$  is the DM and  $q$  is a quark. Taking the expectation value of this operator between two nucleon states ( $N = p$  (proton) or  $n$  (neutron)) determines the effective interaction of the DM with a nucleon,

$$(V.5) \quad \langle N | m_q \bar{q} q | N \rangle = m_N f_{Tq}^{(N)},$$

where the nuclear matrix element  $f_{Tq}^{(N)}$  is determined in chiral perturbation theory from the pion nucleon-scattering sigma term. The coefficient of the effective DM-nucleon interaction,  $f_N(\bar{\chi} \chi)(\bar{N} N)$ , is given by

$$(V.6) \quad \frac{f_N}{m_N} = \sum_{q=u,d,s} f_{Tq}^{(N)} \frac{1}{m_q} c_q + \frac{2}{27} f_{TG}^{(N)} \sum_{q=c,b,t} \frac{1}{m_q} c_q^{(h)},$$

where  $f_{TG}^{(N)} = 1 - \sum_{q=u,d,s} f_{Tq}^{(N)}$  and the  $h$  on  $c_q^{(h)}$  refers to Higgs boson exchange [183].

The nucleon-Higgs interaction is coherent over the nucleus [112] resulting in the well known  $A^2$  enhancement for SI cross sections. To compare between experiments using different nuclei, the elastic scattering cross section is normalized to a per nucleon value [115]:

$$(V.7) \quad \sigma_{\text{SI}}(\chi N \rightarrow \chi N) = \frac{4}{\pi} m_r^2 \frac{1}{A^2} (Z f_p + (A - Z) f_n)^2,$$

where  $m_r$  is the reduced mass between the DM and a nucleon.

We use the DarkSUSY package for numerical analysis [119], so for analytic estimates we will use the same values for the nuclear matrix elements, namely

$$\begin{aligned} f_{Tu}^{(p)} &= 0.023 & f_{Td}^{(p)} &= 0.034 & f_{Ts}^{(p)} &= 0.14 & f_{TG}^{(p)} &= 0.803 \\ f_{Tu}^{(n)} &= 0.019 & f_{Td}^{(n)} &= 0.041 & f_{Ts}^{(n)} &= 0.14 & f_{TG}^{(n)} &= 0.800. \end{aligned}$$

Since these values are derived from the pion nucleon scattering sigma term, their error bars are correlated.

If the Higgs boson,  $h$ , that mediates the interaction between the DM and the nucleon is SM-like, the coefficients  $c_q$  are given by

$$(V.8) \quad c_q = y_q y_\chi \frac{1}{m_h^2},$$

where  $y_q$  ( $y_\chi$ ) is the Yukawa coupling for the quark (DM) and  $m_h$  is the Higgs mass. The per nucleon cross section is then

$$(V.9) \quad \sigma_{\text{SI}}(\chi N \rightarrow \chi N) \approx 5 \times 10^{-8} \text{ pb} \left( \frac{y_\chi}{0.1} \right)^2 \left( \frac{115 \text{ GeV}}{m_h} \right)^4 \quad (\text{SI typical}).$$

Estimates based on recent lattice simulations seem to favor smaller values for the nuclear matrix elements [118]. If these lattice results are correct, the dominant contribution to the SI scattering cross section would be due to the heavy quark content of the nucleon (since  $f_{TG}^{(N)} \rightarrow 1$  in the limit of small  $f_q^{(N)}$ ) and the coefficient in Eq. (V.9) would be replaced by  $2 \times 10^{-8}$  pb. In cases where  $c_d \gg c_u$ , which can occur in models with multiple Higgs bosons such as the MSSM, then uncertainties in the  $f_{Tq}^{(N)}$  can lead to as much as an order of magnitude variation in  $\sigma_{\text{SI}}(\chi N \rightarrow \chi N)$  [98].

### 5.1.2 Spin Dependent

The operator responsible for SD DM-nucleus interactions is

$$(V.10) \quad \mathcal{O}_q^{\text{SD}} = d_q (\bar{\chi} \gamma^\mu \gamma^5 \chi) (\bar{q} \gamma_\mu \gamma^5 q).$$

Taking the expectation value of this operator between two nucleon states allows us to find the effective SD interaction of the DM with a nucleon ( $N = p$  (proton) or  $n$  (neutron)),

$$(V.11) \quad \langle N | \bar{q} \gamma_\mu \gamma^5 q | N \rangle = 2 s_\mu^{(N)} \Delta q^{(N)},$$

where  $s_\mu^{(N)}$  is the spin of the nucleon and the  $\Delta q^{(N)}$  are extracted from polarized deep elastic scattering. The coefficient of the effective DM-nucleon interaction,  $2 a_N (\bar{\chi} \gamma^\mu \gamma^5 \chi) (\bar{N} s_\mu^{(N)} N)$ ,

is given by

$$(V.12) \quad a_N = \sum_{q=u,d,s} d_q \Delta q^{(N)}.$$

The elastic scattering cross section quoted by the experiments is between the DM and a nucleon which is given by

$$(V.13) \quad \sigma_{\text{SD}}(\chi N \rightarrow \chi N) = \frac{6}{\pi} m_r^2 a_N^2,$$

where  $m_r$  is the reduced mass between the DM and a nucleon.

Again we follow DarkSUSY and use the following values for the SD calculations,

$$(V.14) \quad \begin{aligned} \Delta_u^{(p)} &= 0.77 & \Delta_d^{(p)} &= -0.40 & \Delta_s^{(p)} &= -0.12 \\ \Delta_u^{(n)} &= -0.40 & \Delta_d^{(n)} &= 0.77 & \Delta_s^{(n)} &= -0.12. \end{aligned}$$

The prediction for SD scattering is somewhat more robust to variation in the hadronic matrix elements than the SI case: the uncertainties in these values can lead to  $\mathcal{O}(30\%)$  variation in the SD cross section [98].

If the SD interaction is mediated by the  $Z^0$  boson, then the coefficients  $d_q$  are given by

$$(V.15) \quad d_q = \frac{g^2}{2c_w^2} T_3^q \left( \frac{Q_{Z\text{-DM}}}{2} \right) \frac{1}{m_Z^2},$$

where  $Q_{Z\text{-DM}}$  parametrizes the coupling of the DM to the  $Z^0$  and  $c_w \equiv \cos \theta_w$ . For concreteness, (and since it is relevant for calculations of solar capture) when we quote values for SD scattering we will focus on the cross section off of protons. For SD scattering mediated by the  $Z^0$ , the neutron scattering is  $\mathcal{O}(20\%)$  smaller. The SD cross section is

$$(V.16) \quad \sigma_{\text{SD}}(\chi p \rightarrow \chi p) \approx 4 \times 10^{-4} \text{ pb} \left( \frac{Q_{Z\text{-DM}}}{0.1} \right)^2 \quad (\text{SD typical}).$$

In the next section, we discuss the form that  $Q_{Z\text{-DM}}$  takes in the MSSM.



## 5.2 Direct Detection of Neutralino dark matter

The best DM candidate in the MSSM is the lightest neutralino, which is an admixture of Bino ( $\tilde{B}$ ), Wino ( $\tilde{W}$ ), and the up and down-type Higgsinos ( $\tilde{H}_u$  and  $\tilde{H}_d$ ). The stability of the lightest superpartner (LSP) is guaranteed by  $R$ -parity, which is introduced to avoid proton decay. The neutralino mass matrix is given by

$$\mathcal{M} = \begin{pmatrix} M_1 & 0 & -m_Z s_w c_\beta & m_Z s_w s_\beta \\ 0 & M_2 & m_Z c_w c_\beta & -m_Z c_w s_\beta \\ -m_Z s_w c_\beta & m_Z c_w c_\beta & 0 & -\mu \\ m_Z s_w s_\beta & -m_Z c_w s_\beta & -\mu & 0 \end{pmatrix},$$

where  $M_1$  is the Bino mass,  $M_2$  is the Wino mass,  $\mu$  is the Supersymmetric (SUSY) Higgs boson mass parameter,  $m_Z$  is the  $Z^0$  mass,  $\beta = \arctan(v_u/v_d)$ ,  $v_{u,d}$  are the up and down-type Higgs boson vevs,  $s_w \equiv \sin \theta_w$ ,  $c_w \equiv \cos \theta_w$ ,  $s_\beta \equiv \sin \beta$ , and  $c_\beta \equiv \cos \beta$ .

The composition of the lightest neutralino, which we denote  $\chi$ , is specified by

$$(V.17) \quad \chi \equiv Z_B \tilde{B} + Z_W \tilde{W} + Z_{H_d} \tilde{H}_d + Z_{H_u} \tilde{H}_u.$$

If squarks are heavy, the only potentially sizable contributions to SI DD are from both CP-even Higgs bosons,  $h$  and  $H$ , where  $m_h < m_H$ . We comment on the typically subdominant squark exchange contributions in Appendix B.1. The Higgs boson exchange contributions are [32, 97],

$$(V.18) \quad \frac{c_u}{m_u} = -\frac{g^2(Z_W - t_w Z_B)}{4 m_W s_\beta} \times \left[ (Z_{H_d} s_\alpha c_\alpha + Z_{H_u} c_\alpha^2) \frac{1}{m_h^2} + (-Z_{H_d} s_\alpha c_\alpha + Z_{H_u} s_\alpha^2) \frac{1}{m_H^2} \right]$$

$$(V.19) \quad \frac{c_d}{m_d} = \frac{g^2(Z_W - t_w Z_B)}{4 m_W c_\beta} \times \left[ (Z_{H_u} s_\alpha c_\alpha + Z_{H_d} s_\alpha^2) \frac{1}{m_h^2} + (-Z_{H_u} s_\alpha c_\alpha + Z_{H_d} c_\alpha^2) \frac{1}{m_H^2} \right],$$

where  $c_{u,d}$  are the SI operator coefficients given in Eq. (V.4),  $g$  is the  $SU(2)$  gauge coupling,  $m_W$  is the  $W^\pm$  mass,  $t_w \equiv \tan \theta_w$ ,  $\alpha$  is the Higgs mixing angle,  $c_\alpha \equiv \cos \alpha$  and  $s_\alpha \equiv \sin \alpha$ .

In the decoupling ( $m_H \rightarrow \infty$  and  $\alpha \rightarrow \pi/2 + \beta$ ) and large  $t_\beta$  limits, these expressions simplify:

$$(V.20) \quad \frac{c_u}{m_u} = \frac{-g^2}{4m_W} (Z_W - t_w Z_B) \frac{s_\beta}{m_h^2} Z_{H_u},$$

$$(V.21) \quad \frac{c_d}{m_d} = \frac{c_u}{m_u} \left( 1 - \frac{t_\beta}{s_\beta} \frac{m_h^2}{m_H^2} \frac{Z_{H_d}}{Z_{H_u}} \right),$$

where we have only kept the  $t_\beta$  enhanced contribution from  $H$ . We will use these expressions below in Sec. 5.5 when analyzing the allowed suppression of the SI cross section.

The lack of an observation of a Higgs boson at LEP makes it likely that we live in at least a moderate  $t_\beta$  regime (so that the tree-level contribution to the Higgs boson mass  $m_h = m_Z \cos 2\beta$  is maximized), and constraints on the mass of the charged Higgs from flavor experiments point to the decoupling limit. Therefore, Eqs. (V.20) and (V.21) are particularly useful for estimating the expected size of scattering. In Sec. 5.3 we will argue for the typical size of the various neutralino mixing angles which lead to SI cross sections of the order,

$$(V.22) \quad \sigma_{\text{SI}}^{\text{MSSM}}(\chi N \rightarrow \chi N) \approx 5 \times 10^{-9} \text{ pb} \left( \frac{115 \text{ GeV}}{m_h} \right)^4 \left( \frac{(Z_W - t_w Z_B) Z_{H_u}}{0.1} \right)^2 \quad (\text{MSSM: SI typical}),$$

where we have used Eqs. (V.20) and (V.21) and taken  $m_H \rightarrow \infty$ .

In the heavy squark limit, contributions to SD DD come from  $Z^0$  exchange. Since the Bino and Wino are both  $SU(2)$  singlets, they do not couple to the  $Z^0$ . Therefore, SD is controlled by the Higgsino content of the WIMP. The  $Z^0$  exchange contribution takes the form:

$$(V.23) \quad d_q = -\frac{g^2}{4m_Z^2 c_w^2} (|Z_{H_d}|^2 - |Z_{H_u}|^2) T_3^q.$$

A non-zero Higgsino component (so that  $Z_{H_{u,d}} \neq 0$ ) is insufficient to ensure a non-zero SD coupling. If  $M_1, M_2 \rightarrow \infty$ , so that a pure Higgsino is recovered,  $|Z_{H_u}| = |Z_{H_d}| = 1/\sqrt{2}$ ,

and the SD coupling vanishes. Instead, the Higgsino forms a Dirac state, and the large vector scattering of the Dirac neutrino is recovered. Hence, mixing with  $\tilde{B}$  and/or  $\tilde{W}$  (so that  $|Z_{H_u}| \neq |Z_{H_d}|$ ) is required in order for the  $d_q$ 's to be non-zero. This requirement also implies a non-zero SI cross section, giving the correlation demonstrated below.

The typical cross section for SD DD in the MSSM (again see Sec. 5.3) is given by

$$(V.24) \quad \sigma_{\text{SD}}^{\text{MSSM}}(\chi p \rightarrow \chi p) \approx 4 \times 10^{-4} \text{ pb} \left( \frac{|Z_{H_d}|^2 - |Z_{H_u}|^2}{0.1} \right)^2 \quad (\text{MSSM: SD typical}).$$

There are reasons to expect the squarks do not make a sizable contribution to the DD cross sections. In the MSSM, satisfying the LEP bound on the Higgs boson mass requires large radiative corrections from the stop loops. This implies that at least one stop must have a TeV scale mass. Renormalization group flow tends to make the third generation sparticles lighter than the partners for the first and second generations. Therefore, it is plausible that squark contributions to DD scattering are negligible since only the first and second generation squarks contribute (see Appendix B.1 for details about squark exchange). For concreteness, in all scans below we take the scalar superpartners to be  $\mathcal{O}(2 \text{ TeV})$ . This is also why Eqs. (V.22) and (V.24) are expected to be good approximations. For a study which focuses on the effects of light squarks, see [50].

### 5.3 The Argument for a Well-Tempered Neutralino

Arkani-Hamed, Delgado and Giudice [24] argued that when one takes the LEP limits on charginos and sleptons into account, a pure neutralino (*i.e.* composed of only one gaugino eigenstate, usually taken to be Bino) is no longer the “natural” MSSM DM candidate, at least when one imposes the requirement of a thermal cosmology. They claim that one should instead consider a mixed neutralino, which they have dubbed “well-tempered.” Since the relic density of mixed DM is set by annihilations to  $W^+ W^-$  (and  $t\bar{t}$  when kinematically allowed) there is a further condition that  $m_\chi > m_W$ . Hence, we will impose

this requirement when we refer to “thermal” DM in the analysis that follows. In what follows, we review their argument and then discuss some non-thermal options. Note that SI DD has previously been studied for well-tempered models [30, 130], but no dedicated SD study exists.

### 5.3.1 Thermal history

We begin by considering the thermal history of a nearly pure Bino. If one does not allow for co- [122, 94, 95] or resonant [122, 93, 176, 90, 169] annihilations, then Bino freeze-out is controlled by  $t$ -channel sfermion exchange. One can show [24] that in order to produce the observed DM relic density, the sfermion must be  $\lesssim 110$  GeV. Since the LEP limits on sfermions are  $\mathcal{O}(100$  GeV), there is only a small experimentally allowed window for thermal Bino DM.

Either co-annihilations (*e.g.* with the stau or stop) or resonant annihilation through the pseudo-scalar Higgs ( $A^0$ ) also allow dominantly Bino DM. However, both of these options involve numerical coincidences. In the first case the Boltzmann factor will exponentially suppress the density of the would-be co-annihilator unless  $\exp(-\Delta M/T_f)$  is  $\mathcal{O}(1)$ , where  $\Delta M = m_{\text{NLSP}} - m_\chi$ ,  $m_{\text{NLSP}}$  is the mass of the next-to-lightest superpartner, and  $T_f$  is the DM freeze-out temperature. Since  $T_f \approx m_\chi/20$ , this requires a mass degeneracy,  $\Delta M$ , of a few percent. To realize the second case requires a precise relationship between  $m_\chi$  and  $m_A$ . When  $m_\chi < m_W$ , the  $Z^0$  or  $h$  poles may be used to achieve the correct relic density, which requires a similar numerical conspiracy.

Located at the other extreme, far away from the pure Bino, is a pure Wino or a pure Higgsino. In these cases, the requirement of a thermal relic abundance fixes the mass to be  $\mathcal{O}(2.5$  TeV) and  $\mathcal{O}(1$  TeV) respectively. Thus, to realize either of these cases implies

$\mu \gtrsim \mathcal{O}(100 \text{ GeV})$ . Since, in the MSSM, the  $Z^0$  mass is given by

$$(V.25) \quad \frac{m_Z^2}{2} = -|\mu|^2 + \frac{m_{H_d}^2 - m_{H_u}^2 t_\beta^2}{t_\beta^2 - 1},$$

where  $m_{H_{u,d}}^2$  are the Higgs soft-mass squared parameters, this requires a substantial fine-tuning between  $\mu^2$  and  $m_{H_{u,d}}^2$  in order to reproduce the measured  $Z^0$  mass of 91 GeV. Therefore, the desire to alleviate fine-tuning in this expression leads to the requirement that  $\mu \sim \mathcal{O}(100 \text{ GeV})$ . This will also naively lead to well-tempering since the neutralino mixing is proportional to  $m_Z/\mu$ . Though the accuracy of the current measurement of the DM relic density (see Eq. (I.1)) requires a precisely determined neutralino composition, one can easily reproduce the DM abundance for any mass of  $\mathcal{O}(100 \text{ GeV})$ . The Bino/Higgsino mixed LSP as a good thermal WIMP was pointed out in studies of the focus point region on the MSSM [106, 105].

A Higgs boson mass above the LEP bound requires large radiative corrections from a stop squark. This implies that the scale for these particles,  $m_{\text{SUSY}}$ , should be around a TeV. These states yield additive corrections to  $m_{H_{u,d}}^2$ , proportional to  $m_{\text{SUSY}}^2$ . Hence, even in the case when  $\mu \sim \mathcal{O}(100 \text{ GeV})$ , there will naively be fine-tuning between these corrections and the bare value of  $m_{H_{u,d}}^2$  in order to reproduce  $m_Z$ . Solutions to this “little hierarchy problem” have been proposed within the MSSM (*e.g.* [144]) – we will ignore this type of fine-tuning in our arguments, focusing instead on the model independent tuning explicit in Eq. (V.25).

### 5.3.2 Non-thermal options

A thermal history is not the only way to achieve the correct DM relic abundance [166]. It has even been argued [6] that there is a “non-thermal WIMP miracle” when there exist TeV scale states which decay to the DM via Planck suppressed operators. For example, a heavy gravitino (or string-theory moduli fields) can live long enough to dominate the energy density of the universe. Then when these states decay, they will produce superpartners

which will decay down to the lightest neutralino, resulting in a neutralino relic density. This relaxes the relationship between the mass/composition and relic density of a neutralino.

A variety of other options have been proposed. Models where the energy density of the universe at the epoch of DM freeze-out was dominated by something other than radiation were studied in [136]. Alternately, if the DM interacts so feebly that it never achieves thermal equilibrium, one can achieve the correct value of the relic density via “freeze-in” production [125]. Since the total energy density of DM is close to that of the baryons, one can construct models where the DM relic density is set by an asymmetry which is determined by the baryon asymmetry [140]. In [116], it was shown that by varying the reheat temperature and allowing for non-thermal sources, any neutralino composition can result in the correct relic density. In [78], a low temperature phase transition in the early universe changes the DM properties after freeze-out. All of these options involve either non-trivial cosmological histories or other model building challenges. We will focus on the thermal – and hence well-tempered – case, with discussions of the deviations that arise when the thermal assumption is relaxed.

#### 5.4 Spin Dependent Cross Sections for Mixed Dark Matter

In the MSSM, the neutralino mass mixing can often be approximately understood in terms of a two state system: a Dirac Higgsino mixing with either a Bino or a Wino. Thus, to understand the physics of SD scattering via  $Z^0$  exchange, it is useful to consider the simple “Singlet-Doublet Model” (SDM) for DM, where the singlet has the same quantum numbers as either a Bino or a Wino, and the doublets have the same quantum numbers as the Higgsinos:

$$(V.26) \quad \mathcal{L}_{\text{SDM}} \ni \mu_D D \bar{D} + \lambda \mathbf{h} S D + \lambda' \mathbf{h}^* S \bar{D} + \frac{\mu_S}{2} S^2.$$

Here  $D$  and  $\bar{D}$  are a vector-like pair of  $SU(2)$  doublet fermions,  $S$  is an  $SU(2)$  singlet,  $\mathbf{h}$  is the SM Higgs doublet,  $\lambda$  ( $\lambda'$ ) is the Yukawa coupling which leads to the mixing between the  $D$  ( $\bar{D}$ ) and  $S$ ,  $\mu_D$  is the vector-like mass for the  $D$  and  $\bar{D}$ , and  $\mu_S$  is the Majorana mass for  $S$ . For the purposes of SD scattering it is sufficient to replace  $\mathbf{h}$  by its vev,  $\langle \mathbf{h} \rangle \equiv v = 174$  GeV. The exchange of the uneaten component of  $\mathbf{h}$  leads to SI DD.

In the case where  $S$  plays the role of the Bino, the values of  $\lambda$  and  $\lambda'$  are constrained by the supersymmetric relations to be  $\lambda v = -m_Z s_w c_\beta$  and  $\lambda' v = -m_Z s_w s_\beta$ , while in the case where  $S$  is the Wino, the values of  $\lambda$  and  $\lambda'$  are constrained by the supersymmetric relations to be  $\lambda v = m_Z c_w c_\beta$  and  $\lambda' v = m_Z c_w s_\beta$ .

We now use this model to discuss the coupling of the  $Z^0$  boson to the DM in the MSSM. In Appendix B.2 we discuss the diagonalization of the  $3 \times 3$  mixing matrix of the SDM. With appropriate substitutions, these expressions correspond to either Bino/Higgsino ( $M_2 \rightarrow \infty$ ) and Wino/Higgsino ( $M_1 \rightarrow \infty$ ) neutralinos. In these limits we can write down approximate expressions for the effective coupling of the DM to the  $Z^0$ . When there are no degeneracies between parameters in the neutralino mass matrix and  $m_Z$  may be treated as a perturbation, we have (see [24] and Appendix B.2):

$$(V.27) \quad |Z_{H_d}|^2 - |Z_{H_u}|^2 = \begin{cases} \frac{c_{2\beta} s_w^2 m_Z^2}{\mu^2 - M_1^2} & \text{for } |M_1|, |\mu|, |\mu| - |M_1| > m_Z, M_2 \rightarrow \infty \\ \frac{c_{2\beta} c_w^2 m_Z^2}{\mu^2 - M_2^2} & \text{for } |M_2|, |\mu|, |\mu| - |M_2| > m_Z, M_1 \rightarrow \infty. \end{cases}$$

The largest values of  $|Z_{H_d}|^2 - |Z_{H_u}|^2$  do not occur in this limit. Instead, they are found when two parameters of the neutralino mass matrix are degenerate. The reason is simple: a degeneracy allows a large gaugino–Higgsino mixing in spite of the relative smallness of the off-diagonal entries of the neutralino mass matrix (proportional to  $m_Z$ ). It should be said that there is no particular reason to believe that a precise degeneracy should occur, since  $\mu$  and the gaugino masses are SUSY preserving and breaking respectively. However,

since this case maximizes the possible signal at SD experiments, it is worth noting. In the presence of these degeneracies, we have (see Appendix B.2):

$$(V.28) \quad |Z_{H_d}|^2 - |Z_{H_u}|^2 = \begin{cases} \frac{(s_\beta - c_\beta) s_w m_Z}{2\sqrt{2}|\mu|} + \frac{(s_\beta^2 - c_\beta^2) s_w^2 m_Z^2}{8\mu^2} & \text{for } |M_1| = |\mu| > m_Z, M_2 \rightarrow \infty \\ \frac{(s_\beta - c_\beta) c_w m_Z}{2\sqrt{2}|\mu|} + \frac{(s_\beta^2 - c_\beta^2) c_w^2 m_Z^2}{8\mu^2} & \text{for } |M_2| = |\mu| > m_Z, M_1 \rightarrow \infty. \end{cases}$$

Perturbing away from the limit of exact degeneracy gives corrections to these expressions of  $\mathcal{O}((M_i - \mu)/\mu)$ . Note that DM with a mixed Wino/Higgsino has a SD DD rate enhanced relative to a Bino/Higgsino admixture by the appropriate power of  $c_w/s_w = 1.8$ .

What is the largest obtainable SD cross section in the MSSM? A numerical scan yields

$$(V.29) \quad |Z_{H_d}|^2 - |Z_{H_u}|^2 < 0.4 \Rightarrow$$

$$(V.30) \quad (\sigma_{\text{SD}}^{\text{SUSY}}) < 6 \times 10^{-3} \text{ pb} \quad (\text{General MSSM, Non - thermal DM}),$$

when the squarks are heavy. This upper bound is largely a consequence of the LEP bounds on the chargino masses which force the mixing  $\sim m_Z/\mu$  to be less than one. Eq. (V.29) provides a good analytic understanding of this number – it comes within approximately 10% of this value. The deviation is due to mixing effects that occur away from the large  $M_1$  limit.

In many models of SUSY breaking the relation  $M_1/\alpha_1 = M_2/\alpha_2 = M_3/\alpha_3$  holds. We refer to this condition as unified gaugino masses. Because this is equivalent to  $M_2 \approx 2M_1$  at the weak scale, the LSP is mostly Bino and Higgsino. In this case,

$$(V.31) \quad |Z_{H_d}|^2 - |Z_{H_u}|^2 < 0.32 \Rightarrow$$

$$(V.32) \quad (\sigma_{\text{SD}}^{\text{SUSY}}) < 4 \times 10^{-3} \text{ pb} \quad (\text{Unified Gaugino Masses, Non - thermal DM}).$$

Finally, for  $m_\chi > m_W$ , a thermal relic density within  $\pm 3\sigma$  of the WMAP measurement



implies an upper limit on the amount of Higgsino in the DM particle. Therefore,

$$(V.33) \quad |Z_{H_d}|^2 - |Z_{H_u}|^2 < 0.24 \Rightarrow$$

$$(V.34) \quad (\sigma_{\text{SD}}^{\text{SUSY}})_{\text{thermal}} < 2 \times 10^{-3} \text{ pb} \quad (\text{General MSSM, Thermal DM}).$$

This result holds for the case with unified gaugino masses as well. Note that Eqs. (V.30), (V.32), and (V.34) all occur for a DM mass of  $\mathcal{O}(80 \text{ GeV})$ .

To saturate the above bound (*i.e.* maximize  $\sigma_{\text{SD}}$  for thermal, well-tempered DM) requires a Bino/Higgsino mixture (recall that  $d_q$  vanishes for a pure Higgsino), with a negligible Wino contribution. The largest values of SD DD occur when the DM has the largest Bino/Higgsino mixing which happens for the lowest values of the DM mass. As the mass of the DM increases, a larger component of Higgsino or Wino is needed for the DM to efficiently annihilate down to the correct relic density, which in turn typically leads to a decrease in  $\sigma_{\text{SD}}$ .

As shown in Fig. 5.2, there is a tight correlation between the SD cross section and the DM mass, in the decoupling limit when there is gaugino mass unification and a thermal relic abundance.

For low masses, the neutralino is well-tempered for low masses and as  $m_\chi \rightarrow \mathcal{O}(1 \text{ TeV})$  the neutralino approaches a pure Higgsino. Examining Fig. 5.2, except for when the annihilation channel  $\chi\chi \rightarrow t\bar{t}$  opens,  $\sigma_{\text{SD}}$  is a smooth, monotonically decreasing curve. An experiment sensitive to cross sections of  $\mathcal{O}(10^{-4} \text{ pb})$  will probe  $m_\chi \lesssim 200 \text{ GeV}$ . There is a spread in the points in this figure from the liberal range taken on the relic density constraint. For masses approaching  $\mathcal{O}(1 \text{ TeV})$ , there is additional extent from the variation in the Bino content of the neutralino and from contributions from squark exchange. For masses at 1 TeV,  $\sigma_{\text{SD}}$  goes from  $10^{-6} \text{ pb} \rightarrow 0$  for  $M_1$  from  $1300 \text{ GeV} \rightarrow \infty$ . Note that the projected reach of a 1 ton version of COUPP is  $\mathcal{O}(10^{-6}) \text{ pb}$  for  $m_\chi = 1 \text{ TeV}$  [56], *which would probe the entire range of SD cross sections for neutralinos excepting a nearly pure*

TeV *Higgsino*.

Note that the imposition of the unified gaugino mass condition essentially imposes the requirement that there is a tiny Wino content in the LSP. The hatched region in Fig. 5.2 is filled in when non-unified gaugino masses are allowed. In this case, a thermal relic DM candidate can be obtained for a Bino tempered with Wino if  $M_1 \approx M_2$ , which implies that the SD cross section decreases, effectively filling in the region beneath the curve in Fig. 5.2. Note that when  $\sigma_{\text{SD}} \sim \mathcal{O}(10^{-6} \text{ pb})$ , there is additional model dependence since the squark contribution becomes important (see Appendix B.1).

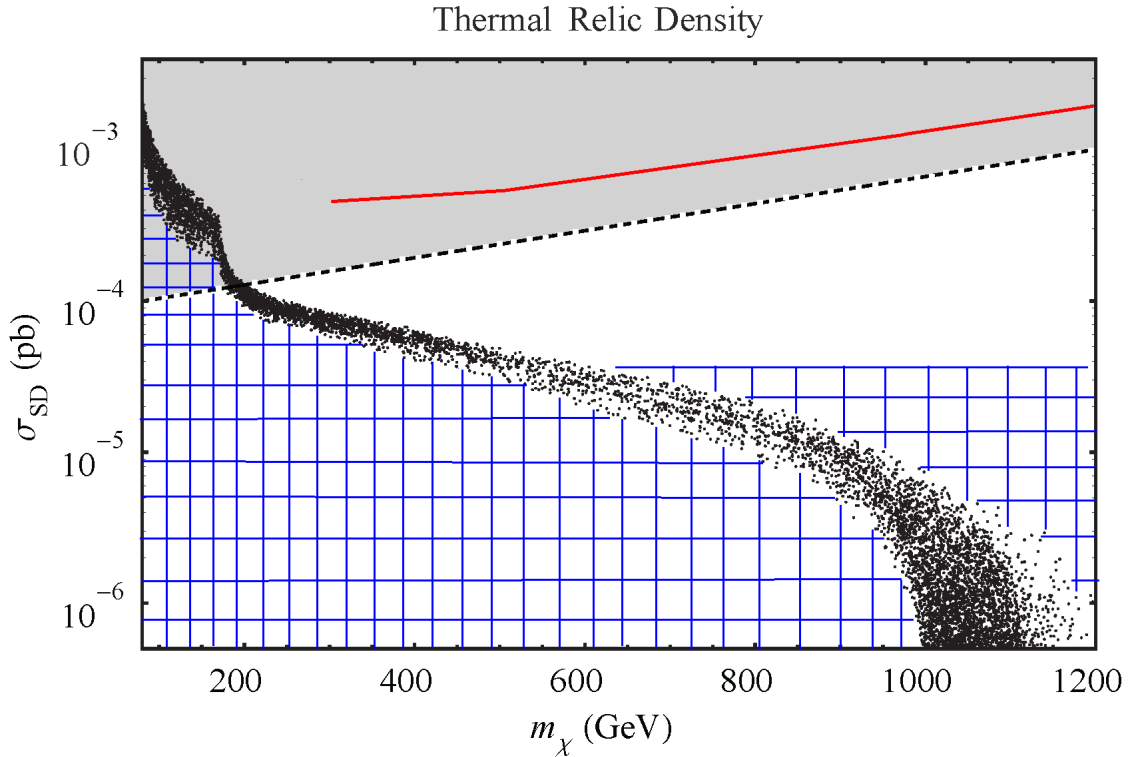


Figure 5.2:  $\sigma_{\text{SD}}^p$ , as a function of  $m_\chi$  for points satisfying the relic density constraint. We have imposed gaugino mass unification and taken the decoupling limit. The shaded region above the dotted line corresponds to “large” SD and will be probed in the near term. The solid red line is the current bound from IceCube, assuming annihilation to  $W^+ W^-$ . The blue hatched region is filled in if the assumption of gaugino mass unification is relaxed. The sfermion masses are taken to be  $\mathcal{O}(2 \text{ TeV})$ .

Finally, we note that there is a region of well-mixed Higgsino–Wino near 2 TeV with a

thermal abundance (where  $M_2 \approx \mu$ ). In this case, the second line of Eq. (V.29) applies, and we find an approximate SD cross section of  $6 \times 10^{-6}$  pb, perhaps able to be probed at a future 1 ton COUPP-like experiment. These are the neutralinos which account for the hatched region above the points in Fig. 5.2.

Not only is the SDM a simplified system useful for understanding the physics of SD scattering in the MSSM, it is potentially of independent interest. The DM may be unrelated to the solution to the hierarchy and simply given by the Lagrangian of Eq. (V.26) [26, 159]. Then the DD story is essentially unchanged except there is greater parametric freedom.

For example, the Higgs boson mass is no longer fixed by SUSY. Then the only constraint is  $m_h \lesssim \mathcal{O}(\text{TeV})$  to unitarize  $W_L^\pm$  scattering. For  $m_h \sim \text{TeV}$ , the SI DD cross section is at most  $10^{-12}$  pb which would not lead to a signal in the next round of SI experiments. While such a large Higgs boson mass is in tension with precision electroweak measurements, it could be reconciled with a contribution to the  $T$  parameter [171] in a way that factorizes from the DM phenomenology.

If one allows for a non-thermal history, the freedom of the SDM allows off-diagonal parameters of the mixing matrix that give  $|Z_{H_d}|^2 - |Z_{H_u}|^2 = 1$ . This maximizes the SD DD signal from  $Z^0$  exchange ( $\sigma_{\text{SD}}^{\text{SDM}} \approx 4 \times 10^{-2}$  pb). Thus, the SDM with a non-thermal history predicts scattering anywhere up to (or even above) the current bounds. Requiring a thermal history limits the amount of doublet allowed in  $m_\chi$ , decreasing  $\sigma_{\text{SD}}^{\text{SDM}}$ . For if a very large doublet component is chosen (in an attempt to maximize the SD cross section), the requirement of reproducing the relic density requires  $\mu_S$  to be  $\mathcal{O}(\text{TeV})$ .

## 5.5 Spin Independent versus Spin Dependent

When a Majorana fermion couples to the  $Z^0$ , there is necessarily an interaction with a Higgs boson, which leads to SD and SI elastic scattering respectively. In the last section, we concentrated on the physics behind the size of the SD cross section. We now ask the

following questions: what is the expected correlation between the SI and SD signals? Is it possible to make one large while the other nearly vanishes?

Since  $m_h$  and  $m_Z$  are known in the MSSM, there exists a correlation between the SI and SD signals, at least in the limit of heavy sfermions and Higgs boson decoupling. For this region of MSSM parameter space, the SI and SD DD cross sections are given by Eqs. (V.22) and (V.24), where only mixing factors and the Higgs boson mass are left unspecified. The light Higgs boson mass is constrained to lie in the tight range  $114 \text{ GeV} < m_h < 130 \text{ GeV}$ , where the lower bound is due to the LEP limit and the upper bound comes from considerations of fine-tuning. For the SplitSUSY model – where the decoupling and heavy sfermion limits certainly apply – the Higgs boson mass is allowed to be larger:  $m_h < 160 \text{ GeV}$ .

In Figs. 5.3, 5.4 and 5.5, we have plotted the  $\max(\sigma_{\text{SI}}^p, \sigma_{\text{SI}}^n)$  vs.  $\sigma_{\text{SD}}^p$  for neutralino scattering with various restrictions. Note that these plots are made from independent scans and we have taken the scalar superpartners to be  $\mathcal{O}(2 \text{ TeV})$ .

As discussed in Section 5.1, we define “large” cross sections to be  $\sigma_{\text{SI}}^{\text{large}} > 5 \times 10^{-9} \text{ pb}$  and  $\sigma_{\text{SD}}^{\text{large}} > 10^{-4} \text{ pb}$ , motivated by the projected near term range of current DD experiments. Hence, the shaded region delineates the (very approximate) reach of the next generation of SI and SD experiments. Note that this neglects the dependence of the sensitivity on the mass of the DM. The maximum for  $\sigma_{\text{SD}}$  in Fig. 5.3 is given by Eq. (V.30) and for Figs. 5.4 and 5.5 is given by Eq. (V.34).

In Fig. 5.3 we show points for both thermal and non-thermal neutralinos. This is our most general framework, and in this case it is clear that the correlation between the relevant mixing angles (and hence cross sections) is weak. By only allowing points which have a thermal relic density within  $\pm 3\sigma$  of the WMAP measurement (see Figs. 5.4 and 5.5), the correlation progressively improves. We will discuss this in detail in what follows.

We will pay special attention to the  $m_H \rightarrow \infty$  limit. In any theory with multiple Higgs bosons, a small SI signal can occur when the diagrams from Higgs boson exchange cancel against one another. Two important points should be made. First, this cancellation is often incomplete and typically cannot be realized for scattering off of both protons and neutrons simultaneously. Second, such a cancellation is a conspiracy – it requires unexpected relationships between parameters in the Higgs sector and nuclear matrix elements. The finer the cancellation, the greater the conspiracy (for further discussion of this cancellation, see Sec. 5.5.3). If one takes the decoupling limit for Fig. 5.3, so that SI DD is determined by  $h$  exchange alone, the maximum SI cross section is  $\sim 3 \times 10^{-8}$  pb. Note that even for  $m_A \sim \mathcal{O}(\text{TeV})$  there can be nontrivial contributions for  $t_\beta \sim \mathcal{O}(50)$  (see Eq. (V.21)).

There is a negative correlation between fine-tuning and the size of DD cross sections (see Eq. (V.25)) [160, 145]. To emphasize this point, in Figs. 5.3, 5.4 and 5.5 we have marked points with  $|\mu| < 500$  GeV by blue dots and points with  $|\mu| > 500$  GeV by red crosses. The apparent feature around  $\sigma_{\text{SI}} \approx 10^{-8}$  pb in Fig. 5.4 is due to the finite range of  $m_A$  taken in this scan ( $m_A < 1$  TeV) – the points above this gap have constructive contributions from  $h$  and  $H$  while the points below have destructive contributions. There are a few interesting features in Fig. 5.5. The gap which extends along the entire plotted range of SD cross sections is due to a slight cancellation between the various contributions from the light Higgs boson (see Eqs. (V.18) and (V.19)) which can occur at finite  $t_\beta$  ( $t_\beta < 50$  in this scan). The small number of points around  $\sigma_{\text{SD}} = 3 \times 10^{-4}$  pb is due to the opening of the top threshold (see Fig. 5.2). The behavior around  $\sigma_{\text{SD}} = 2 \times 10^{-5}$  pb is due to the cross over from dominantly Bino to dominantly Higgsino DM, which occurs around  $m_\chi = 500$  GeV.

### 5.5.1 Large SI and Large SD

To have non-zero SI and SD signals, a Bino-Higgsino, Wino-Higgsino or Bino-Wino-Higgsino mix is required. In fact, appreciable SI and large SD signals can be generated as

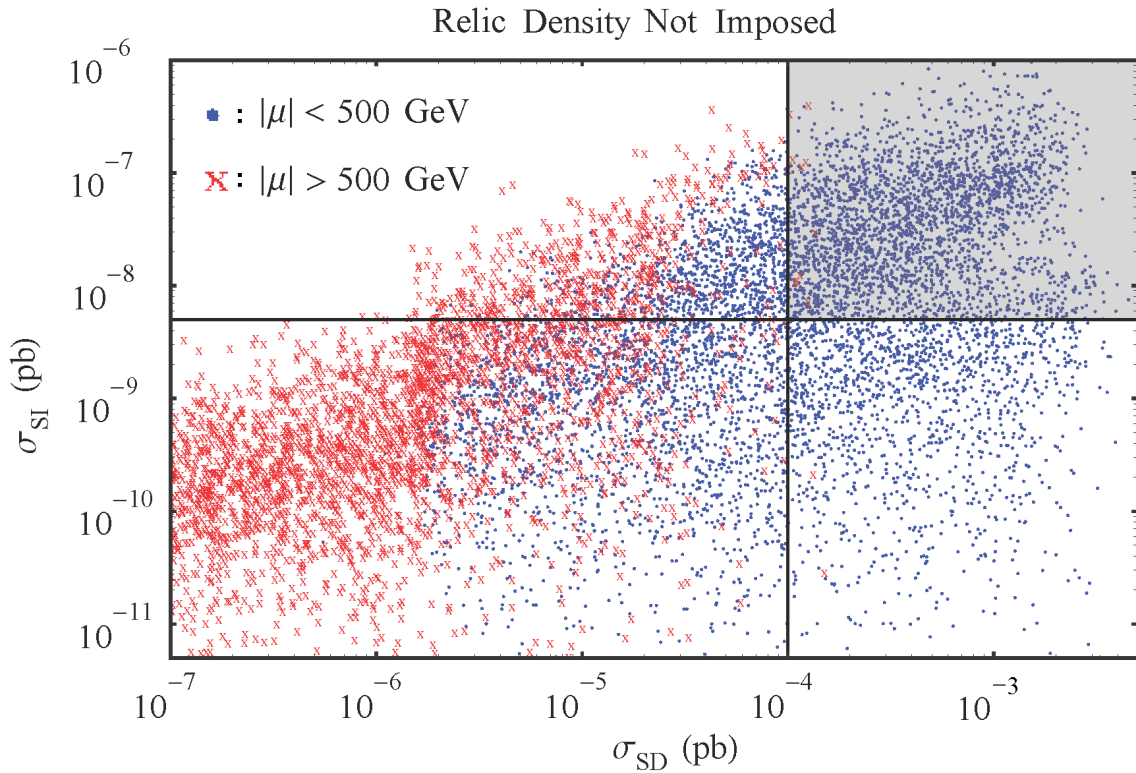


Figure 5.3: The  $\max(\sigma_{\text{SI}}^p, \sigma_{\text{SI}}^n)$  vs.  $\sigma_{\text{SD}}^p$  cross sections in pb for the MSSM. The dots (in blue) and crosses (in red) correspond to  $|\mu| < 500$  GeV and  $|\mu| > 500$  GeV respectively. The horizontal (vertical) line refers to the projected sensitivity for the next generation of SI (SD) experiments. We have shaded the near-term probeable region. Note that we are neglecting the dependence of this sensitivity on the neutralino mass. We have *not* imposed the thermal relic density constraint – all points are taken to have  $\rho_{\text{DM}} = 0.3 \text{ GeV}/\text{cm}^3$ , regardless of thermal abundance. All sfermions have masses of  $\mathcal{O}(2 \text{ TeV})$ . If one takes the decoupling limit, there is a maximum value for  $\sigma_{\text{SD}} = 3 \times 10^{-8}$  pb.

long as the Higgsino fraction is larger than  $\mathcal{O}(10\%)$ . Note that the  $|\mu| < 500$  GeV points, which correspond to less fine-tuning in  $m_Z$ , imply large SD signals. When the gaugino fraction is dominated by Wino rather than Bino, the relative size of  $g$  and  $g'$  gives a slight enhancement in the SI cross section. There can be further enhancement of the SI cross section if  $\text{sgn}(Z_B) \neq \text{sgn}(Z_W)$  (see Eq. (V.18)) which accounts for points with the largest SI values in Figs. 5.3 and 5.4. This cannot occur in models with unified gaugino masses, where  $M_2 \approx 2 M_1$ .

Large SI and SD signals occur as long as there is non-trivial gaugino content in the WIMP. Imposition of the thermal relic density constraint for  $m_\chi > m_W$ , ensures a minimum

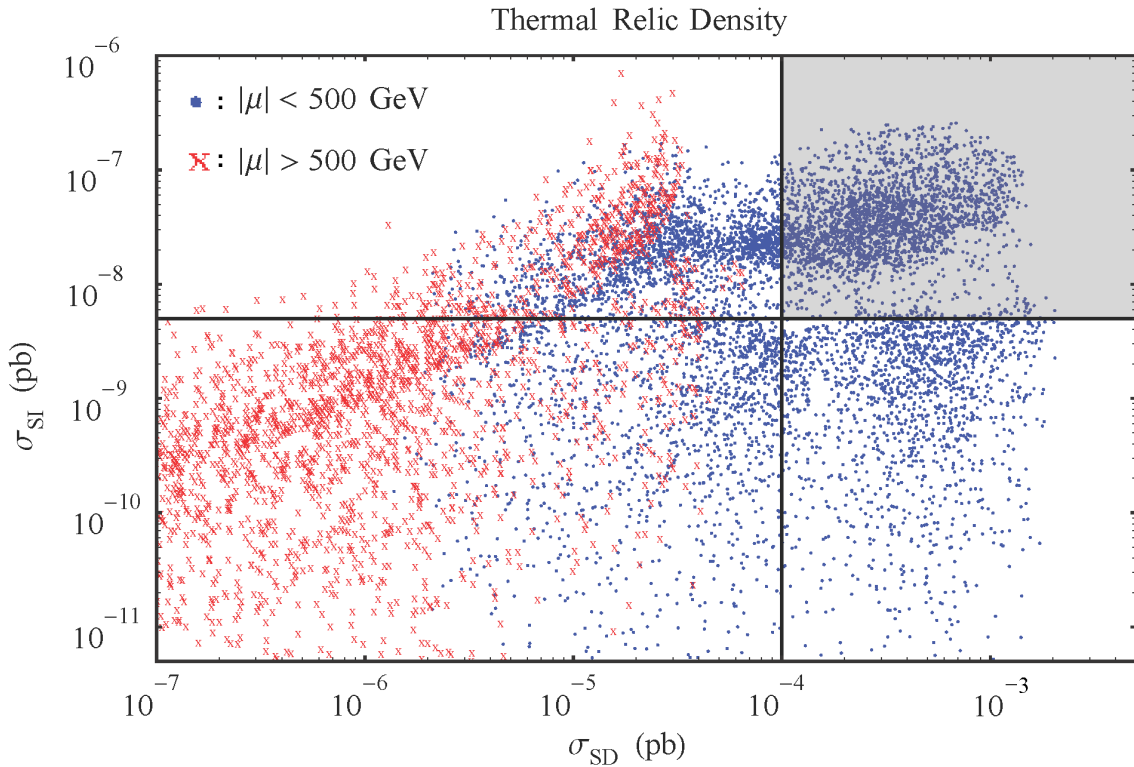


Figure 5.4: The  $\max(\sigma_{\text{SI}}^p, \sigma_{\text{SI}}^n)$  vs.  $\sigma_{\text{SD}}^p$  cross sections in pb for the MSSM. We have imposed that the thermal abundance of the neutralinos is within  $\pm 3\sigma$  of the WMAP measurement. The dots (in blue) and crosses (in red) correspond to  $|\mu| < 500$  GeV and  $|\mu| > 500$  GeV respectively. The horizontal (vertical) line refers to the projected sensitivity for the next generation of SI (SD) experiments. We have shaded the near-term probeable region. Note that we are neglecting the dependence of this sensitivity on the neutralino mass. All sfermions have masses of  $\mathcal{O}(2 \text{ TeV})$ .

required Bino component. If one imposes the large SI and SD conditions,  $|Z_B|^2 \lesssim 0.7$  and  $|Z_B|^2 \lesssim 0.85$  below and above the top threshold respectively. Note that the large SD requirement implies that  $m_\chi < 200 \text{ GeV}$  (see Fig. 5.2). Hence, the assumption of a thermal history is necessary to conclude that the neutralino is a Bino-Higgsino admixture, rather than Wino-Higgsino.

In the next three subsections we will attempt to elucidate the difficulties one encounters when trying to suppress SI and/or SD. This will allow us to argue that large SI and SD DD signals are the generic prediction for a well-tempered MSSM neutralino, since suppression of either SI or SD or both requires doing some gymnastics. While future data may force

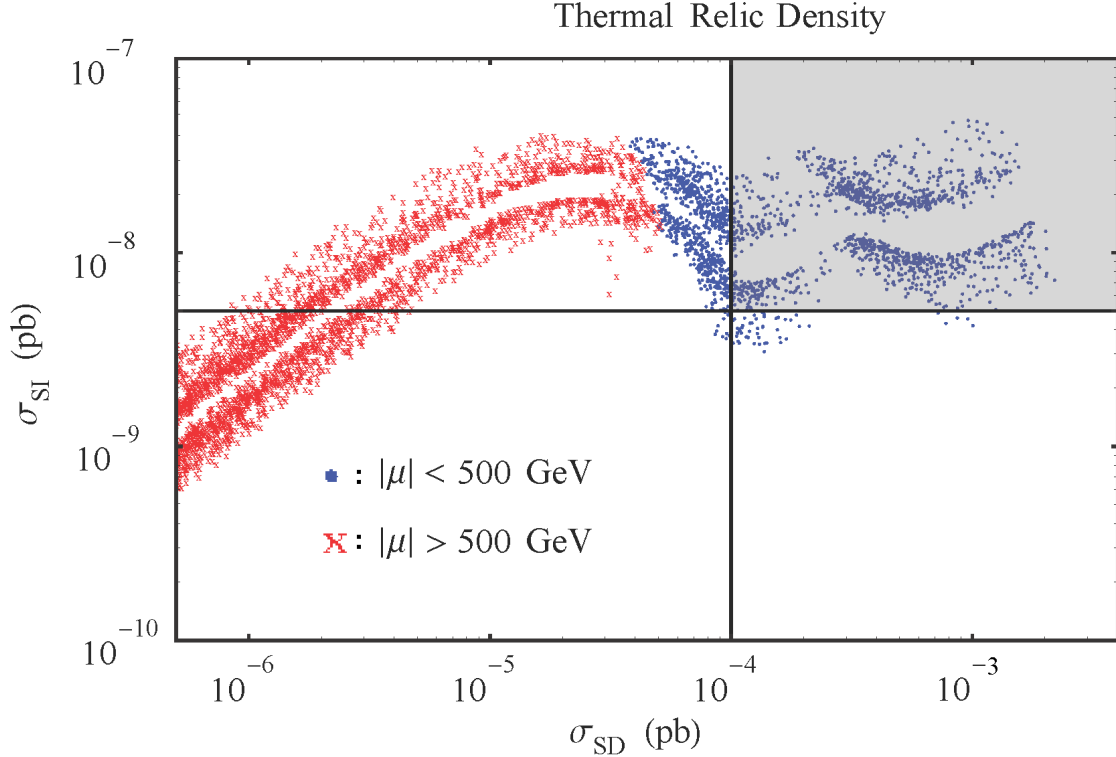


Figure 5.5: The  $\max(\sigma_{SI}^p, \sigma_{SI}^n)$  vs.  $\sigma_{SD}^p$  cross sections in pb for the MSSM with gaugino mass unification. We have imposed that the thermal abundance of the neutralinos is within  $\pm 3\sigma$  of the WMAP measurement. We have taken the decoupling limit ( $m_A = 4$  TeV). The dots (in blue) and crosses (in red) correspond to  $|\mu| < 500$  GeV and  $|\mu| > 500$  GeV respectively (see the text for a discussion). The horizontal (vertical) line refers to the projected sensitivity for the next generation of SI (SD) experiments. We have shaded the near-term probeable region. Note that we are neglecting the dependence of this sensitivity on the neutralino mass. All sfermions have masses of  $\mathcal{O}(2$  TeV).

these contortions upon us, we conjecture that if the DM is a well-tempered neutralino, it is likely to be discovered in the next generation of DD experiments.

### 5.5.2 Small SI and Small SD

There are two ways to suppress both SI and SD. The first is to make  $|Z_{H_u}| = |Z_{H_d}| = 0$ , which is equivalent to the  $\mu \rightarrow \infty$  limit. This limit leads to fine-tuning of the electroweak scale. To achieve the proper thermal relic abundance in this case requires a Bino-Wino mix. Note that the Bino and Wino only mix indirectly through the Higgsino. Therefore, two insertions of the mixing factor are required, and the resulting mixing is of size  $(m_Z/\mu)^2$ .



One can see the effects of this limit by inspecting the red crosses in Figs. 5.3, 5.4 and 5.5. The upper bound in Figs. 5.3 and 5.4 are from points which are either Bino/Higgsino or fully mixed states while the points with the smallest values for SI are due to either Wino/Bino neutralinos or the cancellations discussed in Sec. 5.5.4.

The second option is to take  $M_{1,2} \gg \mu$ . This will imply that  $Z_{B,W} = 0$ , thereby suppressing SI DD, and  $|Z_{H_u}| = |Z_{H_d}|$  so that SD DD is also zero. Reproducing the measured relic density then requires  $\mu \approx 1$  TeV. When one does impose the thermal relic density as a prior, Fig. 5.2 shows that for DM masses of  $\mathcal{O}(\text{TeV})$ , *i.e.* the region of dominantly Higgsino DM, the SD cross section ranges from  $\mathcal{O}(10^{-5} \text{ pb})$  to 0. Fig. 5.5 shows the corresponding SI cross sections for this range. The trend of SI and SD going to zero in this plot is due to the limit  $M_{1,2} \rightarrow \infty$ . Thermal dark matter in either of these two limits ( $\mu$  or  $M_{1,2} \rightarrow \infty$ ) will have a finely-tuned electroweak scale. Note that for either pure Wino or pure Higgsino DM there is a 1-loop diagram which leads to an SI DD cross section of  $\mathcal{O}(10^{-11} \text{ pb})$  or  $\mathcal{O}(10^{-12} \text{ pb})$  and an SD DD cross section of  $\mathcal{O}(10^{-9} \text{ pb})$  or  $\mathcal{O}(10^{-10} \text{ pb})$  for the Wino or Higgsino case respectively [128]. We neglect this tiny contribution in our numerical scans.

### 5.5.3 Large SI and Small SD

There are points which have large SI and SD with a nearly maximal gaugino fraction. If one relaxes the requirement of large SD, then the gaugino fraction can be pushed to nearly 100% while keeping the product  $Z_{B,W} Z_{H_{u,d}}$  approximately fixed, which in turn keeps the SI cross section constant. The relic density constraint can still be satisfied since both Winos and Higgsinos annihilate to  $W^\pm$  bosons with approximately the same rate.

There is another way to have small SD while allowing large SI. In the context of the SDM, one can take  $\lambda = \lambda'$ , *i.e.*  $t_\beta = 1$  in the MSSM. From the SDM mass matrix (see Appendix B.2), one can see that mixing between  $S$  and  $D_-$  will vanish. Since the SD

cross section is proportional to this mixing factor,  $Z_{D-}$ , it will be zero as well. This effect accounts for the empty region in Figs. 5.3 and 5.4 since we restricted  $t_\beta > 5$  in our numerical scans.

For  $\tan\beta \gtrsim 1.5$ , we find that for  $\sigma_{\text{SI}} \sim 5 \times 10^{-9}$  pb the smallest cross section for SD is  $\sigma_{\text{SD}} \sim 10^{-6}$  pb. If one allows  $\sigma_{\text{SI}} < 5 \times 10^{-9}$  pb, then as  $|Z_{H_{u,d}}| \rightarrow 0$ ,  $\sigma_{\text{SD}}/\sigma_{\text{SI}} \rightarrow |Z_{H_{u,d}}|^2 \rightarrow 0$ . Hence, SD falls off faster than SI. However, this is the  $\mu \rightarrow \infty$  limit which leads to fine-tuning as described above.

#### 5.5.4 Small SI and Large SD

Large SD requires a well-tempered neutralino, which naively also leads to large SI DD. In this section we will enumerate the various options one has for suppressing SI signals. We will argue that all options require fine-tuning or numerical coincidences<sup>1</sup>.

Here are the options for minimizing  $\sigma_{\text{SI}}$ :

1. One can make  $m_h$  and  $m_H$  heavy; however  $m_h \approx 115$  GeV in the MSSM in the absence of large fine-tunings. Even in SplitSUSY,  $m_h \lesssim 160$  GeV.
2. Since  $c_{u,d} \sim (Z_W - t_w Z_B)$ , *i.e.* the Higgs couples to the Zino, one could attempt to restrict the DM to only be a photino-Higgsino admixture. In Appendix B.3, we show that this is impossible when one restricts  $M_2$  by the LEP bound.
3. One can tune  $\left(f_{Tu}^{(N)} + 2\frac{2}{27}f_{TG}^{(N)}\right)\frac{c_u}{m_u}$  against  $\left(f_{Td}^{(N)} + f_{Ts}^{(N)} + \frac{2}{27}f_{TG}^{(N)}\right)\frac{c_d}{m_d}$  by tuning the contribution from  $H$  against that from  $h$ . As we will discuss below, it is not possible to precisely tune this quantity to zero simultaneously for the proton and the neutron (see Fig. 5.6). However, an approximate realization of this condition is possible – this is the tuning that underlies large SD/small SI points in Figs. 5.3 and 5.4 and reported in the literature (*e.g.* [168]).

---

<sup>1</sup>Another possibility is that both SI and SD from exchange of the  $Z^0$  and Higgs boson respectively are small. If there exist light squarks, they can give rise to large SD signals [56]. Cross section estimates from light squark exchange are discussed more in Appendix B.1.

4. One can tune the contribution from the proton against the contribution from the neutron. The cancellation would only hold for a specific element. Since all experiments do not use the same elements, we will not pursue this case further.

In what follows, we minimize the SI cross section by tuning the contributions from the  $h$  and  $H$  against each other (point 3 above). From Eq. (V.19), this cancellation requires (in the decoupling/large  $t_\beta$  limit)  $\text{sgn}(Z_{H_u}) = \text{sgn}(Z_{H_d})$ . This condition for cancellations to be possible was first noted in [96]. Using DarkSUSY we have confirmed that this is a necessary condition, not just in this limit, but for any values of the pseudo-scalar Higgs mass ( $m_A$ ) and  $t_\beta$ . This condition only occurs for certain signs of  $M_1$ ,  $M_2$  and  $\mu$ . If large SD/small SI were observed for neutralino DM, this would constrain the signs in the neutralino mass matrix.

Let us estimate the maximum allowed suppression. To good approximation<sup>2</sup>, the best one can do is to tune away the coupling to (for example) the proton:

$$(V.35) \quad \frac{c_u}{m_u} = - \left( \frac{f_{Td}^{(p)} + f_{Ts}^{(p)} + \frac{2}{27} f_{TG}^{(p)}}{f_{Tu}^{(p)} + 2 \frac{2}{27} f_{TG}^{(p)}} \right) \frac{c_d}{m_d} \equiv -f_{d/u}^{(p)} \frac{c_d}{m_d} \approx -1.64 \frac{c_d}{m_d}.$$

In order for Eq. (V.35) to have a guaranteed solution requires independent control of  $\alpha$  and  $m_H$ . Since there is a non-trivial relationship between  $\alpha$  and  $m_H$  (both are determined by  $m_A$ ), our lower bound provides a conservative estimate. Using Eq. (V.8) to estimate  $c_q$  and plugging in the relationship between  $c_u$  and  $c_d$  from Eq. (V.35) gives  $\sigma_{\text{SI}}^p = 0$  and

$$(V.36) \quad \sigma_{\text{SI}} = \sigma_{\text{SI}}^n = \frac{4}{\pi} m_n^2 \frac{(A-Z)^2}{A^2} m_r^2 y_\chi^2 \frac{1}{m_h^4} \left( \left( f_{Tu}^{(n)} + 2 \frac{2}{27} f_{TG}^{(n)} \right) f_{d/u}^{(p)} - \left( f_{Td}^{(n)} + f_{Ts}^{(n)} + \frac{2}{27} f_{TG}^{(n)} \right) \right)^2$$

$$(V.37) \quad \approx 8 \times 10^{-13} \text{ pb} \left( \frac{115 \text{ GeV}}{m_h} \right)^4 \left( \frac{y_\chi}{0.1} \right)^2 \quad (\text{SI with cancellations}).$$

This gives an estimate for how small SI can be, absent taking some of  $M_1, M_2, \mu \rightarrow \infty$ . The effects of the current uncertainties on the hadronic matrix elements described in Sec. 5.1.1

<sup>2</sup>From Fig. 5.6 the absolute minimum of the total SI cross section occurs between the region where the coupling to the proton and neutron vanish. Therefore, the following analytic estimate will be off by a factor of a few.

can change the amount of cancellation allowed (the coefficient in Eq. (V.35)), altering the lower bound in Eq. (V.37) by  $\mathcal{O}(50\%)$ .

In Fig. 5.6 we show the SI cross section on the proton, the neutron and both as a function of  $m_A$  for a 93 GeV neutralino with a thermal relic density of  $\Omega_{\text{DM}} h^2 = 0.1$ ,  $\sigma_{\text{SD}}^p = 9 \times 10^{-4}$  pb and  $\sigma_{\text{SD}}^n = 6 \times 10^{-4}$  pb. One can clearly see that both contributions to SI DD cannot both be canceled simultaneously. At the minimum,  $\sigma_{\text{SI}}^{\text{min}} = 3 \times 10^{-12}$  pb for  $m_A = 751$  GeV. For a shift in  $m_A$  of  $\sim 5\%$ , the cross section becomes  $\sim 2 \times 10^{-10}$  pb – a change of almost 2 full orders of magnitude. This emphasizes the delicacy of the cancellation. Other than in the limited region where the cancellation occurs, the entire range is probeable by the next generation of SI experiments.

Numerically, we find that for  $\sigma_{\text{SD}} > 10^{-4}$  pb, the smallest  $\sigma_{\text{SI}}$  can be is  $\mathcal{O}(10^{-14})$  pb where the suppression beyond the value in Eq. (V.37) is due to small mixing angles.

Finally, we note that while these kinds of conspiracies are allowed, there is no reason to expect that the SUSY breaking parameters have anything to do with the nuclear matrix elements. We take this as evidence that such cancellations are unlikely.

## 5.6 Conclusions

In this work we have explored the physics of SD DD with an emphasis on the correlations with SI experiments. In the process, we have determined some expectations for the SD cross sections. In particular, in the MSSM,  $(\sigma_{\text{SD}}^{\text{SUSY}}) < 6 \times 10^{-3}$  pb without making any assumptions about the thermal history. Again, allowing for a non-trivial cosmic history, but imposing the unified gaugino mass condition, we find  $(\sigma_{\text{SD}}^{\text{SUSY}}) < 4 \times 10^{-3}$  pb. Finally,  $(\sigma_{\text{SD}}^{\text{SUSY}}) < 2 \times 10^{-3}$  pb when a thermal relic density is imposed. These represent important targets for future experiments. If one includes the possibility of squark exchange, a SD cross section as high as  $2 \times 10^{-2}$  pb can be reached for a neutralino which has a thermal abundance by utilizing the squark pole [47, 48]. We note that in the absence of light

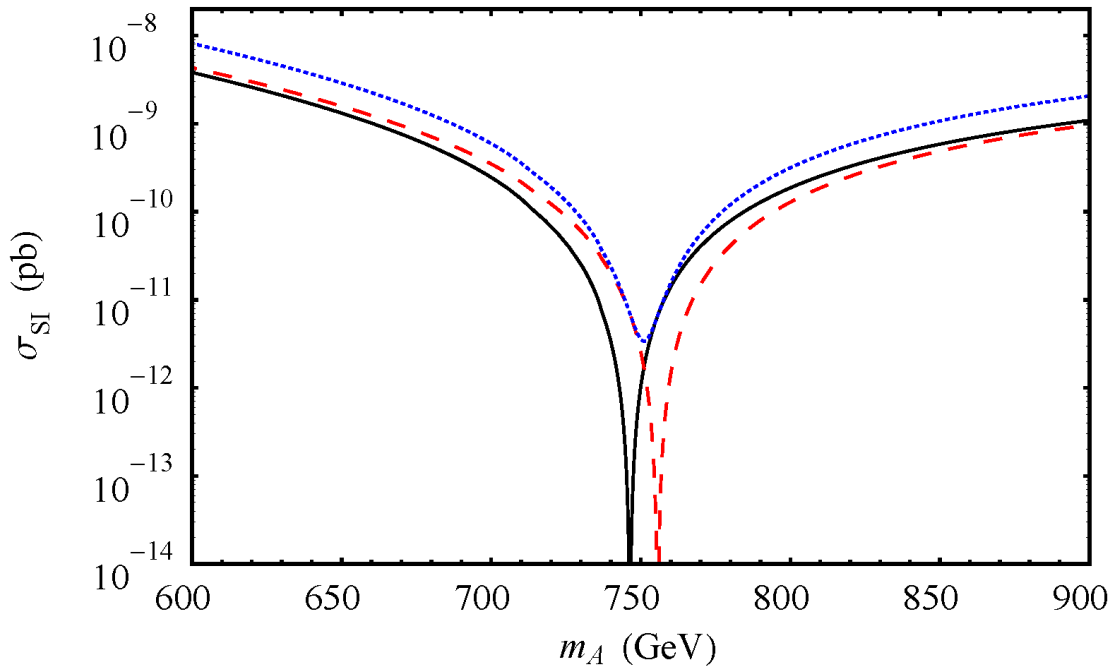


Figure 5.6: Plot of the SI DD cross section for the neutralino scattering off of a proton (solid), a neutron (dashed) and both (dotted) as a function of  $m_A$ . For reference, the size of the SD cross section is about  $9 \times 10^{-4}$  pb (proton) and  $6 \times 10^{-4}$  pb (neutron) and  $m_\chi = 93$  GeV. The thermal relic density is  $\Omega_{\text{DM}} h^2 = 0.1$ . The minimum value for the total SI DD is  $\sigma_{\text{SI}}^{\text{min}} = 3 \times 10^{-12}$  pb for  $m_A = 751$  GeV. By changing  $m_A$  by 5%, the cross section becomes  $\sim 2 \times 10^{-10}$  pb. For small  $m_A$  the cross section is on the order of  $\sigma_{\text{SI}} \sim 10^{-7}$  pb and in the decoupling limit the cross section is on the order of  $\sigma_{\text{SI}} \sim 10^{-9}$  pb – the entire region where there are not any conspiratorial cancellations is within the reach of the next generation of SI experiments.

squarks, if SD cross sections larger than  $\sim 6 \times 10^{-3}$  pb were observed, the DM would not be an MSSM neutralino. This would point to more exotic theories like the SDM or models with light mediators [66]. For models which reproduce the relic density, in the decoupling limit, and unified gaugino masses, a 1-ton COUPP-like experiment could probe the entire range of SD cross sections up to WIMP masses of  $\mathcal{O}(1 \text{ TeV})$ .

More generally, we have argued that given the experimental constraints from LEP, neutralino DM is likely to be well-tempered with possible signals for the next generation of SI and SD DD experiments. In fact, any model (such as the SDM) which interacts with the SM via a light Higgs boson can imply a signal in SI experiments and any model of Majorana

fermions with non-trivial couplings to the  $Z^0$  can imply a signal in SD experiments. We have enumerated the ways to avoid these arguments. Since all of these options involve a numerical conspiracy or some new source of tuning, we take them to be disfavored. With available methods we should be able to probe the majority of the natural range for the SI and SD DD signals of both thermal and non-thermal neutralino DM.

## CHAPTER VI

# Extracting the Dark Matter Mass from Single Stage Cascade Decays at the LHC

### 6.1 Introduction

This chapter was completed in collaboration with Eric Kuffik and Kathryn Zurek [77].

In this chapter we will explore one aspect of DM phenomenology at the LHC. Making DM mass measurements at the LHC, for example in models of supersymmetry (SUSY) or Universal Extra Dimensions (UED), is a difficult problem, since the DM particle is typically produced in pairs as products of complicated decay chains of parent particles. In fact, the number of states participating in the event can vary dramatically depending on the specific model. The identities, couplings, and masses of the particles involved in these processes may be unknown. Let  $n$  be the number of steps in the cascade between the production of the parent and the appearance of the DM child in the event. For  $n > 1$ , if all visible particles in the decay are detected, all masses of the parent, intermediate and visible and invisible child particles can, in principle, be determined uniquely (see for example [59] for a discussion). The simplest case of  $n = 1$  proves to be more challenging. In Fig. 6.1 we show a schematic of an  $n = 1$  process. We have also included the possibility that additional visible states are produced before the parents, which we refer to as Up-Stream Radiation (USR). In Sec. 6.2 below, we will discuss the relevance of USR for DM mass determination. Refs. [123, 37, 163, 172, 164] also study  $n = 1$  decay chains.

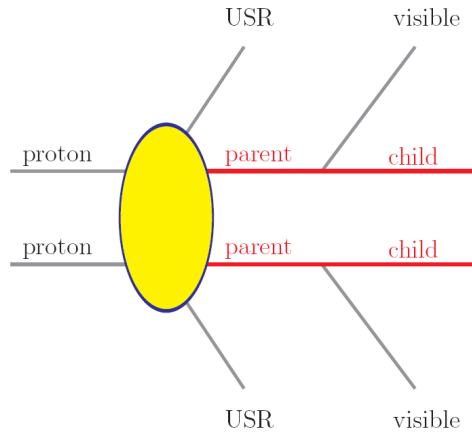


Figure 6.1: Schematic representation of the  $n = 1$  class of processes considered in this work, with additional Up-Stream Radiation (USR). The parent particle is the state which decays to the visible particles and the child DM particles.

The motivation for studying DM mass determination in  $n = 1$  processes is many fold – we mention two here. First, within SUSY or UED,  $n = 1$  processes with additional USR can be important. For example, decays  $\tilde{\ell}^\pm \rightarrow \ell^\pm \tilde{\chi}^0$  with initial state radiation, and  $\tilde{q} \rightarrow j \tilde{\chi}^\pm \rightarrow j \ell^\pm \tilde{\nu}$  (for a sneutrino lightest SUSY particle), are of the type shown in Fig. 6.1, where  $\tilde{\ell}^\pm$  is a slepton,  $\ell^\pm$  is a lepton,  $\tilde{\chi}^0$  is a neutralino,  $\tilde{q}$  is a squark,  $j$  is a jet,  $\tilde{\chi}^\pm$  is a chargino and  $\tilde{\nu}$  is a sneutrino. Although higher  $n$  chains may also be present in many models, the combinatoric backgrounds can make mass extraction in such decay chains complicated. By contrast  $n = 1$  events are clean, and involve only two visible objects plus missing transverse momentum (hereafter referred to as missing energy). Also, since one will potentially observe  $n = 1$  chains if one of these theories is correct, it will be useful to extract as much information as possible from these signals. Second, the observations of astrophysical anomalies, *e.g.* PAMELA [7] and Fermi [4], have led many to conjecture that the DM is leptophilic. Models which generate such signals can, for example, be constructed by connecting the DM to the lepton asymmetry [81], or by positing that mixed sneutrinos constitute the DM [28, 126, 190]. The simplest such dark sectors involve only a new mediator state and the leptophilic DM state, so that the DM is produced at a collider



through the leptonic decay of the mediator. Hence, the study of these processes is well motivated. The reader is referred to Appendix C.1 for more detail on models where  $n = 1$  decay chains with USR are important.

As shown in Appendix C.2, the phase space for  $n = 1$  processes without USR depends on the combination  $\mu = (m_p^2 - m_c^2)/(2m_p)$  and weakly on  $\hat{s}/(4m_p^2)$  where  $m_p$  is the parent mass,  $m_c$  is the child mass and  $\sqrt{\hat{s}}$  is the partonic center-of-mass energy. Hence, extracting  $\mu$  is simple, while measuring  $m_p$  proves to be more challenging. Current experimental methods for mass determination in events with missing energy rely on matrix element techniques. Here, one begins by assuming a model which implies a matrix element with additional dependence on  $m_p$ . Then by fitting measured differential distributions, one can extract, in addition to the combination  $\mu$ , the overall mass scale  $m_p$  by observing how quickly the event rate falls off with  $\sqrt{\hat{s}}$ .

In this paper we explore a different technique where the overall mass scale is determined from the transverse boosts given to the parent particles by USR. Since the boost depends only on  $m_p$ , *i.e.* it is independent of the matrix element, the result is a model independent method for determining the overall mass scale. We explore a particular  $M_{T2}$  variant proposed in [149], which utilizes events with USR to separately extract the parent and child masses. We carry out the first full scale simulation of these  $M_{T2}$  based variants for dark matter mass determination, including detector effects, emphasizing the size of statistical errors and discussing various difficulties this method presents.

The outline of this paper is as follows. We begin with a discussion of the  $M_{T2}$  variable, and the possibility of extracting parent and child mass separately in  $n = 1$  events with USR. Next we turn to a numerical analysis of this  $M_{T2}$  based method and its efficiency in DM mass determination for a given number of  $n = 1$  events at the LHC. We then discuss additional sources of error beyond those explicitly contained in the previous section.

Finally, we conclude. In Appendix C.1 we outline some example models where this method would be relevant and in Appendix C.2 we show how the phase space for  $n = 1$  processes depends on the  $M_{T2}$  endpoint.

## 6.2 $M_{T2}$ Preliminaries

We begin by reviewing the  $M_{T2}$  variable [153, 36]. Since the LHC is a hadron collider, the initial parton longitudinal momenta are unknown. Hence, only the total transverse momentum is constrained to be zero, and thus it becomes necessary to use transverse variables, such as  $M_{T2}$ , a generalization of the transverse mass (see also [68, 38, 143]). For the class of processes studied here (see Fig. 6.1), there will be two missing particles in each event, so that the 4-momenta of the invisible child particles cannot be determined. Thus, only the total transverse missing momentum,  $\vec{p}_T^{\text{miss}}$ , can be measured. In addition, the child particle mass,  $m_c$ , is not known. However, a trial DM mass can be guessed,  $\tilde{m}_c$ , and  $M_{T2}$  formed for each event as

$$(VI.1) \quad M_{T2}(\tilde{m}_c) \equiv \min \left[ \max \left\{ M_T^{(1)}, M_T^{(2)} \right\} \right],$$

where the minimization is performed over trial missing momenta for the two child particles,  $\vec{p}_T^{\text{miss}(1)}$ ,  $\vec{p}_T^{\text{miss}(2)}$ , subject to the constraint that their sum be the total missing  $\vec{p}_T$ :

$$(VI.2) \quad \vec{p}_T^{\text{miss}(1)} + \vec{p}_T^{\text{miss}(2)} = \vec{p}_T^{\text{miss}} = -\vec{p}_T^{\text{vis}(1)} - \vec{p}_T^{\text{vis}(2)},$$

where  $\vec{p}_T^{\text{vis}(i)}$  is the transverse momentum of the  $i^{\text{th}}$  visible particle, and we are neglecting here the possibility of additional USR. In Eq. (VI.1),  $M_T^{(i)}$  is the transverse mass of the visible and child particles using the guessed missing momentum,  $\vec{p}_T^{\text{miss}(i)}$ , and child trial mass  $\tilde{m}_c$ :

$$(VI.3) \quad M_T^{(i)} = \sqrt{\left(m_{\text{vis}}^{(i)}\right)^2 + \tilde{m}_c^2 + 2 \left(E_T^{\text{vis}(i)} E_T^{\text{miss}(i)} - \vec{p}_T^{\text{vis}(i)} \cdot \vec{p}_T^{\text{miss}(i)}\right)},$$

where  $m_{\text{vis}}^{(i)}$  is the mass of the  $i^{\text{th}}$  visible particle. The energies are formed in the usual way,

$$(VI.4) \quad E_T^{\text{vis}(i)} \equiv \sqrt{\left(\vec{p}_T^{\text{vis}(i)}\right)^2 + \left(m_{\text{vis}}^{(i)}\right)^2}, \quad E_T^{\text{miss}(i)} \equiv \sqrt{\left(\vec{p}_T^{\text{miss}(i)}\right)^2 + \tilde{m}_c^2}.$$

When there is no USR, there exists a value of  $M_{T2}$ , referred to as an endpoint, above which the differential cross section,  $d\sigma/dM_{T2}$ , rapidly approaches zero, which is given by [73]

$$(VI.5) \quad M_{T2}^{\text{max}} = \mu + \sqrt{\mu^2 + \tilde{m}_c^2},$$

where

$$(VI.6) \quad \mu \equiv \frac{m_p^2 - m_c^2}{2m_p},$$

is the momentum of the invisible child in the parents' rest frame. As we show in Appendix C.2,  $n = 1$  chains only depend on  $\mu$  up to small corrections due to the parent mass (which is exploited by the matrix element methods). Methods which do not capitalize on these corrections do not have enough information to extract both masses separately. This neglects, however, the potential for additional USR in the event. The USR can be in the form of jets coming from the initial state QCD radiation (ISR), or jets coming from the decays of heavy colored objects in  $n > 1$  processes, where the decay chain ends in the  $n = 1$  process of interest. By including the USR, Eq. (VI.2) no longer obtains, and instead the total momentum of the visible and invisible particles must be balanced against the momentum of the radiation,  $\vec{p}_T^{\text{USR}} \equiv \vec{P}_T$ ,

$$(VI.7) \quad \vec{p}_T^{\text{miss}(1)} + \vec{p}_T^{\text{miss}(2)} = \vec{p}_T^{\text{miss}} = -\vec{p}_T^{\text{vis}(1)} - \vec{p}_T^{\text{vis}(2)} - \vec{P}_T.$$

Now the  $M_{T2}$  endpoint will depend on the upstream momentum [59, 172, 164]:

$$(VI.8) \quad M_{T2}^{\text{max}}(\tilde{m}_c, P_T) = \begin{cases} \left[ \left( \mu(P_T) + \sqrt{\left( \mu(P_T) + \frac{P_T}{2} \right)^2 + \tilde{m}_c^2} \right)^2 - \frac{P_T^2}{4} \right]^{1/2}, & \text{if } \tilde{m}_c \leq m_c \\ \left[ \left( \mu(-P_T) + \sqrt{\left( \mu(-P_T) - \frac{P_T}{2} \right)^2 + \tilde{m}_c^2} \right)^2 - \frac{P_T^2}{4} \right]^{1/2}, & \text{if } \tilde{m}_c \geq m_c \end{cases}$$

and

$$(VI.9) \quad \mu(P_T) \equiv \frac{m_p^2 - m_c^2}{2m_p} \left( \sqrt{1 + \left(\frac{P_T}{2m_p}\right)^2} - \frac{P_T}{2m_p} \right).$$

The functional form for the  $M_{T2}$  endpoint depends on whether the test mass is larger or smaller than the true DM mass. Hence, there is a discontinuity in the derivative with respect to the trial child mass of Eq. (VI.8) above and below the true DM mass,  $m_c$ , giving rise to a kink [123, 37, 163, 72] in the  $M_{T2}^{\max}(\tilde{m}_c, P_T)$  curve which can be utilized for extracting additional information beyond Eq. (VI.5). In principle, given an event with a specific value for the  $P_T$  of the USR, one can now extract the parent and child masses. However, since one must do this analysis for a particular bin in  $P_T$ , there is competition between the size of the bin – small bins imply small statistical samples – and the accuracy of the measurement.

Another method was proposed in [149], which sidesteps the problem of binning by utilizing the whole range of  $P_T$ . From Eqs. (VI.5) and (VI.8), it can be seen that  $M_{T2}^{\max}$  is unchanged by the effects of the  $P_T$  when  $\tilde{m}_c = m_c$ . Furthermore, it has been shown [149] that

$$(VI.10) \quad M_{T2}^{\max}(\tilde{m}_c, P_T) - M_{T2}^{\max}(\tilde{m}_c, 0) \geq 0,$$

where the equality only holds when  $\tilde{m}_c = m_c$ . Thus one can construct a new variable [149]

$$(VI.11) \quad N(\tilde{m}_c) \equiv \sum_{\text{all events}} \Theta \left( M_{T2}^{\text{measured}}(\tilde{m}_c) - M_{T2}^{\max}(\tilde{m}_c, 0) \right),$$

where  $\Theta(\dots)$  is the Heaviside function and  $M_{T2}^{\text{measured}}(\tilde{m}_c)$  is the measured value of  $M_{T2}(\tilde{m}_c)$ . It is this variable we will be minimizing to find the correct child mass. In Fig. 6.2, we plot  $N(\tilde{m}_c)$  vs.  $\tilde{m}_c$  for  $m_p = 300$  GeV and  $m_c = 150$  GeV. Since the shape is “bowl”-like, we refer to this construction as an  $M_{T2}$  bowl. Unless otherwise specified, all events were simulated with the MadGraph 4.4 event generator [13], showered by PYTHIA 6.4 [184],

and run through the detector simulation software PGS 3.3 [84]. Note that we use the MadGraph default settings which defines a lepton as having  $p_T > 10$  GeV and a jet as having  $p_T > 20$  GeV.

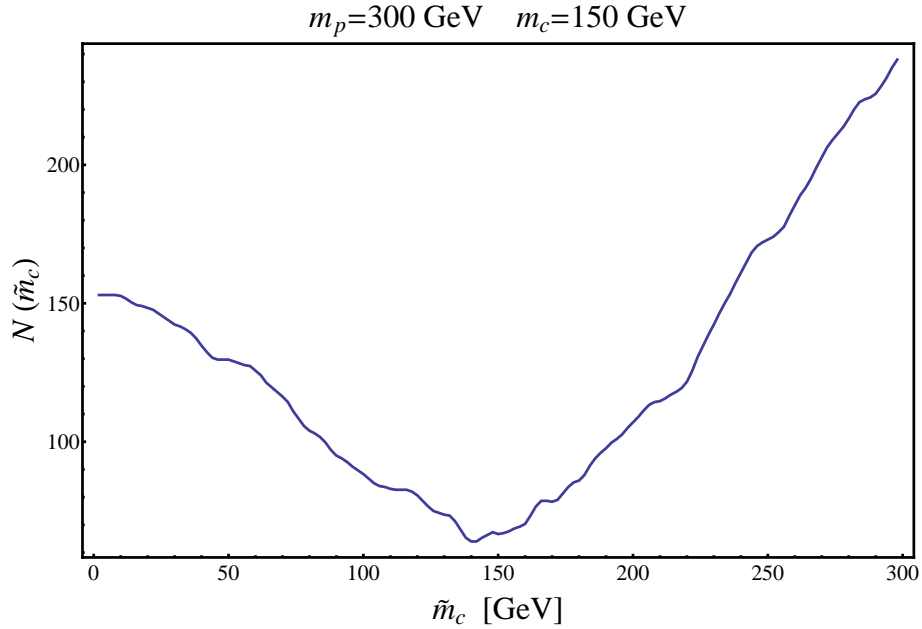


Figure 6.2: Example of an  $M_{T2}$  bowl for 50,000 smuon pair production events with QCD USR. The parent mass is 300 GeV and the child mass is 150 GeV. The events were run through the PGS detector simulator.

### 6.3 Mass Determination from $M_{T2}$ Bowls

In this section we will calculate the statistical errors for child mass determination with  $M_{T2}$  bowls. Clearly, Eq. (VI.9) only depends on the kinematics of the event, *i.e.* it is independent of the quantum numbers, including the spin, of the underlying particles. Then, up to small corrections due to the steepness of the  $M_{T2}$  distribution about this endpoint, there are only  $\mathcal{O}(1)$  differences in the bowls around the minimum for different parent spins. Hence, we can study the effectiveness of this variable for a wide variety of

models by only scanning over the masses of the parent and child particles. We take

$$\begin{aligned}
 m_p &= 100 \text{ GeV}, & m_c &= 25, 50, 75 \text{ GeV}, \\
 m_p &= 300 \text{ GeV}, & m_c &= 75, 150, 225 \text{ GeV}, \\
 \text{(VI.12)} \quad m_p &= 500 \text{ GeV}, & m_c &= 125, 250, 375 \text{ GeV}
 \end{aligned}$$

as our benchmark parameters.

For reference we provide the overall cross section for these benchmark models in Table 6.1, where we have assumed that the production occurs via electroweak processes, including the effects of QCD ISR. Neglecting diagrams which involve additional new-physics states, the overall rates only depend on the spin of the parent up to  $\mathcal{O}(1)$  factors due to the choice of  $SU(2) \times U(1)$  representation. For reference, the scalar example process is  $pp \rightarrow \tilde{\ell}^+ \tilde{\ell}^- \rightarrow \ell^+ \ell^- \tilde{\chi}^0 \tilde{\chi}^0$  where  $\tilde{\ell}^\pm$  is a slepton and  $\tilde{\chi}^0$  is the lightest neutralino. This is the process we simulate for our benchmarks with QCD ISR. For reference, a fermionic example process is  $pp \rightarrow \tilde{\chi}^+ \tilde{\chi}^- \rightarrow \ell^+ \ell^- \tilde{\nu} \tilde{\nu}^*$  where  $\tilde{\chi}^\pm$  is a chargino and  $\tilde{\nu}$  is a sterile sneutrino. For some details of these and other models which have  $n = 1$  processes, see Appendix C.1. Our results below will be given in terms of the number of events before cuts, so Table 6.1 can be used to estimate the reach of actual models.

$m_p$	$\sigma_{\text{scalar}}$	$\sigma_{\text{fermion}}$
100 GeV	0.4 pb	20 pb
300 GeV	$9 \times 10^{-3}$ pb	0.4 pb
500 GeV	$10^{-3}$ pb	$6 \times 10^{-2}$ pb

Table 6.1: Cross sections for electroweak pair production of parent particles with various masses and spins including the effects of QCD ISR. We neglect any  $t$ -channel processes involving additional states.

There are also models which have more complicated decay chains but can be interpreted as  $n = 1$  processes with additional ISR. For example, one can have new colored objects which decay to jets and the parent particle. As long as the ISR can be distinguished from the decay product of the parent, our method is applicable. This will improve the

prospects for this method dramatically since the overall rate will increase due to colored production instead of electroweak production, and additionally the majority of events will have very hard  $P_T$  for the USR. Hence, we also choose a set of benchmark models with colored objects up-stream with masses

$$\begin{aligned}
 & m_{\text{col}} = 600 \text{ GeV}, \quad m_p = 300 \text{ GeV}, \quad m_c = 150 \text{ GeV}, \\
 & m_{\text{col}} = 1000 \text{ GeV}, \quad m_p = 300 \text{ GeV}, \quad m_c = 150 \text{ GeV}, \\
 \text{(VI.13)} \quad & m_{\text{col}} = 1400 \text{ GeV}, \quad m_p = 300 \text{ GeV}, \quad m_c = 150 \text{ GeV},
 \end{aligned}$$

where  $m_{\text{col}}$  is the mass of the colored state which decays to the parent particle and jets. The example process we will simulate for these benchmarks is  $pp \rightarrow \tilde{q}\tilde{q} \rightarrow jj\tilde{\chi}^+\tilde{\chi}^- \rightarrow \ell^+\ell^-\tilde{\nu}\tilde{\nu}^*$  where  $\tilde{q}$  is a squark,  $\tilde{\chi}^\pm$  is a chargino and  $\tilde{\nu}$  is a sterile sneutrino. While one might be able to use additional handles from viewing such events as  $n = 2$  processes (instead of  $n = 1$  with USR), here we wish to examine only the effect of harder USR from colored particle decay on the error for DM mass determination in  $n = 1$ . For additional models of  $n = 1$  processes which can be produced in the decays of colored states see Appendix C.1.

As discussed above, the additional radiation shifts all events, including those near the  $M_{T2}$  endpoint. For reference, the radiation distributions for our benchmark models are shown in Figs. 6.3 and 6.4. From Eq. (VI.8), the correction to the  $M_{T2}$  endpoint due to USR is of the form  $P_T/m_p$ . Hence, the  $P_T$  distribution of jets determines how well the parent and child masses can be extracted separately. From Fig. 6.3, we see that heavier parents lead to harder  $P_T$  distributions due to the larger recoil occurring from production of a heavier state. However, since the correction to  $M_{T2}$  goes as  $1/m_p$ , this enhancement is tempered by the parent mass. In addition, heavier parents have smaller production cross sections (see Table 6.1). Hence, assuming they can be seen above the backgrounds, lower parent mass states give rise to more defined bowls. The trade-off between background rejection, which is optimized for high masses, and the quality of the  $M_{T2}$  bowls, which

is optimized for low masses due to the dependence on the ISR, leads to a sweet spot in the range of  $\mathcal{O}(200 \text{ GeV})$  to  $\mathcal{O}(500 \text{ GeV})$ , with significant dependence on the spin of the parent. In the cases with colored states upstream this tension is alleviated since now the  $P_T$  distributions are harder and the production cross sections are larger, as in Fig. 6.4.

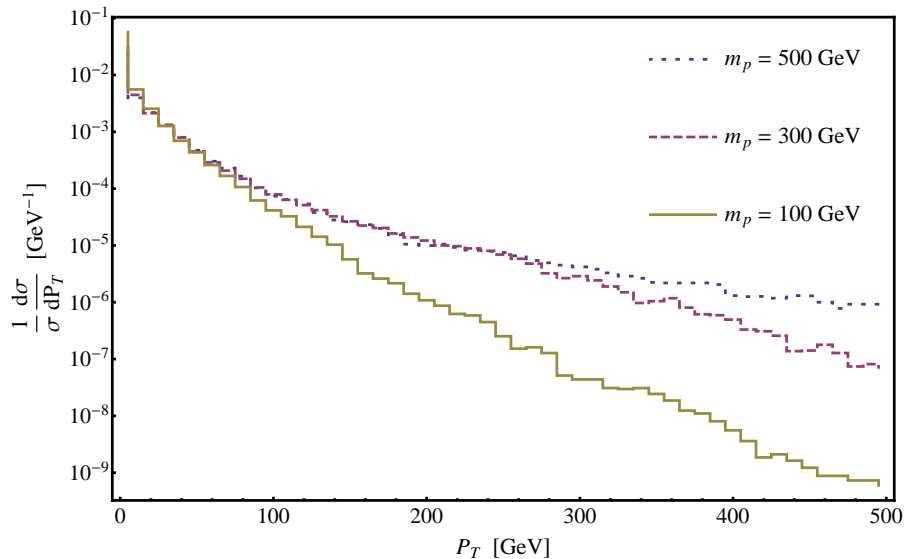


Figure 6.3:  $P_T$  of the hardest jet for slepton events with only QCD ISR. The blue dotted line is for  $m_p = 500 \text{ GeV}$ , the red dashed line is for  $m_p = 300 \text{ GeV}$  and the yellow solid line is for  $m_p = 100 \text{ GeV}$ . Note from Eq. (VI.8) that the correction to  $M_{T2}$  due to USR is of the form  $P_T/m_p$ .

The effects of the radiation on the  $M_{T2}$  endpoint are shown by plotting  $N(\tilde{m}_c)$  as a function of  $\tilde{m}_c$  in Fig. 6.2, for 50,000 smuon pair production events with two muons and missing energy, with no background events (also see Fig. 6.11). As we will show in the next section, the backgrounds can be very efficiently cut away, and will be insignificant near the  $M_{T2}$  endpoint (see Sec. 6.4.2). In what follows, we will present statistical error bars on the DM mass determination using the  $M_{T2}$  bowl and will discuss in detail various sources of error and their effect on this analysis.



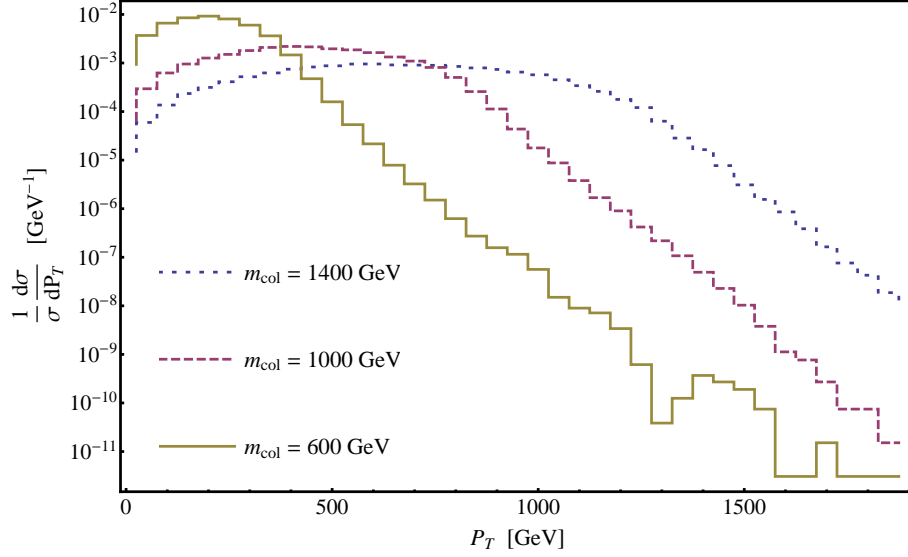


Figure 6.4:  $P_T$  of the hardest jet with new colored state dominating the USR. Specifically, these colored states are squarks. The blue dotted line is for  $m_{\text{col}} = 1400$  GeV, the red dotted line is for  $m_{\text{col}} = 1000$  GeV and the yellow solid line is for  $m_{\text{col}} = 600$  GeV. We have fixed  $m_p = 300$  GeV in all cases. From Eq. (VI.8), the correction to  $M_{T2}$  due to USR is of the form  $P_T/m_p$ .

### 6.3.1 Statistical Analysis of $M_{T2}$ Bowls

Contributions to adjacent bins in the  $M_{T2}$  bowls from the same events imply that it is inappropriate to use simple  $\sqrt{N}$  statistics in computing errors. Removing one event from a given bin in the distribution can in principle remove one event from *each* bin. Therefore, we utilized the well-known “bootstrapping” method to do the statistical error analysis. We employed the following method when doing this. We begin by generating a sample of  $\mathcal{O}(100,000)$  signal events (we take  $\sqrt{s} = 14$  TeV). From those 100,000 events, we choose a subset of size  $N_{\text{events}}$ , and make 100 independent random selections of  $N_{\text{events}}$  events from the original data set. Then for each of these selections we calculate  $N(\tilde{m}_c)$  using Eq. (VI.11). This gives us a random sampling of bowls for a given number of events. Since there is often a degeneracy of minima for each of these random bowls, especially for a low number of events, we take the geometric mean of these multiple minima to give us an average minimum for each bowl. Note that we do this assuming the theoretical value

of  $M_{T2}^{\max}$  (see Sec. 6.4.3). Finally, we find the mean and standard deviation of these 100 average minima. To find the standard deviation we used the formula  $\sum(x_i - x_{\text{mean}})^2 / (N - 1)$  and checked to confirm that this corresponds to  $1\text{-}\sigma$  error for a Gaussian distribution to good approximation.

This method allows for a statistical sampling of the distribution of possible bowls for a given number of events. We present our results as a function of  $N_{\text{events}}$ , the number of events *before* any cuts are made. Note that the events which contribute to the bowl have very special kinematics which allow them to go beyond  $M_{T2}^{\max}$  – the overwhelming majority of events will not have any bearing on the mass determination. Hence, cuts designed to remove backgrounds will not cut away these special events which contribute near the minimum of the  $M_{T2}$  bowl where the DM mass determination occurs. This is an expectation we check explicitly in the next section.<sup>1</sup> Also note that by working with the mean we will systematically underestimate the DM mass due to the asymmetric shape of the bowl. This asymmetry is due to the shape of the  $M_{T2}$  distribution near the endpoint as a function of  $\tilde{m}_c$  – the slope becomes steeper as  $\tilde{m}_c$  is taken larger. The events used for the bowls were generated using the PGS detector simulator so that they do include detector effects which also adds to the consistent underestimates. As we discuss in Sec. 6.4.1, detector simulations must be utilized to determine the required correction to account for this off-set. Further sources of error are discussed below in Sec. 6.4.

In Figs. 6.5 - 6.8, we show the statistical error bars for the DM mass determination for a given parent and child mass combination as a function of the number of events before cuts. Note that for a given child mass, the error bars grow smaller as the DM mass approaches the parent mass, due to the width of the minimum of the bowl. This occurs because the minimum of the bowl becomes more well-defined as the  $M_{T2}$  distribution becomes steeper. The error bars grow smaller as  $N_{\text{events}}$  grows larger, but not as quickly as  $1/\sqrt{N_{\text{events}}}$ .

---

<sup>1</sup>This assumption is not true when  $M_{T2}^{\max} \approx m_W$  as in the case of, for example,  $m_p = 100$  GeV and  $m_c = 25$  GeV.

This is because events contribute to multiple bins so that errors from adjacent bins are correlated. Also notice that error bars in Fig. 6.8 are much smaller for a given  $N_{\text{events}}$  than those in Fig. 6.6 for  $m_c = 150$  GeV. The error bars are also smaller for larger values of  $m_{\text{col}}$ . This is due to the enhanced  $P_T$  of the USR as shown by comparing Figs. 6.3 and 6.4. In what remains we will discuss the various additional errors and will argue to what degree we expect them to degrade the results.

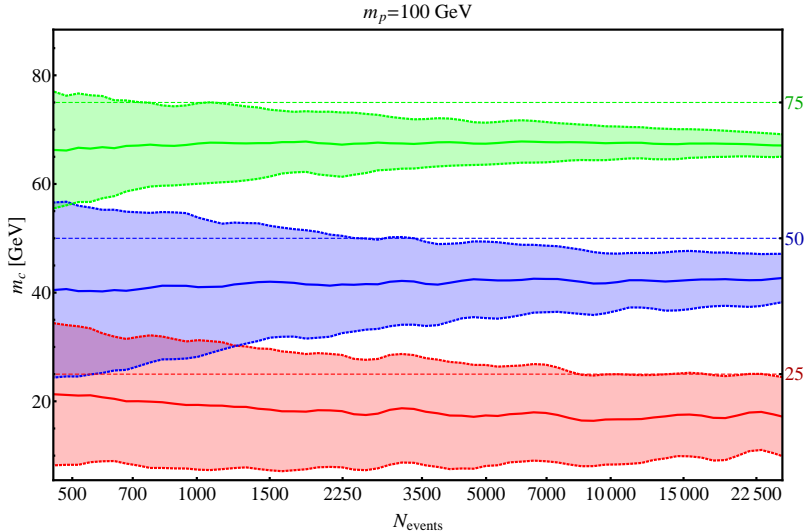


Figure 6.5: Mean and  $\pm 1\sigma$  statistical error bars for a DM mass measurement as a function of the number of signal events *before* cuts. The only source of USR is initial state radiation. The process we simulated is electroweak smuon production. The error bars will improve by  $\mathcal{O}(1)$  for fermionic parents. The parent mass is 100 GeV and the child masses are 75 GeV (green), 50 GeV (blue) and 25 GeV (red) from top to bottom. The dashed lines show the actual child mass. Note that detector effects have been simulated for the underlying events and that the DM mass measurement systematically undershoots the actual value on account of these effects.

## 6.4 Sources of Error

The results of Figs. 6.5 - 6.8 only incorporate statistical and detector effects. In this section we argue that the errors we have included in our analysis are a realistic estimate of the precision with which the DM mass can be extracted from simple cascade decays. We further qualify the additional sources of error below.

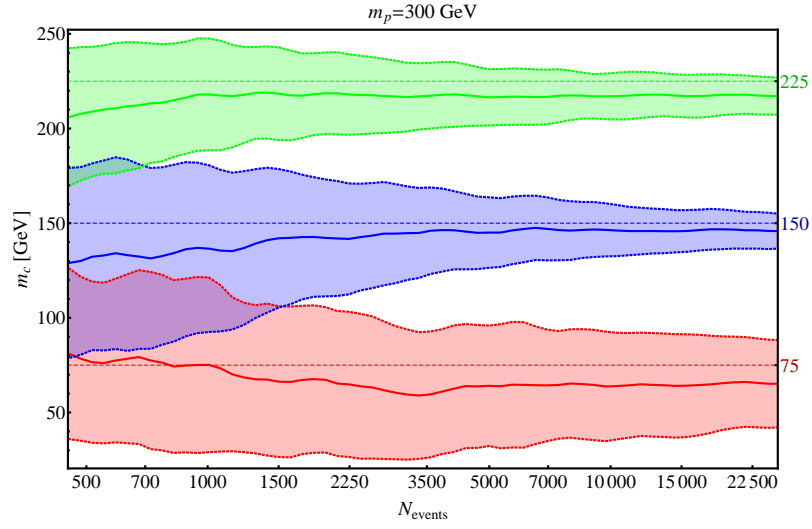


Figure 6.6: Same as Fig. 6.5 except that the parent mass is 300 GeV and the child masses are 225 GeV (green), 150 GeV (blue) and 75 GeV (red) from top to bottom. As explained in the text, we find that cuts designed to eliminate the background will not change these results.

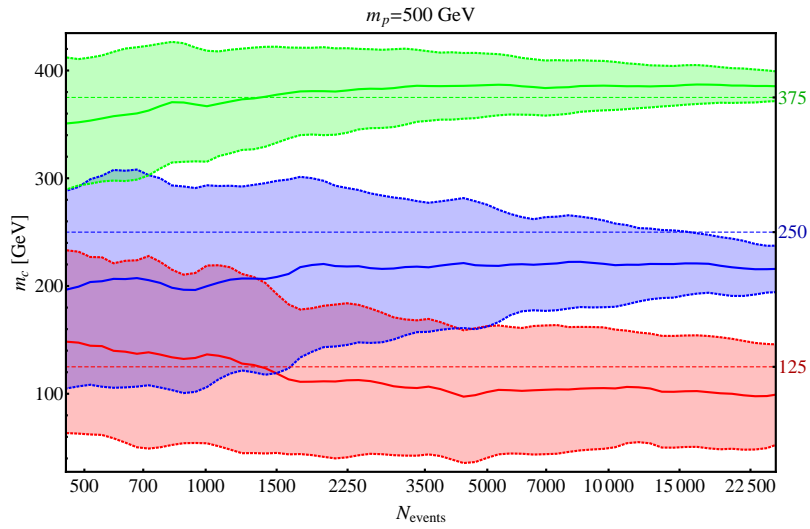


Figure 6.7: Same as Fig. 6.5 except that the parent mass is 500 GeV and the child masses are 375 GeV (green), 250 GeV (blue) and 125 GeV (red) from top to bottom. As explained in the text, we find that cuts designed to eliminate the background will not change these results.

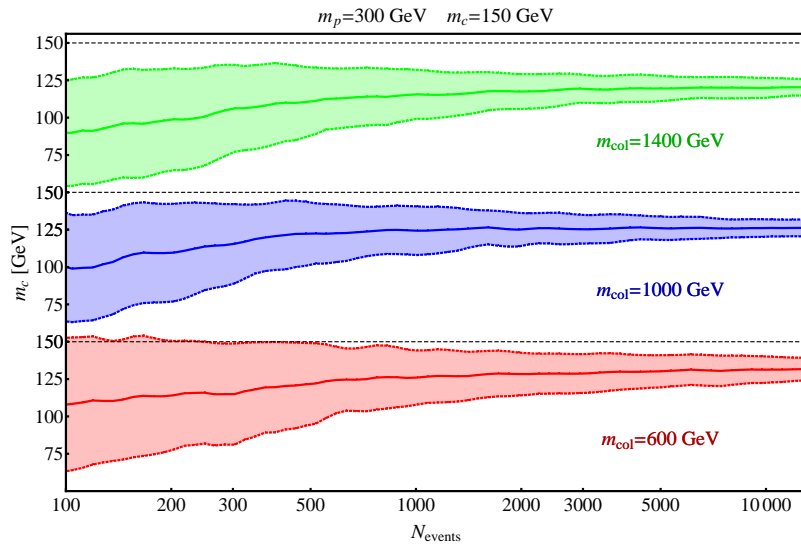


Figure 6.8: Same as Fig. 6.6 except that the dominant source of USR is new heavy colored states. These colored states are squarks which produce chargino parents and jets. The parent mass is 300 GeV and the child mass is 150 GeV for all three cases. The mass of the colored objects are 1400 GeV (green), 1000 GeV (blue) and 600 GeV (red) from top to bottom. As explained in the text, we find that cuts designed to eliminate the background will not change these results.

#### 6.4.1 Detector Effects

With the inclusion of detector effects, the events at the  $M_{T2}$  endpoint become smeared out. This implies that some events which do not have the correct kinematics to make a contribution to the bowl can have  $M_{T2} > M_{T2}^{\max}$ . This leads to a degradation of the minimum of the bowl. Since the  $M_{T2}$  distribution is steeper for larger test masses, this degradation will tend to contribute to a larger underestimate of the DM mass. This is the reason for the systematic under-shooting of the DM mass in Figs. 6.5 - 6.8. To illustrate this effect we have generated the analog of Fig. 6.6 for parton level events as shown in Fig. 6.9. Note that the  $1\text{-}\sigma$  error bars overlap with the actual DM mass except in the case where  $m_c = 75$  GeV since here the bowl is essentially flat below  $\tilde{m}_c \sim 75$  GeV (see Fig. 6.11). Hence detector simulations would have to correct for this systematic effect in any real DM mass measurement.

After generating bowls using the parton level events, the value  $N(\tilde{m}_c)$  (see Eq. (VI.11))

at the minimum is  $\sim 0$ . For the same bowls, but with detector effects, the value  $N(\tilde{m}_c = m_c)$  is no longer 0 – for  $\mathcal{O}(100,000)$  events,  $N(\tilde{m}_c = m_c) \sim \mathcal{O}(100)$ . Hence one can attempt to clean up the bowl by removing the events from the data sample which contribute at the minimum. This will increase the steepness of the bowl and might be helpful in minimizing the error since all removed events are guaranteed to be pathological. However, since this cleaning process does not change the minimum, this will not change the error bars presented above.

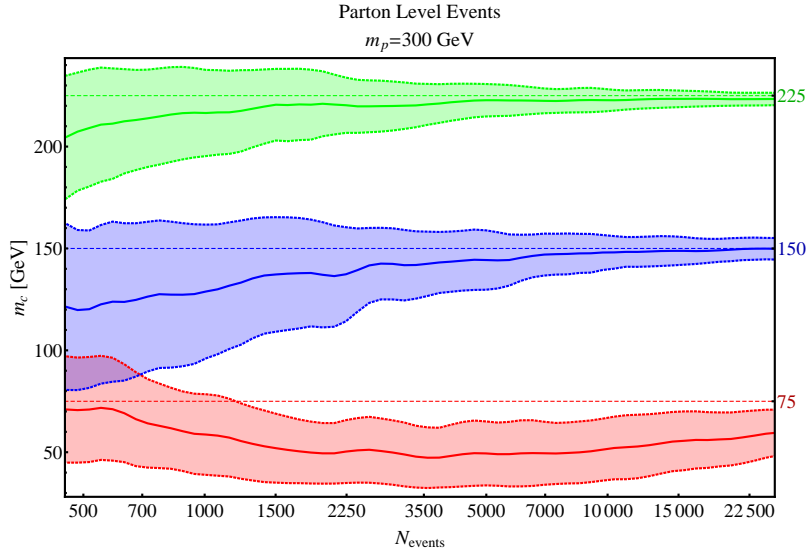


Figure 6.9: Same as Fig. 6.6 except that the underlying events are parton level.

#### 6.4.2 Background Contamination and Cuts

In this section we will argue that a generic set of cuts designed to remove backgrounds will not degrade the minimum of the  $M_{T2}$  bowl and hence will not affect our conclusions. Motivated by the choices taken in [35], we have analyzed the following cuts for illustration, which are relevant for di-lepton events with jets and missing energy (*i.e.* slepton pair production):

1. Require 2 opposite sign, same flavor leptons ( $e$  or  $\mu$ ).
2. Hardest lepton:  $p_T > 40$  GeV.

3. Second hardest lepton:  $p_T > 30$  GeV.
4.  $p_T^{\text{miss}} > 100$  GeV.
5. A  $Z^0$  veto: the invariant mass of the two leptons,  $m_{\ell\ell}$ , must not lie in the range
 
$$80 \text{ GeV} < m_{\ell\ell} < 100 \text{ GeV}.$$
6. No  $b$ -tagged jets.

While cuts should be tailored to the particular model under consideration, these are fairly generic, and will serve to illustrate the point that our results are not significantly degraded by background removal. We also explored the effect of a cut on  $M_{T2}$  by requiring  $M_{T2}(\tilde{m}_c = 0) > 100$  GeV. These cuts will be very efficient for eliminating standard model (SM) backgrounds, the worst of which is  $W^+ W^-$  plus jets, where the  $W^\pm$  bosons decay leptonically. In particular, this di-boson process is dominated by  $t\bar{t}$  production.

An  $M_{T2}$  cut on the  $t\bar{t}$  background is a powerful discriminator, and in many cases it will have no effect on the DM mass determination. To see this, first note that the  $t\bar{t}$  background falls into the same class of  $n = 1$  processes we have been studying already, with the tops as the colored particles leading to hard USR, the  $W^\pm$  as parents and the neutrinos as children. Since the child is a neutrino,  $m_c = 0$ , and the minimum of the bowl will occur at  $\tilde{m}_c = 0$ . Then (neglecting detector effects which will only add a small perturbation) the  $t\bar{t}$  background will be largely eliminated for an  $M_{T2}$  cut of  $\mathcal{O}(100 \text{ GeV})$ . In Fig. 6.10 we plot this  $M_{T2}$  distribution including detector effects. Clearly, there is an endpoint at  $m_W$ . The cross section for  $t\bar{t} \rightarrow b\bar{b}\mu^-\mu^+\nu_\mu\bar{\nu}_\mu$  is 5 pb. Then starting with a 100,000 event sample, the cuts 1-6 described above reduce this background to  $0.065 \pm 0.002$  pb. Then the  $M_{T2}(\tilde{m}_c = 0) > 100$  GeV cut eliminates all remaining events. In this way, the worst of the SM backgrounds can be easily removed for  $m_p \gtrsim 100$  GeV.

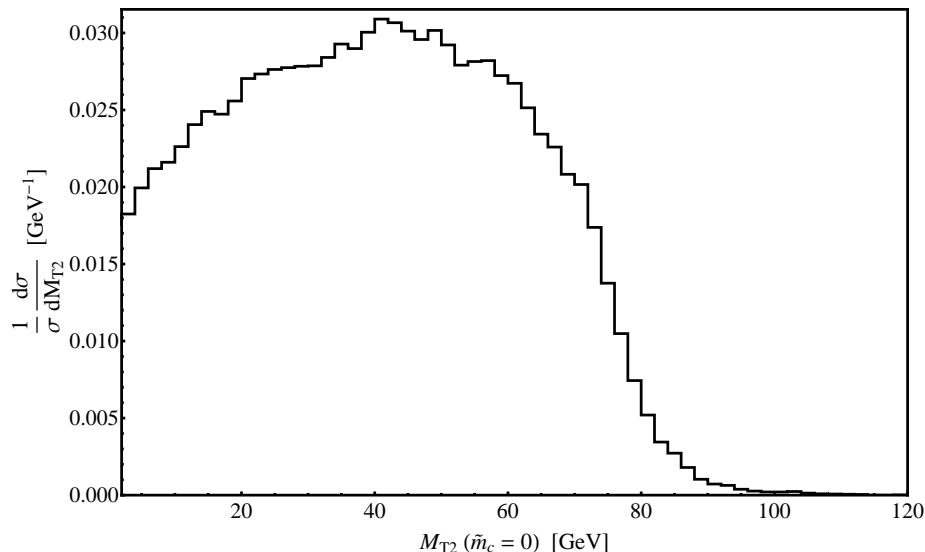


Figure 6.10:  $M_{T2}(\tilde{m}_c = 0)$  distribution for  $t\bar{t}$  events where we have treated this as an  $n = 1$  process where the  $b$ -jets are USR and the  $W^\pm$  are the parent particles. This plot is made before cuts and we have included detector effects. There is an endpoint at  $m_W$  since the child, *i.e.* the neutrino, mass is zero in these events.

In Fig. 6.11 we have plotted a series of  $M_{T2}$  bowls before and after this set of cuts to check that the signal in the DM mass determination region of the  $M_{T2}$  bowl is not degraded. For  $m_p = 100$  GeV there is a significant degradation of the bowl. However, for this value of  $m_p$ , there will be tremendous difficulties disentangling the signal from the  $W^+W^-$  background since they have very similar  $M_{T2}$  endpoints. For the models with heavier parents or with additional colored states producing hard USR, the minimum is maintained for these cuts. Additionally, the  $M_{T2}$  cut has no effect on these plots (excluding the example with  $m_p = 100$  GeV). We also checked that this statement is robust under variations in the cut parameter choices made above.

#### 6.4.3 Variation in $M_{T2}^{\max}$

In generating Figs. 6.5-6.8 we assumed that the  $M_{T2}^{\max}$  endpoint has been measured precisely and matches the theoretical value. In [149], another  $M_{T2}$  based variable,  $M_{T2\perp}$ , was introduced, which is the projection of  $M_{T2}$  along the direction perpendicular to the USR. They show that the endpoint of this distribution is independent of the USR momentum



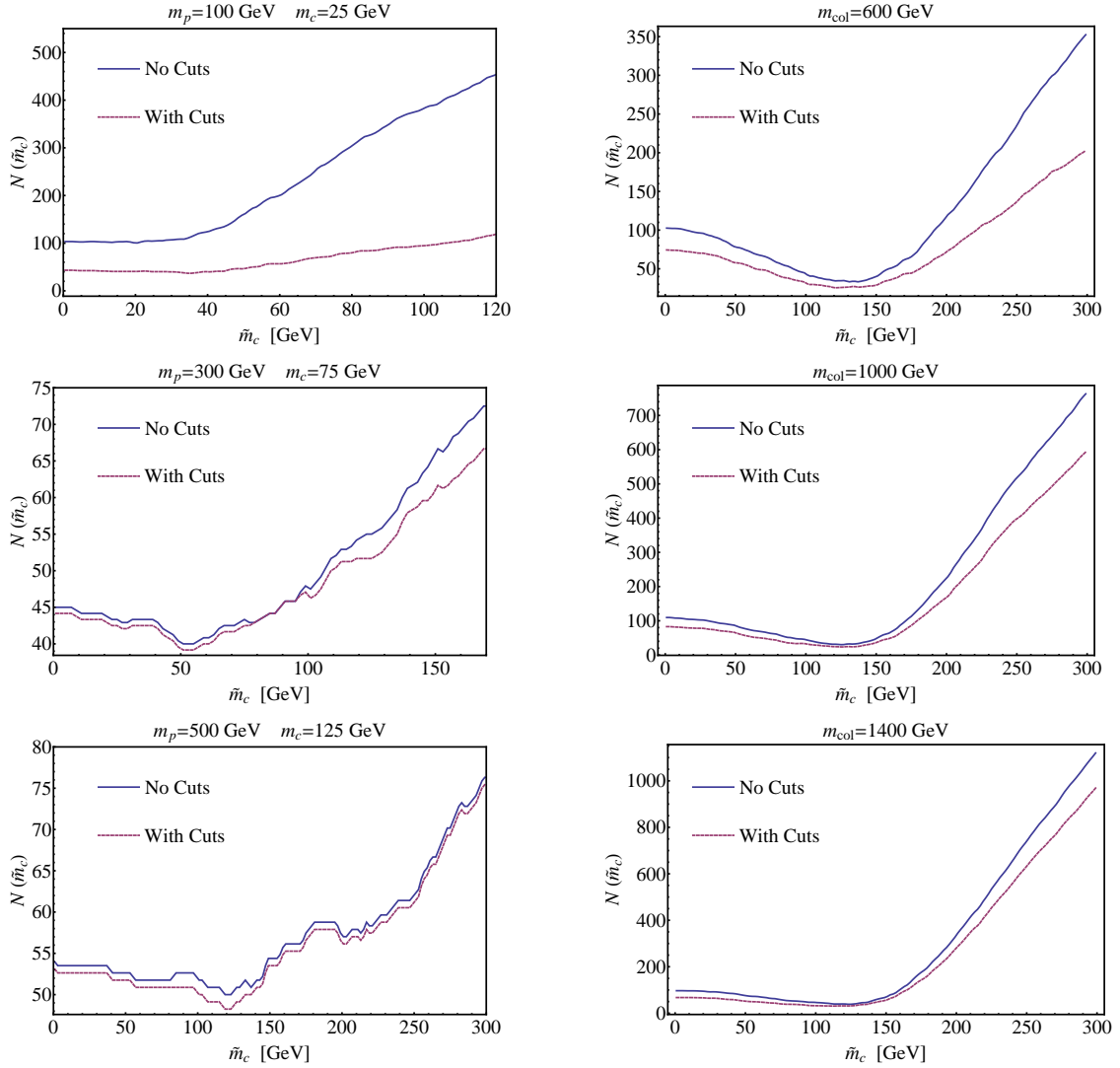


Figure 6.11:  $M_{T2}$  bowl for 25,000 (10,000) slepton (squark) pair production events which give jets, two muons and missing energy. The bowls on the left column only have QCD ISR. The bowls on the right have additional colored states which dominate the USR, and we have taken  $m_p = 300$  GeV and  $m_c = 150$  GeV for these cases. Note that the cuts preserve the minimum in all cases except  $m_p = 100$  GeV. Additionally, when one does a cut on  $M_{T2}(\tilde{m}_c = 0)$ , the bowl will be unaffected as long as this cut is taken below  $M_{T2}^{\max}$  for the bowl in question.

and identical to  $M_{T_2}^{\max}(\tilde{m}_c, 0)$  endpoint. Hence, even in cases with large USR, it is possible to extract the required input to construct the bowls.

However, the level of accuracy with which  $M_{T_2}^{\max}(\tilde{m}_c, 0)$  can be measured depends on detector effects. For the purposes of illustration, in Fig. 6.12, we show how the  $M_{T_2}$  bowl is degraded as one varies the  $M_{T_2}^{\max}$  endpoint by  $\pm 2\%$  and  $\pm 5\%$  for  $m_p = 300$  GeV and  $m_c = 150$  GeV. For variations on the order of  $-5\%$  the minimum is shifted by a non-trivial amount and can even disappear in some cases. For overestimates of  $M_{T_2}^{\max}$  of order  $5\%$ , the width of the minimum becomes much broader than the statistical error bars presented above. Therefore, it is crucial to the success of this method that an accurate measurement of the  $M_{T_2}$  endpoint be made. On the other hand, the steepness of the bowl around the minimum is maximized for the correct choice of  $M_{T_2}^{\max}$ . By combining this observation with the direct measurement of the endpoint, the accuracy with which  $M_{T_2}^{\max}$  could be determined would be improved. The accuracy with which this can be done is left for future work, though it can likely be done with high precision due to the larger amount of statistics available than for the bowls.

## 6.5 Discussion and Conclusions

In this work we studied the possibility of using  $n = 1$  single stage cascade decays to measure the DM mass at the LHC. We have argued, using the particular  $M_{T_2}$  variant of [149], that if a signal is observable and backgrounds can be eliminated, it is possible to make  $\mathcal{O}(10\%)$  measurements of the DM mass with  $\mathcal{O}(10,000)$  events before cuts for optimal values of  $m_p$  and  $m_c$ . We have shown that this requires a precise determination of  $M_{T_2}^{\max}(\tilde{m}_c, 0)$ .

In [14] the matrix element technique was used to ascertain how well the neutralino mass could be measured in an  $n = 1$  squark decay for a benchmark model with a parent mass of 561 GeV and a child mass of 97 GeV. Using parton level events so that jet smearing

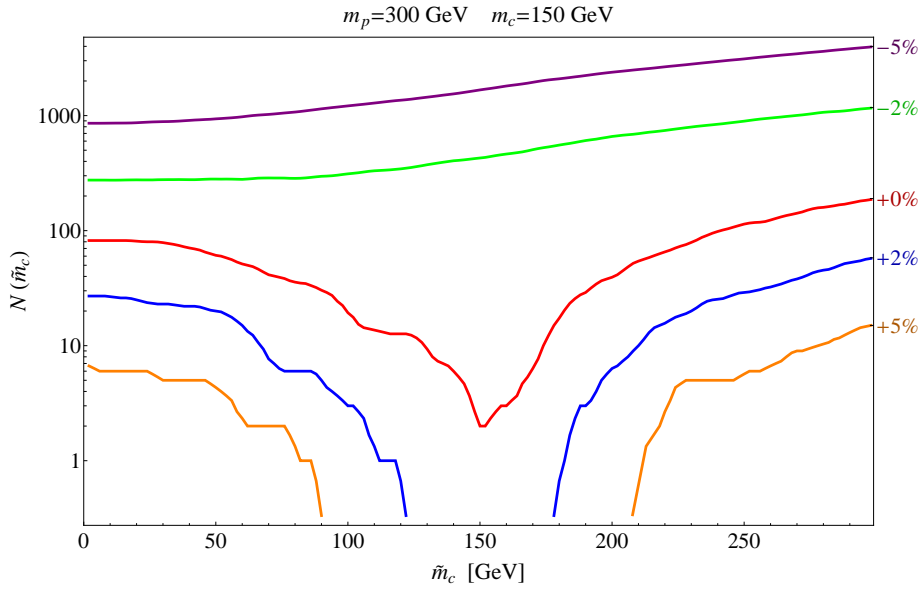


Figure 6.12: Plot of  $M_{T2}$  bowls allowing for variations in the  $M_{T2}^{\max}$  endpoint of  $\pm 5\%$  and  $\pm 2\%$ . All bowls are made with 50,000 smuon pair production events before cuts. For clarity we have not simulated detector effects for these events.

effects, *etc.*, are not considered, they found that with 3000 events before cuts only an upper limit on the child mass could be determined and with 7500 events a measurement could be made with an  $\mathcal{O}(100\%)$  error bar. This can be compared with our Fig. 6.7 for the benchmark  $m_p = 500$  GeV and  $m_c = 125$  GeV<sup>2</sup>. We find that with 3000 events we can make an  $\mathcal{O}(70\%)$  determination and for 7500 events error bar goes down to  $\mathcal{O}(50\%)$  once the correction for detector effects is applied as described above in Sec. 6.4.1. Hence, the methods seem to be competitive, but ultimately a detailed study will be required to determine which will lead to the best DM mass determination.

Finally, we would like to emphasize the model independence of these results, even when there are complicated cascade decays. A large class of events can be interpreted as  $n = 1$  processes with USR. All that is required is that the only missing energy in event is produced at the end of the chain as the result of the decay of an on-shell parent, and that the USR be distinguishable from the decay product of the parent. When this isolation is possible (*e.g.* the two photon plus missing energy signal of some gauge mediated SUSY breaking

<sup>2</sup>Note that since they did not include the effects of ISR, these error bars are a conservative estimate.

models) our results can be applied up to differences due to detector effects.

## CHAPTER VII

### Summary and Conclusions

This is an exciting era for fundamental physics. The LHC is running, direct detection (DD) experiments are probing a well motivated region of parameter space, and data from indirect detection experiments continues to accumulate. It is not unreasonable to believe that all of this information will culminate in a new and deeper understanding of the laws of nature and the composition of our Universe. The goal of this thesis is to attempt progress in exploring some new theoretical ideas in dark matter (DM) model building while also working to understanding what we can actually learn from the upcoming experimental results.

We presented three new possible explanations for DM and the corresponding phenomenology. The first model demonstrates that it is possible for the DM mass and/or couplings at freeze-out, which are relevant for determining the relic abundance, could have been different from the ones we would observe today. This requires the introduction of a new scalar field which would have undergone a low temperature phase transition. We discussed the experimental implications of this type of phase transition sector and the possibilities for reconstructing this cosmological history.

The next two theories are both examples of asymmetric dark matter (ADM) — models where the DM relic density is set by the baryon asymmetry. The first one provides a simple SUSY realization of the ADM paradigm by introducing a new DM sector with an Abelian

gauge symmetry. By introducing kinetic mixing between this new “dark photon” and the hypercharge gauge boson, we can generate the GeV scale for the DM mass dynamically, efficiently annihilate away the symmetric component of the DM relic density, and predict observable signals for DD.

The second ADM model is motivated by the PAMELA positron excess. The requirement of a leptophilic DM candidate implies that the DM carries lepton number and its relic density is therefore set by the lepton asymmetry. In order to explain the PAMELA signal, the DM must have a mass of order 100 GeV. Hence, the process which transfers the asymmetry must be in equilibrium until after the DM becomes non-relativistic. A small Majorana mass for the DM must be introduced in order for the relic density to be symmetric today. Since this mass term violates lepton number, it can be utilized to generate masses for the SM neutrinos at 1-loop. The renormalizable completion of the model implies the existence of an additional Higgs boson which could be discovered at the LHC.

The rest of this thesis was devoted to exploring future experimental results in a semi-model independent fashion. Typically the two largest effective DM-nucleon operators which imply signal in DD experiments are spin-independent (SI) and spin-dependent (SD). If SD signals are the result of coupling to the  $Z^0$  boson, we argue that there will likely be observable signals in SI experiments as a consequence of Higgs boson exchange between the DM and nuclei. By exploring the conditions required for a robust correlation between these two signals, we show that if signals could appear in one type of experiment without implying a signal for the other there would be a non-trivial fine-tuning of unrelated parameters. Within the context of the MSSM, a desire to alleviate fine-tuning in the  $Z^0$  mass (and by assuming a thermal history for the Universe) implies that SI and SD experiments should see signals in currently running, or at least the next generation, of experiments.

We concluded with a study of DM mass determination at the LHC by utilizing single-

stage cascade decays. In order to extract the DM mass from this class of events we utilize a variation of the  $M_{T2}$  kinematic variable. In order to break kinematic degeneracies requires the modification of  $M_{T2}$  to include the effect of upstream radiation. We compute 1-sigma error bars on DM determination for a variety of parent and DM masses for events where the upstream radiation is due to initial state radiation and for the case when it comes from the decays of heavier states. We found that a measurement of a 150 GeV dark matter candidate can be made to  $\mathcal{O}(10\%)$  for a parent mass of 300 GeV with a production cross section of 100 fb and 100 fb<sup>-1</sup> of integrated luminosity at the 14 TeV LHC.

In anticipation of future signals, it is up to the theoretical physics community to be prepared for any possible scenario for how nature behaves. This means a continued push to explore consequences of the endless possibilities of the theory landscape by looking for new ways to generate the DM relic density, by finding new correlations between seemingly unrelated theoretical issues, by discovering (and eliminating?) tricky degeneracies among the signals from different models, and by proposing new experimental tests which will allow us to untangle the mathematical structures that underlie reality. Hopefully within the next few years we will make progress towards an answer to the nearly 80 year question — what is the dark matter?

## APPENDICES



## APPENDIX A

### Asymmetric Dark Matter from a GeV Hidden Sector

#### A.1 Models with $\mathcal{O}_{\text{asym}} \sim S^2 L H_u$ are not allowed

In this appendix, we argue that this operator is excluded. We begin by arguing for the allowed size of  $m_{\text{DM}}$  in models with this operator.

Since the size of  $m_{\text{DM}}$  is determined by when the asymmetry transfer decouples with respect to the EWPT, it depends on the size of  $M_{(-1)}$ . In particular, the process  $\psi\psi \leftrightarrow \nu^\dagger \tilde{\gamma}_d$ , which proceeds via  $t$ -channel  $S$  exchange, controls the transfer once  $\langle H_u \rangle \neq 0$ . Since the rate for this process is proportional to  $T$  for  $T_{\text{EWPT}} > T > m_S$ , it becomes more important as the temperature decreases. Therefore, if this process were ever in equilibrium it would necessarily lead to some washout since its decoupling would be controlled by the Boltzmann suppression of the DM. Requiring that this process not be in equilibrium for any  $T > m_S$  implies a bound

$$(A.1) \quad M_{(-1)} \gtrsim 3 \times 10^8 \text{ GeV} \left( \frac{\lambda}{0.1} \right) \left( \frac{14 \text{ GeV}}{m_S} \right)^{1/2}.$$

For the asymmetry transfer to decouple before  $T = T_{\text{EWPT}}$ , requires examination of the operator with  $\langle H_u \rangle = 0$ , which gives the condition:

$$(A.2) \quad M_{(-1)} \gtrsim 6 \times 10^7 \text{ GeV} \left( \frac{\lambda}{0.1} \right).$$

These two conditions together imply that in order to avoid washout, the asymmetry transfer must decouple at  $T > T_{\text{EWPT}}$ , and the DM mass is 14.2 GeV (see Eq. (III.15)).

For this operator, the decay  $\psi \rightarrow S^\dagger \nu^\dagger$  is allowed. This could give a non-trivial symmetric component of the DM today. If this decay rate is sizable, the constraints described in Sec. 3.3.3 are relevant which implies that  $\lambda \lesssim 0.1$ . In fact, given the CMB constraint, it is not possible to achieve a DM mass as large as the required 14.2 GeV. As described in Sec. 3.3.3, maximizing the ratio  $\epsilon/g_d$  yields the largest possible DM mass. Using Fig. 3.2, this ratio attains its maximum at  $(\epsilon/g_d)_{\max} \sim (7 \times 10^{-3}/7 \times 10^{-3})$ , which when combined with  $\lambda \sim 0.1$  implies  $m_S = 7.2$  GeV. Since this is far below 14.2 GeV, this scenario is excluded.

One might hope that the CMB constraint could be mitigated by ensuring that symmetric decays  $\psi \rightarrow \tilde{G}S$  dominate over the asymmetric decays. The decay width to gravitinos is given in Eq. (III.21) and to neutrinos is given by

$$(A.3) \quad \Gamma(\psi \rightarrow S^\dagger \nu^\dagger) = \frac{1}{32\pi} \frac{v^2 \sin^2 \beta (m_\psi^2 - m_S^2)^2}{M_{(-1)}^2 m_\psi^3}.$$

Then the branching ratio is given by

$$(A.4) \quad \text{BR}(\psi \rightarrow S\tilde{G}) = 1 - \text{BR}(\psi \rightarrow S^\dagger \nu^\dagger) = \frac{2M_{(-1)}^2 (m_\psi^2 - m_S^2)^2}{F^2 v^2 s_\beta^2 + 2M_{(-1)}^2 (m_\psi^2 - m_S^2)^2}.$$

To satisfy the CMB constraint for  $\lambda = 1$  requires that  $\text{BR}(\psi \rightarrow S^\dagger \nu) \lesssim 10^{-4}$ . For  $g_d = 10^{-1}$  and  $\epsilon = 4 \times 10^{-3}$ ,  $M_{(-1)} \gtrsim 10^{16}$  GeV. This implies the reheat temperature after inflation must be  $\sim 10^{16}$  GeV in order for this operator to ever have been in equilibrium, inconsistent with the lack of observation of tensor modes at WMAP [108].

## APPENDIX B

### On the Correlation Between the Spin-Independent and Spin-Dependent Direct Detection of Dark Matter

#### B.1 Squark Contributions to Direct Detection

The neutralino can scatter off of quarks via  $s$ -channel squark exchange, giving contributions to  $\mathcal{O}_q^{\text{SI}}$  or  $\mathcal{O}_q^{\text{SD}}$ . Only squarks that couple to the light quarks ( $u, d, s$ ) will be able to contribute to the SI and SD cross sections since only the light quarks have non-negligible nuclear matrix elements.

A non-zero “left-right” squark mixture is required since SI scattering converts a left-handed quark into a right-handed quark. Though a Bino/Wino mixture maximizes the coupling between the quarks and the neutralino, the scattering cross section for a pure Bino is of the same order.

If one makes the standard assumption that left-right squark mixing (*i.e.*  $a$ -terms) are proportional to Yukawa couplings, then the squark mixing angle is proportional to  $m_q/\tilde{m}_q$ . Therefore, all SI couplings will be proportional to a quark mass and there is no enhancement for the light squarks over Higgs boson exchange. The maximum cross section is

$$(B.1) \quad \left( \sigma_{\text{SI}}^{\text{squark}}(\chi N \rightarrow \chi N) \right)_{\text{max}} = 6 \times 10^{-9} \text{ pb} \left( \frac{200 \text{ GeV}}{\tilde{m}_s} \right)^4,$$

for a Bino-Wino mix. This is subdominant to the Higgs boson exchange contribution

barring the cancellations discussed in Sec. 5.5.4<sup>1</sup>.

The maximum  $\sigma_{\text{SD}}(\chi p \rightarrow \chi p)$  contribution from squark exchange is for a “left-handed” up-type squark coupling to a pure Wino, due to the larger  $SU(2)$  gauge coupling:

$$(B.2) \quad \left( \sigma_{\text{SD}}^{\text{squark}}(\chi p \rightarrow \chi p) \right)_{\text{max}} = 3 \times 10^{-4} \text{ pb} \left( \frac{200 \text{ GeV}}{\tilde{m}_u} \right)^4.$$

This is typically subdominant to the  $Z^0$  contribution to SD DD. Thus, we will focus on the effects of  $Z^0$  exchange in our discussions of the expected SD cross section.

## B.2 The Bino/Higgsino and Wino/Higgsino Limits

In the limit of large  $M_1$  ( $M_2$ ) the neutralino is dominantly a Wino/Higgsino (Bino/Higgsino) admixture. We can explore this effective 3 state system using the SDM defined as (see Eq. (V.26) above):

$$(B.3) \quad \mathcal{L}_{\text{SDM}} \ni \mu_D D \bar{D} + \lambda \mathbf{h} S D + \lambda' \mathbf{h}^* S \bar{D} + \frac{\mu_S}{2} S^2.$$

The resulting lightest eigenstate ( $\chi$ ) is specified by

$$(B.4) \quad \chi \equiv Z_S S + Z_D D + Z_{\bar{D}} \bar{D}.$$

Following [24], it is useful to write this system in a basis defined by  $S$  and  $D_{\pm} \equiv \frac{1}{\sqrt{2}}(D \pm \bar{D})$ .

Note that the labels  $\pm$  have nothing to do with electric charge. The mass matrix is then, in the  $(S, D_+, D_-)$  basis,

$$\mathcal{M}_{\text{SDM}} = \begin{pmatrix} \mu_S & \frac{1}{\sqrt{2}}(\lambda + \lambda')v & \frac{1}{\sqrt{2}}(\lambda - \lambda')v \\ \frac{1}{\sqrt{2}}(\lambda + \lambda')v & \mu_D & 0 \\ \frac{1}{\sqrt{2}}(\lambda - \lambda')v & 0 & -\mu_D \end{pmatrix},$$

with the resulting lightest eigenstate,

$$(B.5) \quad \chi \equiv Z_S S + Z_{D_+} D_+ + Z_{D_-} D_-.$$

<sup>1</sup>If exceptionally large left-right in the squark sector is allowed (perhaps through abnormally large  $a$ -terms) a contribution to  $\sigma_{\text{SI}}(\chi N \rightarrow \chi N)$  of  $\mathcal{O}(10^{-3} \text{ pb})$  may be obtained.

Since we are interested in the SD DD cross section, our goal is to extract the coupling of  $\chi$  to the  $Z^0$ . The coefficient of the operator  $\mathcal{O}_q^{\text{SD}}$  of Eq. (V.10) is given by

$$(B.6) \quad d_q = -\frac{g^2}{4m_Z^2 c_w^2} |2Z_{D+} Z_{D-}|^2 T_3^q.$$

Note that  $|2Z_{D+} Z_{D-}| \equiv |Z_D|^2 - |Z_{\bar{D}}|^2$ . One can find analytic expressions for the mass eigenstates and the combination  $|2Z_{D+} Z_{D-}|$  in various useful limits. To second order in  $v$ , for  $|\mu_D|, |\mu_S|, (|\mu_D| - |\mu_S|) \gg \lambda v, \lambda' v$

$$(B.7) \quad m_\chi = \mu_S - \frac{2\lambda\lambda'v^2}{\mu_D} - \frac{(\lambda^2 + \lambda'^2)v^2\mu_S}{\mu_D^2}$$

$$(B.8) \quad |2Z_{D+} Z_{D-}| = \frac{(\lambda'^2 - \lambda^2)v^2}{\mu_D^2 - \mu_S^2},$$

and for  $|\mu_D| = |\mu_S| \gg \lambda v, \lambda' v$ ,

$$(B.9) \quad m_\chi = \mu_S - \frac{1}{\sqrt{2}}|\lambda + \lambda'|v + \frac{(\lambda - \lambda')^2 v^2}{8\mu_S}$$

$$(B.10) \quad |2Z_{D+} Z_{D-}| = \frac{(\lambda' - \lambda)v}{2\sqrt{2}|\mu_S|} + \frac{(\lambda'^2 - \lambda^2)v^2}{8\mu_S^2}.$$

Perturbing away from the limit of exact degeneracy gives corrections to these expressions of  $\mathcal{O}((\mu_S - \mu_D)/\mu_D)$ . Note we have assumed that there is no CP violation for simplicity.

In order to apply these expressions to the MSSM one can make the identifications

SDM	Bino/Higgsino	Wino/Higgsino
$\mu_S$	$M_1$	$M_2$
$\mu_D$	$\mu$	$\mu$
$\lambda v$	$-m_Z s_w c_\beta$	$m_Z c_w c_\beta$
$\lambda' v$	$-m_Z s_w s_\beta$	$m_Z c_w s_\beta$

where we neglect terms of  $\mathcal{O}(1/M_2)$  for the Bino/Higgsino system and  $\mathcal{O}(1/M_1)$  for the Wino/Higgsino system.

Explicitly making the substitutions for the MSSM we have

$$(B.11) \quad \begin{aligned} |Z_{H_d}|^2 &= |Z_{H_u}|^2 \\ &= \begin{cases} \frac{c_{2\beta} s_w^2 m_Z^2}{\mu^2 - M_1^2} & \text{for } |M_1|, |\mu|, |\mu| - |M_1| > m_Z, M_2 \rightarrow \infty \\ \frac{c_{2\beta} c_w^2 m_Z^2}{\mu^2 - M_2^2} & \text{for } |M_2|, |\mu|, |\mu| - |M_2| > m_Z, M_1 \rightarrow \infty, \end{cases} \end{aligned}$$

and

$$(B.12) \quad \begin{aligned} |Z_{H_d}|^2 &= |Z_{H_u}|^2 \\ &= \begin{cases} \frac{(s_\beta - c_\beta) s_w m_Z}{2\sqrt{2}|\mu|} + \frac{(s_\beta^2 - c_\beta^2) s_w^2 m_Z^2}{8\mu^2} & \text{for } |M_1| = |\mu| > m_Z, M_2 \rightarrow \infty \\ \frac{(s_\beta - c_\beta) c_w m_Z}{2\sqrt{2}|\mu|} + \frac{(s_\beta^2 - c_\beta^2) c_w^2 m_Z^2}{8\mu^2} & \text{for } |M_2| = |\mu| > m_Z, M_1 \rightarrow \infty. \end{cases} \end{aligned}$$

### B.3 No-go Theorem for photino-Higgsino DM

The neutralino mass matrix in the  $(\tilde{\gamma}, \tilde{Z}, \tilde{H}_d, \tilde{H}_u)$  basis is given by

$$\mathcal{M} = \begin{pmatrix} M_1 c_w^2 + M_2 s_w^2 & (M_1 - M_2) c_w s_w & -m_Z s_{2w} c_\beta & m_Z s_{2w} s_\beta \\ (M_1 - M_2) c_w s_w & M_1 s_w^2 + M_2 c_w^2 & m_Z c_{2w} c_\beta & -m_Z c_{2w} s_\beta \\ -m_Z s_{2w} c_\beta & m_Z c_{2w} c_\beta & 0 & -\mu \\ m_Z s_{2w} s_\beta & -m_Z c_{2w} s_\beta & -\mu & 0 \end{pmatrix}.$$

Is it possible to generate a large SD/SI ratio by having DM which is only a mixture of photino and Higgsino? The Higgsino component is required for a non-trivial coupling to the  $Z^0$  and an admixture of photino (and not Zino) will allow  $(|Z_{H_d}|^2 - |Z_{H_u}|^2) \neq 0$  without introducing a coupling to the Higgs. We show that current phenomenological bounds preclude this possibility.

There are two potential options. The first is decoupling the Zino by making it heavy while tuning the photino mass to be  $\sim \mu$ . This implies taking the limit where  $M_1$  and  $M_2$  are large while the combination  $M_1 c_w^2 + M_2 s_w^2$  stays small, which requires  $\text{sgn}(M_1) \neq \text{sgn}(M_2)$ . Then the Zino-photino mixing will go like  $(M_1 - M_2)/m_{\tilde{Z}} > \mathcal{O}(1)$ . Note that we are free to take  $M_1 < m_Z$  to suppress this mixing, but due to the LEP bound on the

chargino mass,  $M_2 > m_Z$ . The second option is to try to eliminate the photino-Zino mixing by taking  $M_1 = M_2$ . Then the Zino and photino have the same mass and the Higgsino will mix with both, resulting in a DM state which is an equal admixture of all 4 gauge eigenstates. Therefore, a neutralino cannot be a mixture of only photino and Higgsino.

## APPENDIX C

## Extracting the Dark Matter Mass from Single Stage Cascade Decays at the LHC

### C.1 Benchmark Models

The  $n = 1$  events studied here are the simplest class of events at the LHC which involve the DM. Perhaps the most commonly studied of such processes is  $pp \rightarrow \tilde{q}\tilde{q} \rightarrow jj\tilde{\chi}^0\tilde{\chi}^0$ . In such models, however, one expects there to be higher  $n$  processes present as well which will give additional kinematic information. In this appendix we will outline examples of  $n = 1$  process with scalar, fermionic and vector parents. Estimates for the electroweak LHC cross sections for these models are given in Table 6.1.

#### C.1.1 Scalar Parents

We begin by motivating scalar parents. Recently, a wave of leptophilic DM models have been proposed to explain measured cosmic ray anomalies. A non-supersymmetric example, which is additionally motivated by the baryon-DM coincidence, can be constructed by simply extending the SM by two additional fields: a new Higgs doublet,  $H'$ , and a leptophilic DM state,  $X$ , interacting via [140]

$$(C.1) \quad \mathcal{L} = \bar{X}LH' + m_X\bar{X}X.$$

When the additional term

$$(C.2) \quad \Delta\mathcal{L} = \lambda(H^\dagger H')^2 + \text{h.c.}$$



is added to the Lagrangian, where  $H$  is the SM Higgs doublet, and the  $H'$  is integrated out, the effective operator

$$(C.3) \quad \mathcal{L}_{\text{asym}} = \frac{\bar{X}^2 L H L H}{M^4}$$

is generated, where  $M$  is the effective suppression scale. This operator transfers the lepton asymmetry to the DM sector, so that the DM density is set by an asymmetry and not thermal freeze-out. Also note that such leptophilic DM candidates can be viable as an explanation for the observation of an excesses of cosmic ray positrons by the PAMELA experiment [81]. Although the DM would be asymmetric (*i.e.* mostly  $\bar{X}$ ) when its density freezes in, that asymmetry could be erased through Majorana mass terms for  $\bar{X}$  and  $X$ . Then in the universe today,  $X\bar{X} \rightarrow \ell^+\ell^-$  may give rise to significant cosmic ray positron signals.

The DM would be created at the collider through the electroweak production of the  $H'$ ,

$$(C.4) \quad pp \rightarrow H' H' \rightarrow X \bar{X} \ell^+ \ell^-.$$

However, production rates for  $pp \rightarrow H' H' \rightarrow X \bar{X} \ell^+ \ell^-$  will be low (see Table 6.1). While these events could be extracted from the large di-boson background with high luminosity, DM mass determination will be difficult.

Note that this process is identical to the electroweak pair production of sleptons (see [35] for a study which determines how feasible it is to find these processes at the LHC),

$$(C.5) \quad pp \rightarrow \tilde{\ell}^+ \tilde{\ell}^- \rightarrow \ell^+ \ell^- \tilde{\chi}^0 \tilde{\chi}^0.$$

### C.1.2 Fermionic Parents

For an example with fermionic parents, we turn to a model which is embedded within the MSSM. Introduce a superfield DM candidate,  $X$ , with the quantum numbers of a sterile neutrino. Then the active sneutrino can mix with scalar partner for  $X$ ,  $\tilde{X}$ , leading

to mixed sneutrino DM. In [28, 126, 190],  $\tilde{X}$  has been shown to be a viable DM candidate.

At the LHC, electroweak production can go through

$$(C.6) \quad pp \rightarrow \tilde{\chi}^+ \tilde{\chi}^- \rightarrow \tilde{X} \tilde{X}^* \ell^+ \ell^-,$$

where  $\tilde{\chi}^\pm$  is a chargino. Since the parent particles are fermions instead of scalars, the production rates are larger (see Table 6.1).

With a slight modification, these classes of DM models can be related to the lepton asymmetry. One can add a new pair of electroweak doublet superfields,  $D$  and  $\bar{D}$ , and a new superpotential term,

$$(C.7) \quad \Delta\mathcal{W} = m_D \bar{D} D + \lambda \bar{X} D H_u + y_i L_i \bar{D} \bar{X} + m_X \bar{X} X,$$

where  $m_D$  is the mass for  $D$ ,  $m_X$  is the mass for  $X$  and  $\lambda$  is a new yukawa coupling.

Integrating out these doublet states results in the lepton number transferring operator

$$(C.8) \quad \mathcal{W}_{\text{asym}} = \frac{\bar{X}^2 L H_u}{M},$$

where  $M$  is the effective suppression scale. This operator can be used to generate the relic density. The production at the collider then goes through the electroweak production of the fermionic  $\tilde{D}$ :

$$(C.9) \quad pp \rightarrow \tilde{D}^+ \tilde{D}^- \rightarrow \tilde{X} \tilde{X}^* \ell^+ \ell^-.$$

Production rates in all these fermionic parent models can further be enhanced by embedding the  $n = 1$  process into squark decays:

$$(C.10) \quad pp \rightarrow \tilde{q} \tilde{q} \rightarrow \tilde{\chi}^+ \tilde{\chi}^- j j \rightarrow \tilde{\nu} \tilde{\nu}^* \ell^+ \ell^- j j$$

As described above (see Fig. 6.4), this will lead to a much harder USR distribution, which in turn will imply better DM mass determination.

### C.1.3 Vector Parents

Lastly, we note that within UED models, pair production of vectors gives rise to similar signals. For example,

$$(C.11) \quad pp \rightarrow W^{(1)+} W^{(1)-} \rightarrow \ell^+ \ell^- \nu^{(1)} \bar{\nu}^{(1)},$$

where  $W^{(1)\pm}$  is a KK  $W$ -boson,  $\nu^{(1)}$  is a KK neutrino is an  $n = 1$  chain. This process can similarly be embedded in the decay of new colored states, which gives rise to harder USR:

$$(C.12) \quad pp \rightarrow Q^{(1)} \bar{Q}^{(1)} \rightarrow W^{(1)+} W^{(1)-} jj \rightarrow \ell^+ \ell^- \nu^{(1)} \bar{\nu}^{(1)} jj,$$

where  $Q^{(1)}$  is a KK quark. Note that if  $\nu^{(1)}$  is the DM its mass is restricted to be greater than  $\mathcal{O}(50 \text{ TeV})$  by direct detection experiments [181].

## C.2 Phase Space Dependence on $M_{T2}$

To show the phase space dependence on  $M_{T2}$  and the overall scale  $m_p$ , we will assume that the parents are produced on-shell so that the  $2 \rightarrow 4$  production in Fig. C.1 can be approximated by the  $2 \rightarrow 2$  cross section  $\sigma_{2 \rightarrow 2}$  and parent particle decay width  $\Gamma$ .

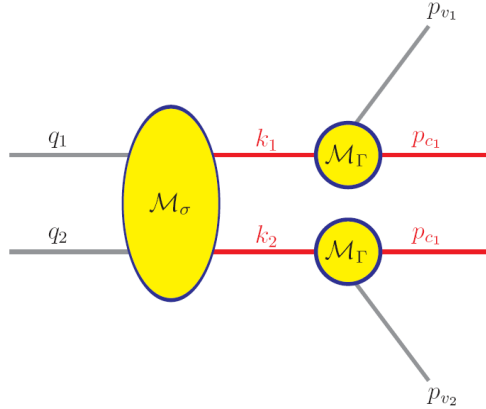


Figure C.1: Process considered in this section. The proton momenta are  $q_i$ , the parent momenta are  $k_i$ , the visible momenta are  $p_{v_i}$  and the child momenta are  $p_{c_i}$ .

We begin by simplifying the general  $2 \rightarrow 2$  differential cross-section and  $1 \rightarrow 2$  differential decay width. Throughout the calculation we will drop overall constants since they do not contribute to the normalized distributions. The  $2 \rightarrow 2$  differential cross-section is given by

$$(C.13) \quad d\sigma_{2 \rightarrow 2} = \frac{1}{4 |\vec{q}_1|_{\text{CM}} \sqrt{\hat{s}}} |\mathcal{M}_\sigma|^2 (2\pi)^4 \delta^4(q_1 + q_2 - k_1 - k_2) \frac{1}{2 E_1} \frac{d^3 k_1}{(2\pi)^3} \frac{1}{2 E_2} \frac{d^3 k_2}{(2\pi)^3},$$

where  $\sqrt{\hat{s}}$  is the parton center-of-mass (CM) energy and  $E_i$  is the energy of the  $i^{\text{th}}$  parent.

Integrating over  $\vec{k}_2$  in the CM frame to eliminate  $\delta^3(\vec{q}_1 + \vec{q}_2 - \vec{k}_1 - \vec{k}_2)$  gives

$$(C.14) \quad d\sigma_{2 \rightarrow 2} \propto \frac{1}{\hat{s}} |\mathcal{M}_\sigma|^2 \frac{1}{E_1 E_2} \delta(\sqrt{\hat{s}} - E_2 - E_1) d^3 k_1,$$

where  $\vec{k}_2 = -\vec{k}_1$ . Similarly, we simplify the  $1 \rightarrow 2$  differential decay widths

$$(C.15) \quad d\Gamma_i = \frac{1}{2 E_i} |\mathcal{M}_\Gamma|^2 (2\pi)^4 \delta^4(k_i - p_{v_i} - p_{c_i}) \frac{1}{2 E_{v_i}} \frac{d^3 p_{v_i}}{(2\pi)^3} \frac{1}{2 E_{c_i}} \frac{d^3 p_{c_i}}{(2\pi)^3},$$

where  $c$  and  $v$  stand for child and visible, respectively, and  $i = 1, 2$ . Integrating over  $\vec{p}_{c_i}$  to eliminate  $\delta^3(\vec{k}_i - \vec{p}_{c_i} - \vec{p}_{v_i})$  gives

$$(C.16) \quad d\Gamma_i \propto \frac{1}{E_i E_{c_i} E_{v_i}} |\mathcal{M}_\Gamma|^2 \delta(E_i - E_{c_i} - E_{v_i}) d^3 p_{v_i},$$

where the  $\delta$ -function enforces  $\vec{p}_{c_i} = \vec{k}_i - \vec{p}_{v_i}$ . Since for  $1 \rightarrow 2$  decays the summed and squared matrix elements  $|\mathcal{M}_{\Gamma_i}|^2$  are only functions of the masses, they will not contribute to the normalized distributions. We drop these factors from here forward.

Convolving the differential parent decay width with the differential  $2 \rightarrow 2$  cross section, and again dropping overall constant factors gives

$$(C.17) \quad d\sigma = d\sigma_{2 \rightarrow 2} d\Gamma_1 d\Gamma_2 \\ \propto \frac{|\mathcal{M}_\sigma|^2}{\hat{s}} \frac{\delta(\sqrt{\hat{s}} - 2 E_1) \delta(E_1 - E_{c_1} - E_{v_1}) \delta(E_2 - E_{c_2} - E_{v_2})}{E_1^4 E_{c_1} E_{v_1} E_{c_2} E_{v_2}} d^3 k_1 d^3 p_{v_1} d^3 p_{v_2}.$$

Define  $\cos \beta_i$  to be the angle between the visible particle momenta and the parent particle:

$$(C.18) \quad \vec{k}_i \cdot \vec{p}_{v_i} \equiv k_i p_{v_i} \cos \beta_i.$$

Rewriting the phase space delta functions so that  $\cos \beta_1$ ,  $\cos \beta_2$ , and  $k_1/m_p$  are the integration variables, the integrand takes on a more revealing form

$$\begin{aligned}
d\sigma_{2 \rightarrow 2} d\Gamma_1 d\Gamma_2 &\propto d\left(\frac{k_1}{m_p}\right) dp_{v_1} dp_{v_2} d\Omega_1 d(\cos \beta_{v_1}) d(\cos \beta_{v_2}) d\phi_{v_1} d\phi_{v_2} \\
&\times \frac{|\mathcal{M}_\sigma|^2}{\tilde{s}^{5/2} \sqrt{\tilde{s}-1}} \mathcal{J}(\theta_1, \theta_{v_1}, \theta_{v_2} : \theta_1, \beta_{v_1}, \beta_{v_2}) \delta\left(\frac{k_1}{m_p} - \sqrt{\tilde{s}-1}\right) \\
\text{(C.19)} \quad &\times \delta\left(\cos \beta_1 - \frac{\mu - p_{v_1} \sqrt{\tilde{s}}}{p_{v_1} \sqrt{\tilde{s}-1}}\right) \delta\left(\cos \beta_2 - \frac{\mu - p_{v_2} \sqrt{\tilde{s}}}{p_{v_2} \sqrt{\tilde{s}-1}}\right),
\end{aligned}$$

where  $\mathcal{J}(\dots)$  is the Jacobian for converting from integration over the  $\theta$  angles to the  $\beta$  angles, which does not depend on any mass parameters,  $\mu$  is defined as in the main body of the paper (see Eq. (VI.6)), and

$$\text{(C.20)} \quad \tilde{s} \equiv \frac{\hat{s}}{4m_p^2}.$$

Hence, Eq. (C.19) shows that the phase space only depends on the parent and child mass through the two functions  $\tilde{s}$  and  $\mu$ . Note that when integrating over the parton distribution functions (PDFs), the factor  $1/(1-\tilde{s})^2$  will cause the differential cross-section to be dominated by values  $\tilde{s} \sim 1$ , which corresponds to threshold production of the parent particles. Therefore, for a trivial cross section matrix element, *the differential cross section only depends on the  $m_p$  and  $m_c$  through the combination  $2\mu = M_{T_2}^{\max}(\tilde{m}_c = 0) = (m_p^2 - m_c^2)/m_p$* . Note that in some cases,  $\mathcal{M}_\sigma$  will depend explicitly on  $m_p$ , or masses of particles being exchanged in the corresponding Feynmann diagram, causing slight deviations in the normalized distributions for the same  $M_{T_2}^{\max}$ , but different parent mass.

In Fig. C.2, we plot various normalized distributions with the same  $M_{T_2}^{\max}(\tilde{m}_c = 0)$  endpoint. With the exception of a weak dependence on the parent mass, due to  $\hat{s}$  dependence, the distributions look virtually identical. Note that it is this weak  $\hat{s}$  dependence that the matrix element methods seek to capitalize on.

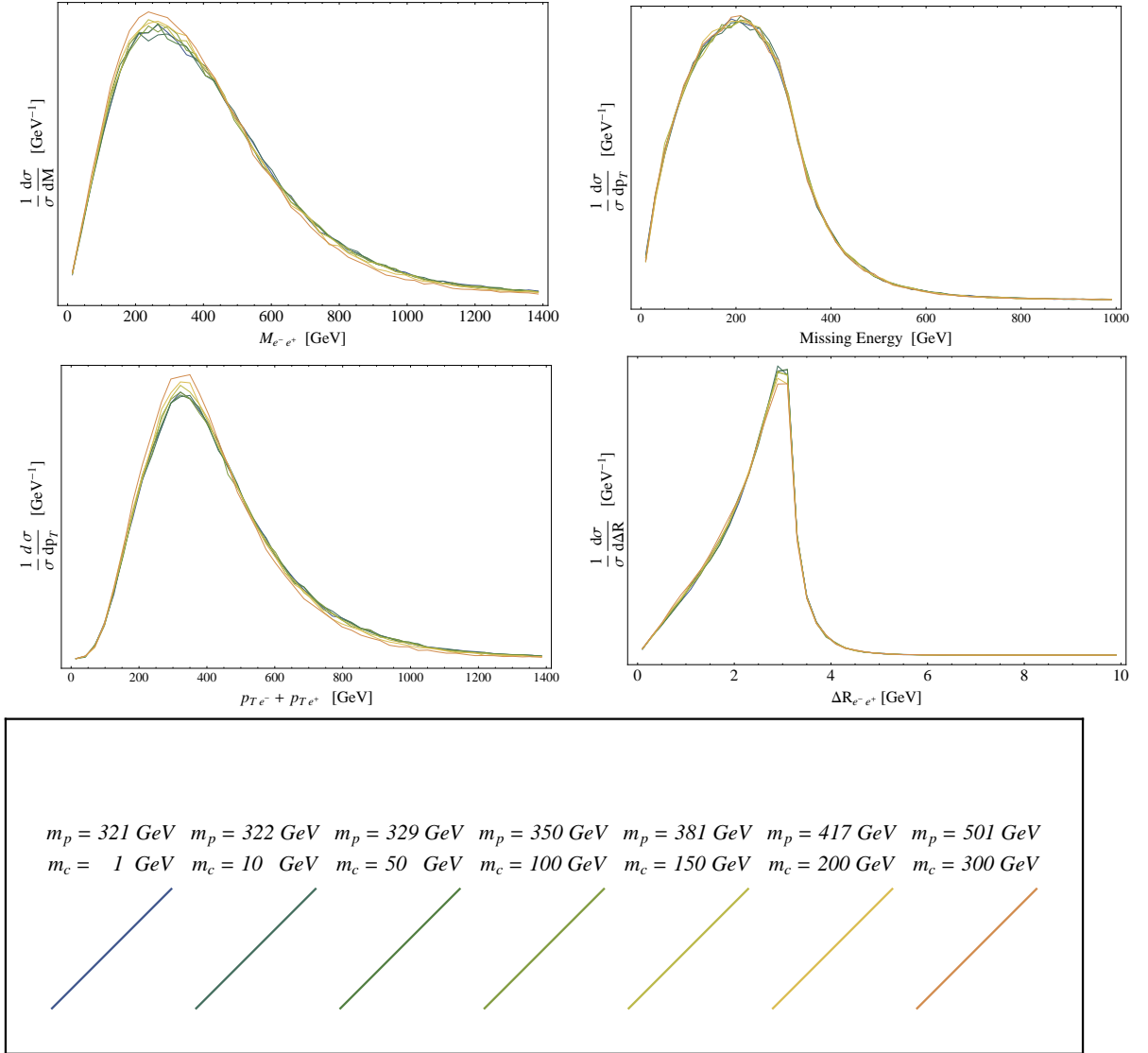


Figure C.2: Various distributions for points with the same  $M_{T2}$  endpoint for  $pp \rightarrow \tilde{\ell}^+ \tilde{\ell}^- \rightarrow \ell^+ \ell^- \tilde{\chi}^0 \tilde{\chi}^0$ . As shown in Appendix C.2, the data only depends on  $M_{T2}^{\text{max}}$  with a slight variation due to  $\hat{s}/(4m_p^2)$ . The distributions plotted are the invariant mass of the two visible particles (upper left), the total missing transverse energy (upper right), the total transverse momentum of the visible particles (lower left), and  $\Delta R = \sqrt{\Delta\eta^2 + \Delta\phi^2}$  between the two visible particles (lower right).

## BIBLIOGRAPHY

## BIBLIOGRAPHY

- [1] C. E. Aalseth et al. Results from a Search for Light-Mass Dark Matter with a P- type Point Contact Germanium Detector. 2010.
- [2] V. M. Abazov et al. Search for dark photons from supersymmetric hidden valleys. *Phys. Rev. Lett.*, 103:081802, 2009.
- [3] R. Abbasi et al. Limits on a muon flux from neutralino annihilations in the Sun with the IceCube 22-string detector. *Phys. Rev. Lett.*, 102:201302, 2009.
- [4] Aous A. Abdo et al. Measurement of the Cosmic Ray  $e^+$  plus  $e^-$  spectrum from 20 GeV to 1 TeV with the Fermi Large Area Telescope. *Phys. Rev. Lett.*, 102:181101, 2009.
- [5] S. A. Abel, Subir Sarkar, and P. L. White. On the cosmological domain wall problem for the minimally extended supersymmetric standard model. *Nucl. Phys.*, B454:663–684, 1995.
- [6] Bobby Samir Acharya, Gordon Kane, Scott Watson, and Piyush Kumar. A Non-thermal WIMP Miracle. *Phys. Rev.*, D80:083529, 2009.
- [7] Oscar Adriani et al. An anomalous positron abundance in cosmic rays with energies 1.5-100 GeV. *Nature*, 458:607–609, 2009.
- [8] Ian Affleck and Michael Dine. A New Mechanism for Baryogenesis. *Nucl.Phys.*, B249:361, 1985.
- [9] Kaustubh Agashe, Adam Falkowski, Ian Low, and Geraldine Servant. KK Parity in Warped Extra Dimension. *JHEP*, 0804:027, 2008.
- [10] M. Aguilar et al. Cosmic-ray positron fraction measurement from 1-GeV to 30- GeV with AMS-01. *Phys. Lett.*, B646:145–154, 2007.
- [11] Z. Ahmed et al. Results from the Final Exposure of the CDMS II Experiment. 2009.
- [12] Z. Ahmed et al. Search for Weakly Interacting Massive Particles with the First Five-Tower Data from the Cryogenic Dark Matter Search at the Soudan Underground Laboratory. *Phys. Rev. Lett.*, 102:011301, 2009.
- [13] Johan Alwall, Pavel Demin, Simon de Visscher, Rikkert Frederix, Michel Herquet, et al. MadGraph/MadEvent v4: The New Web Generation. *JHEP*, 0709:028, 2007.
- [14] Johan Alwall, Ayres Freitas, and Olivier Mattelaer. Measuring Sparticles with the Matrix Element. *AIP Conf.Proc.*, 1200:442–445, 2010.
- [15] C. Amsler et al. Review of particle physics. *Phys. Lett.*, B667:1, 2008.
- [16] Haipeng An, Shao-Long Chen, Rabindra N. Mohapatra, Shmuel Nussinov, and Yue Zhang. Energy Dependence of Direct Detection Cross Section for Asymmetric Mirror Dark Matter. 2010.
- [17] Greg W. Anderson and Sean M. Carroll. Dark matter with time-dependent mass. 1997.



- [18] J. Angle et al. First Results from the XENON10 Dark Matter Experiment at the Gran Sasso National Laboratory. *Phys. Rev. Lett.*, 100:021303, 2008.
- [19] J. Angle et al. First Results from the XENON10 Dark Matter Experiment at the Gran Sasso National Laboratory. *Phys. Rev. Lett.*, 100:021303, 2008.
- [20] Thomas Appelquist, Hsin-Chia Cheng, and Bogdan A. Dobrescu. Bounds on universal extra dimensions. *Phys.Rev.*, D64:035002, 2001.
- [21] E. Aprile et al. First Dark Matter Results from the XENON100 Experiment. *Phys.Rev.Lett.*, 105:131302, 2010.
- [22] S. Archambault et al. Dark Matter Spin-Dependent Limits for WIMP Interactions on 19-F by PICASSO. *Phys. Lett.*, B682:185–192, 2009.
- [23] N. Arkani-Hamed, A.G. Cohen, E. Katz, and A.E. Nelson. The Lightest Higgs. *JHEP*, 0207:034, 2002.
- [24] N. Arkani-Hamed, A. Delgado, and G. F. Giudice. The well-tempered neutralino. *Nucl. Phys.*, B741:108–130, 2006.
- [25] Nima Arkani-Hamed, Savas Dimopoulos, and G.R. Dvali. The Hierarchy problem and new dimensions at a millimeter. *Phys.Lett.*, B429:263–272, 1998.
- [26] Nima Arkani-Hamed, Savas Dimopoulos, and Shamit Kachru. Predictive landscapes and new physics at a TeV. 2005.
- [27] Nima Arkani-Hamed, Douglas P. Finkbeiner, Tracy R. Slatyer, and Neal Weiner. A Theory of Dark Matter. *Phys. Rev.*, D79:015014, 2009.
- [28] Nima Arkani-Hamed, Lawrence J. Hall, Hitoshi Murayama, David Tucker-Smith, and Neal Weiner. Small neutrino masses from supersymmetry breaking. *Phys.Rev.*, D64:115011, 2001.
- [29] Nima Arkani-Hamed and Neal Weiner. LHC Signals for a SuperUnified Theory of Dark Matter. *JHEP*, 12:104, 2008.
- [30] Howard Baer, Azar Mustafayev, Eun-Kyung Park, and Xerxes Tata. Target dark matter detection rates in models with a well-tempered neutralino. *JCAP*, 0701:017, 2007.
- [31] R. Barate et al. Search for the standard model Higgs boson at LEP. *Phys. Lett.*, B565:61–75, 2003.
- [32] Riccardo Barbieri, M. Frigeni, and G. F. Giudice. DARK MATTER NEUTRALINOS IN SUPERGRAVITY THEORIES. *Nucl. Phys.*, B313:725, 1989.
- [33] Vernon Barger, Wai-Yee Keung, and Gabe Shaughnessy. Spin Dependence of Dark Matter Scattering. *Phys. Rev.*, D78:056007, 2008.
- [34] M. Barnabe-Heider et al. Improved Spin Dependent Limits from the PICASSO Dark Matter Search Experiment. *Phys. Lett.*, B624:186–194, 2005.
- [35] A.J. Barr. Measuring slepton spin at the LHC. *JHEP*, 0602:042, 2006.
- [36] Alan Barr, Christopher Lester, and P. Stephens.  $m(T_2)$ : The Truth behind the glamour. *J.Phys.G*, G29:2343–2363, 2003.
- [37] Alan J. Barr, Ben Gripaios, and Christopher G. Lester. Weighing Wimps with Kinks at Colliders: Invisible Particle Mass Measurements from Endpoints. *JHEP*, 0802:014, 2008.
- [38] Alan J. Barr, Ben Gripaios, and Christopher G. Lester. Transverse masses and kinematic constraints: from the boundary to the crease. *JHEP*, 0911:096, 2009.

- [39] Stephen M. Barr, R. Sekhar Chivukula, and Edward Farhi. ELECTROWEAK FERMION NUMBER VIOLATION AND THE PRODUCTION OF STABLE PARTICLES IN THE EARLY UNIVERSE. *Phys. Lett.*, B241:387–391, 1990.
- [40] John D. Barrow. MASSIVE PARTICLES AS A PROBE OF THE EARLY UNIVERSE. *Nucl. Phys.*, B208:501–508, 1982.
- [41] S. W. Barwick et al. Measurements of the cosmic-ray positron fraction from 1- GeV to 50-GeV. *Astrophys. J.*, 482:L191–L194, 1997.
- [42] Brian Batell, Maxim Pospelov, and Adam Ritz. Exploring Portals to a Hidden Sector Through Fixed Targets. *Phys. Rev.*, D80:095024, 2009.
- [43] Brian Batell, Maxim Pospelov, and Adam Ritz. Multi-lepton Signatures of a Hidden Sector in Rare B Decays. 2009.
- [44] Brian Batell, Maxim Pospelov, and Adam Ritz. Probing a Secluded U(1) at B-factories. *Phys. Rev.*, D79:115008, 2009.
- [45] Christian W. Bauer, Zoltan Ligeti, Martin Schmaltz, Jesse Thaler, and Devin G. E. Walker. Supermodels for early LHC. 2009.
- [46] J. J. Beatty et al. New measurement of the cosmic-ray positron fraction from 5-GeV to 15-GeV. *Phys. Rev. Lett.*, 93:241102, 2004.
- [47] V.A. Bednyakov and H.V. Klapdor-Kleingrothaus. Update of the direct detection of dark matter and the role of the nuclear spin. *Phys.Rev.*, D63:095005, 2001.
- [48] V.A. Bednyakov and H.V. Klapdor-Kleingrothaus. On dark matter search after DAMA with Ge-73. *Phys.Rev.*, D70:096006, 2004.
- [49] E. Behnke et al. Improved Spin-Dependent WIMP Limits from a Bubble Chamber. *Science*, 319:933–936, 2008.
- [50] G. Belanger, E. Nezri, and A. Pukhov. Discriminating dark matter candidates using direct detection. *Phys. Rev.*, D79:015008, 2009.
- [51] Alexander V. Belikov and Dan Hooper. How Dark Matter Reionized The Universe. *Phys. Rev.*, D80:035007, 2009.
- [52] Maria Beltran, Dan Hooper, Edward W. Kolb, Zosia A. C. Krusberg, and Tim M. P. Tait. Maverick dark matter at colliders. 2010.
- [53] Carola F. Berger, James S. Gainer, JoAnne L. Hewett, and Thomas G. Rizzo. Supersymmetry Without Prejudice. *JHEP*, 02:023, 2009.
- [54] R. Bernabei et al. First results from DAMA/LIBRA and the combined results with DAMA/NaI. *Eur. Phys. J.*, C56:333–355, 2008.
- [55] R. Bernabei et al. New results from DAMA/LIBRA. 2010.
- [56] G. Bertone, David G. Cerdeno, J. I. Collar, and Brian C. Odom. WIMP identification through a combined measurement of axial and scalar couplings. *Phys. Rev. Lett.*, 99:151301, 2007.
- [57] James D. Bjorken, Rouven Essig, Philip Schuster, and Natalia Toro. New Fixed-Target Experiments to Search for Dark Gauge Forces. *Phys. Rev.*, D80:075018, 2009.
- [58] M. Boezio. Presentation given at idm08 conference. 2008.
- [59] Michael Burns, Kyoungchul Kong, Konstantin T. Matchev, and Myeonghun Park. Using Subsystem MT2 for Complete Mass Determinations in Decay Chains with Missing Energy at Hadron Colliders. *JHEP*, 0903:143, 2009.

- [60] Qing-Hong Cao, Ernest Ma, and Gabe Shaughnessy. Dark Matter: The Leptonic Connection. *Phys.Lett.*, B673:152–155, 2009.
- [61] Marcela Carena, Tao Han, Gui-Yu Huang, and Carlos E. M. Wagner. Higgs Signal for  $h$  to  $aa$  at Hadron Colliders. *JHEP*, 04:092, 2008.
- [62] Riccardo Catena and Piero Ullio. A novel determination of the local dark matter density. *JCAP*, 1008:004, 2010. \* Brief entry \*.
- [63] J. Chang. prepared for 29th International Cosmic Ray Conferences (ICRC 2005). 2005.
- [64] Spencer Chang, Jia Liu, Aaron Pierce, Neal Weiner, and Itay Yavin. CoGeNT Interpretations. 2010.
- [65] Spencer Chang and Markus A. Luty. Displaced Dark Matter at Colliders. 2009.
- [66] Spencer Chang, Aaron Pierce, and Neal Weiner. Momentum Dependent Dark Matter Scattering. *JCAP*, 1001:006, 2010.
- [67] Chuan-Hung Chen, Chao-Qiang Geng, and Dmitry V. Zhuridov. Neutrino Masses, Leptogenesis and Decaying Dark Matter. *JCAP*, 0910:001, 2009.
- [68] Hsin-Chia Cheng and Zhenyu Han. Minimal Kinematic Constraints and  $m(T2)$ . *JHEP*, 0812:063, 2008.
- [69] Hsin-Chia Cheng and Ian Low. TeV symmetry and the little hierarchy problem. *JHEP*, 0309:051, 2003.
- [70] Clifford Cheung, Joshua T. Ruderman, Lian-Tao Wang, and Itay Yavin. Kinetic Mixing as the Origin of Light Dark Scales. *Phys. Rev.*, D80:035008, 2009.
- [71] Kingman Cheung, Jeonghyeon Song, and Qi-Shu Yan. Role of  $h$   $\rightarrow$   $\eta$   $\eta$  in Intermediate-Mass Higgs Boson Searches at the Large Hadron Collider. *Phys. Rev. Lett.*, 99:031801, 2007.
- [72] Won Sang Cho, Kiwoon Choi, Yeong Gyun Kim, and Chan Beom Park. Gluino Stranverse Mass. *Phys.Rev.Lett.*, 100:171801, 2008.
- [73] Won Sang Cho, Kiwoon Choi, Yeong Gyun Kim, and Chan Beom Park. Measuring super-particle masses at hadron collider using the transverse mass kink. *JHEP*, 0802:035, 2008.
- [74] Ilias Cholis, Lisa Goodenough, Dan Hooper, Melanie Simet, and Neal Weiner. High Energy Positrons From Annihilating Dark Matter. 2008.
- [75] Marco Cirelli, Mario Kadastik, Martti Raidal, and Alessandro Strumia. Model-independent implications of the  $e^+e^-$ , anti-proton cosmic ray spectra on properties of Dark Matter. *Nucl.Phys.*, B813:1–21, 2009.
- [76] Andrew G. Cohen, D.B. Kaplan, and A.E. Nelson. Spontaneous baryogenesis at the weak phase transition. *Phys.Lett.*, B263:86–92, 1991.
- [77] Timothy Cohen, Eric Kuflik, and Kathryn M. Zurek. Extracting the Dark Matter Mass from Single Stage Cascade Decays at the LHC. *JHEP*, 1011:008, 2010.
- [78] Timothy Cohen, David E. Morrissey, and Aaron Pierce. Changes in Dark Matter Properties After Freeze-Out. *Phys. Rev.*, D78:111701, 2008.
- [79] Timothy Cohen, Daniel J. Phalen, and Aaron Pierce. On the Correlation Between the Spin-Independent and Spin- Dependent Direct Detection of Dark Matter. 2010.
- [80] Timothy Cohen, Daniel J. Phalen, Aaron Pierce, and Kathryn M. Zurek. Asymmetric Dark Matter from a GeV Hidden Sector. *Phys.Rev.*, D82:056001, 2010.

- [81] Timothy Cohen and Kathryn M. Zurek. Leptophilic Dark Matter from the Lepton Asymmetry. *Phys. Rev. Lett.*, 104:101301, 2010.
- [82] ATIC Collaboration. *Nature*, 456:362, 2008.
- [83] Juan Collar. *Talk at ITS/CUNY Emerging Problems in Particle Phenomenology Workshop*, April 2010.
- [84] J. Conway. PGS: Pretty Good Simulation software.
- [85] Cedric Delaunay, Christophe Grojean, and James D. Wells. Dynamics of Non-renormalizable Electroweak Symmetry Breaking. *JHEP*, 04:029, 2008.
- [86] S. Desai et al. Search for dark matter WIMPs using upward through-going muons in Super-Kamiokande. *Phys. Rev.*, D70:083523, 2004.
- [87] S. Dimopoulos, R. Esmailzadeh, Lawrence J. Hall, and N. Tetradis. Electroweak phase transition and dark matter abundance. *Phys. Lett.*, B247:601–606, 1990.
- [88] S. Dimopoulos, S. Raby, and Frank Wilczek. Supersymmetry and the Scale of Unification. *Phys.Rev.*, D24:1681–1683, 1981.
- [89] Savas Dimopoulos, Scott D. Thomas, and James D. Wells. Sparticle spectroscopy and electroweak symmetry breaking with gauge-mediated supersymmetry breaking. *Nucl. Phys.*, B488:39–91, 1997.
- [90] Abdelhak Djouadi, Manuel Drees, and Jean-Loic Kneur. Neutralino dark matter in mSUGRA: Reopening the light Higgs pole window. *Phys. Lett.*, B624:60–69, 2005.
- [91] L. Dolan and R. Jackiw. Symmetry Behavior at Finite Temperature. *Phys. Rev.*, D9:3320–3341, 1974.
- [92] F. Donato, D. Maurin, P. Brun, T. Delahaye, and P. Salati. Constraints on WIMP Dark Matter from the High Energy PAMELA  $\bar{p}/p$  data. *Phys.Rev.Lett.*, 102:071301, 2009.
- [93] Manuel Drees and Mihoko M. Nojiri. The Neutralino relic density in minimal  $N = 1$  supergravity. *Phys. Rev.*, D47:376–408, 1993.
- [94] John R. Ellis, Toby Falk, and Keith A. Olive. Neutralino-Stau Coannihilation and the Cosmological Upper Limit on the Mass of the Lightest Supersymmetric Particle. *Phys. Lett.*, B444:367–372, 1998.
- [95] John R. Ellis, Toby Falk, Keith A. Olive, and Mark Srednicki. Calculations of neutralino stau coannihilation channels and the cosmologically relevant region of MSSM parameter space. *Astropart. Phys.*, 13:181–213, 2000.
- [96] John R. Ellis, Andrew Ferstl, and Keith A. Olive. Re-evaluation of the elastic scattering of supersymmetric dark matter. *Phys. Lett.*, B481:304–314, 2000.
- [97] John R. Ellis, Andrew Ferstl, and Keith A. Olive. Exploration of elastic scattering rates for supersymmetric dark matter. *Phys. Rev.*, D63:065016, 2001.
- [98] John R. Ellis, Keith A. Olive, and Christopher Savage. Hadronic Uncertainties in the Elastic Scattering of Supersymmetric Dark Matter. *Phys. Rev.*, D77:065026, 2008.
- [99] Rouven Essig, Jared Kaplan, Philip Schuster, and Natalia Toro. On the Origin of Light Dark Matter Species. 2010.
- [100] Rouven Essig, Philip Schuster, and Natalia Toro. Probing Dark Forces and Light Hidden Sectors at Low-Energy  $e+e-$  Colliders. *Phys. Rev.*, D80:015003, 2009.

- [101] Rouven Essig, Philip Schuster, Natalia Toro, and Bogdan Wojtsekhowski. An Electron Fixed Target Experiment to Search for a New Vector Boson  $A'$  Decaying to  $e+e-$ . 2010.
- [102] Rob Fardon, Ann E. Nelson, and Neal Weiner. Dark energy from mass varying neutrinos. *JCAP*, 0410:005, 2004.
- [103] Brian Feldstein and A. Liam Fitzpatrick. Discovering Asymmetric Dark Matter with Anti-Neutrinos. 2010.
- [104] Jonathan L. Feng and Jason Kumar. The WIMPless Miracle: Dark-Matter Particles without Weak- Scale Masses or Weak Interactions. *Phys. Rev. Lett.*, 101:231301, 2008.
- [105] Jonathan L. Feng, Konstantin T. Matchev, and Frank Wilczek. Neutralino dark matter in focus point supersymmetry. *Phys.Lett.*, B482:388–399, 2000.
- [106] Jonathan L. Feng, Konstantin T. Matchev, and Frank Wilczek. Prospects for indirect detection of neutralino dark matter. *Phys.Rev.*, D63:045024, 2001.
- [107] Pavel Fileviez Perez and Mark B. Wise. On the Origin of Neutrino Masses. *Phys.Rev.*, D80:053006, 2009.
- [108] Fabio Finelli, Jan Hamann, Samuel M. Leach, and Julien Lesgourgues. Single-field inflation constraints from CMB and SDSS data. *JCAP*, 1004:011, 2010.
- [109] A. Liam Fitzpatrick, Dan Hooper, and Kathryn M. Zurek. Implications of CoGeNT and DAMA for Light WIMP Dark Matter. 2010.
- [110] Patrick J. Fox and Erich Poppitz. Leptophilic Dark Matter. *Phys.Rev.*, D79:083528, 2009.
- [111] Paul H. Frampton, Masahiro Kawasaki, Fuminobu Takahashi, and Tsutomu T. Yanagida. Primordial Black Holes as All Dark Matter. *JCAP*, 1004:023, 2010. \* Temporary entry \*.
- [112] Daniel Z. Freedman, David N. Schramm, and David L. Tubbs. The Weak Neutral Current and Its Effects in Stellar Collapse. *Ann. Rev. Nucl. Part. Sci.*, 27:167–207, 1977.
- [113] Joshua A. Frieman, Christopher T. Hill, and Richard Watkins. Late time cosmological phase transitions. 1. Particle physics models and cosmic evolution. *Phys. Rev.*, D46:1226–1238, 1992.
- [114] Hiroki Fukuoka, Jisuke Kubo, and Daijiro Suematsu. Anomaly Induced Dark Matter Decay and PAMELA/ATIC Experiments. *Phys.Lett.*, B678:401–406, 2009.
- [115] R. J. Gaitskell. Direct detection of dark matter. *Ann. Rev. Nucl. Part. Sci.*, 54:315–359, 2004.
- [116] Graciela B. Gelmini and Paolo Gondolo. Neutralino with the right cold dark matter abundance in (almost) any supersymmetric model. *Phys. Rev.*, D74:023510, 2006.
- [117] H. Georgi, Helen R. Quinn, and Steven Weinberg. Hierarchy of Interactions in Unified Gauge Theories. *Phys.Rev.Lett.*, 33:451–454, 1974.
- [118] Joel Giedt, Anthony W. Thomas, and Ross D. Young. Dark matter, the CMSSM and lattice QCD. 2009.
- [119] P. Gondolo et al. DarkSUSY: Computing supersymmetric dark matter properties numerically. *JCAP*, 0407:008, 2004.
- [120] Shrihari Gopalakrishna, Sunghoon Jung, and James D. Wells. Higgs boson decays to four fermions through an abelian hidden sector. *Phys. Rev.*, D78:055002, 2008.

- [121] Phill Grajek, Gordon Kane, Daniel J. Phalen, Aaron Pierce, and Scott Watson. Neutralino Dark Matter from Indirect Detection Revisited. 2008.
- [122] Kim Griest and David Seckel. Three exceptions in the calculation of relic abundances. *Phys. Rev.*, D43:3191–3203, 1991.
- [123] Ben Gripaios. Transverse observables and mass determination at hadron colliders. *JHEP*, 0802:053, 2008.
- [124] Howard E. Haber and Heather E. Logan. Radiative corrections to the  $Z$   $b$  anti- $b$  vertex and constraints on extended Higgs sectors. *Phys. Rev.*, D62:015011, 2000.
- [125] Lawrence J. Hall, Karsten Jedamzik, John March-Russell, and Stephen M. West. Freeze-In Production of FIMP Dark Matter. 2009.
- [126] Lawrence J. Hall, Takeo Moroi, and Hitoshi Murayama. Sneutrino cold dark matter with lepton number violation. *Phys.Lett.*, B424:305–312, 1998.
- [127] Jeffrey A. Harvey and Michael S. Turner. Cosmological baryon and lepton number in the presence of electroweak fermion number violation. *Phys. Rev.*, D42:3344–3349, 1990.
- [128] Junji Hisano, Shigeki Matsumoto, Mihoko M. Nojiri, and Osamu Saito. Direct detection of the Wino- and Higgsino-like neutralino dark matters at one-loop level. *Phys. Rev.*, D71:015007, 2005.
- [129] Junji Hisano, Shigeki Matsumoto, Mihoko M. Nojiri, and Osamu Saito. Non-perturbative effect on dark matter annihilation and gamma ray signature from galactic center. *Phys.Rev.*, D71:063528, 2005.
- [130] Junji Hisano, Kazunori Nakayama, and Masato Yamanaka. Implications of CDMS II result on Higgs sector in the MSSM. 2009.
- [131] Bob Holdom. Two  $U(1)$ 's and Epsilon Charge Shifts. *Phys.Lett.*, B166:196, 1986.
- [132] Dan Hooper and Kathryn M. Zurek. A Natural Supersymmetric Model with MeV Dark Matter. *Phys. Rev.*, D77:087302, 2008.
- [133] <http://dendera.berkeley.edu/plotter/entryform.html>.
- [134] Karsten Jedamzik. Big bang nucleosynthesis constraints on hadronically and electromagnetically decaying relic neutral particles. *Phys. Rev.*, D74:103509, 2006.
- [135] Gerard Jungman, Marc Kamionkowski, and Kim Griest. Supersymmetric dark matter. *Phys. Rept.*, 267:195–373, 1996.
- [136] Marc Kamionkowski and Michael S. Turner. THERMAL RELICS: DO WE KNOW THEIR ABUNDANCES? *Phys. Rev.*, D42:3310–3320, 1990.
- [137] Gordon Kane, Ran Lu, and Scott Watson. PAMELA Satellite Data as a Signal of Non-Thermal Wino LSP Dark Matter. *Phys.Lett.*, B681:151–160, 2009. \* Brief entry \*.
- [138] Junhai Kang, Paul Langacker, and Brent D. Nelson. Theory and Phenomenology of Exotic Isosinglet Quarks and Squarks. *Phys.Rev.*, D77:035003, 2008.
- [139] David B. Kaplan, Howard Georgi, and Savvas Dimopoulos. Composite Higgs Scalars. *Phys.Lett.*, B136:187, 1984.
- [140] David E. Kaplan, Markus A. Luty, and Kathryn M. Zurek. Asymmetric Dark Matter. *Phys. Rev.*, D79:115016, 2009.
- [141] Andrey Katz and Raman Sundrum. Breaking the Dark Force. *JHEP*, 06:003, 2009.

- [142] Masahiro Kawasaki, Kazunori Kohri, Takeo Moroi, and Akira Yotsuyanagi. Big-Bang Nucleosynthesis and Gravitino. *Phys. Rev.*, D78:065011, 2008.
- [143] Ian-Woo Kim. Algebraic Singularity Method for Mass Measurement with Missing Energy. *Phys.Rev.Lett.*, 104:081601, 2010.
- [144] Ryuichiro Kitano and Yasunori Nomura. A solution to the supersymmetric fine-tuning problem within the MSSM. *Phys. Lett.*, B631:58–67, 2005.
- [145] Ryuichiro Kitano and Yasunori Nomura. Dark matter before the LHC in a natural supersymmetric standard model. *Phys. Lett.*, B632:162–166, 2006.
- [146] Edward W. Kolb and Michael S. Turner. The Early universe. *Front. Phys.*, 69:1–547, 1990.
- [147] E. Komatsu et al. Five-Year Wilkinson Microwave Anisotropy Probe (WMAP) Observations:Cosmological Interpretation. *Astrophys. J. Suppl.*, 180:330–376, 2009.
- [148] E. Komatsu et al. Seven-Year Wilkinson Microwave Anisotropy Probe (WMAP) Observations: Cosmological Interpretation. *Astrophys.J.Suppl.*, 192:18, 2011.
- [149] Partha Konar, Kyoungchul Kong, Konstantin T. Matchev, and Myeonghun Park. Superpartner Mass Measurement Technique using 1D Orthogonal Decompositions of the Cambridge Transverse Mass Variable  $M_{T2}$ . *Phys.Rev.Lett.*, 105:051802, 2010.
- [150] Joachim Kopp, Thomas Schwetz, and Jure Zupan. Global interpretation of direct Dark Matter searches after CDMS-II results. *JCAP*, 1002:014, 2010.
- [151] George Lazarides, C. Panagiotakopoulos, and Q. Shafi. BARYOGENESIS AND THE GRAVITINO PROBLEM IN SUPERSTRING MODELS. *Phys. Rev. Lett.*, 56:557, 1986.
- [152] H. S Lee. et al. Limits on WIMP-nucleon cross section with CsI(Tl) crystal detectors. *Phys. Rev. Lett.*, 99:091301, 2007.
- [153] C.G. Lester and D.J. Summers. Measuring masses of semiinvisibly decaying particles pair produced at hadron colliders. *Phys.Lett.*, B463:99–103, 1999.
- [154] Ilan Levine. *Private Communication*, 2009.
- [155] Ilan Levine. The COUPP Dark Matter Search Experiment. *Talk at DPF*, 2009.
- [156] W. Love et al. Search for Light CP-odd Higgs in Radiative Decays of Upsilon(1S). 2008.
- [157] David H. Lyth and Ewan D. Stewart. Thermal inflation and the moduli problem. *Phys. Rev.*, D53:1784–1798, 1996.
- [158] Rakhi Mahbubani and Leonardo Senatore. The minimal model for dark matter and unification. *Phys. Rev.*, D73:043510, 2006.
- [159] Rakhi Mahbubani and Leonardo Senatore. The minimal model for dark matter and unification. *Phys. Rev.*, D73:043510, 2006.
- [160] Vuk Mandic, Aaron Pierce, Paolo Gondolo, and Hitoshi Murayama. The Lower bound on the neutralino nucleon cross-section. 2000.
- [161] M. Markevitch et al. A Textbook Example of a Bow Shock in the Merging Galaxy Cluster 1E0657-56. *Astrophys. J.*, 567:l27, 2002.
- [162] Stephen P. Martin. *A Supersymmetry Primer*. 1997.
- [163] Konstantin T. Matchev, Filip Moortgat, Luc Pape, and Myeonghun Park. Precision sparticle spectroscopy in the inclusive same-sign dilepton channel at LHC. *Phys.Rev.*, D82:077701, 2010.

- [164] Konstantin T. Matchev and Myeonghun Park. A General method for determining the masses of semi-invisibly decaying particles at hadron colliders. 2009.
- [165] Patrick Meade, Michele Papucci, Alessandro Strumia, and Tomer Volansky. Dark Matter Interpretations of the  $e^+$ - Excesses after FERMI. *Nucl.Phys.*, B831:178–203, 2010.
- [166] Takeo Moroi and Lisa Randall. Wino cold dark matter from anomaly mediated SUSY breaking. *Nucl.Phys.*, B570:455–472, 2000.
- [167] David E. Morrissey, David Poland, and Kathryn M. Zurek. Abelian Hidden Sectors at a GeV. *JHEP*, 07:050, 2009.
- [168] Emmanuel Moulin, F. Mayet, and D. Santos. Supersymmetric dark matter search via spin-dependent interaction with He-3. *Phys. Lett.*, B614:143–154, 2005.
- [169] Pran Nath and Richard L. Arnowitt. Predictions in SU(5) supergravity grand unification with proton stability and relic density constraints. *Phys. Rev. Lett.*, 70:3696–3699, 1993.
- [170] Brian Patt and Frank Wilczek. Higgs-field portal into hidden sectors. 2006.
- [171] Michael Edward Peskin and James Daniel Wells. How can a heavy Higgs boson be consistent with the precision electroweak measurements? *Phys. Rev.*, D64:093003, 2001.
- [172] Giacomo Polesello and Daniel R. Tovey. Supersymmetric particle mass measurement with the boost-corrected contranverse mass. *JHEP*, 1003:030, 2010.
- [173] Georg G. Raffelt. Astrophysical axion bounds. *Lect. Notes Phys.*, 741:51–71, 2008.
- [174] Lisa Randall and Raman Sundrum. A Large mass hierarchy from a small extra dimension. *Phys.Rev.Lett.*, 83:3370–3373, 1999.
- [175] Rogerio Rosenfeld. Relic abundance of mass-varying cold dark matter particles. *Phys. Lett.*, B624:158–161, 2005.
- [176] Leszek Roszkowski, Roberto Ruiz de Austri, and Takeshi Nihei. New cosmological and experimental constraints on the CMSSM. *JHEP*, 08:024, 2001.
- [177] Vera C. Rubin and W. Kent Ford, Jr. Rotation of the Andromeda Nebula from a Spectroscopic Survey of Emission Regions. *Astrophys. J.*, 159:379–403, 1970.
- [178] P. Salucci, F. Nesti, G. Gentile, and C.F. Martins. The dark matter density at the Sun’s location. *Astron.Astrophys.*, 523:A83, 2010. \* Temporary entry \*.
- [179] Robert Schabinger and James D. Wells. A minimal spontaneously broken hidden sector and its impact on Higgs boson physics at the Large Hadron Collider. *Phys. Rev.*, D72:093007, 2005.
- [180] Philip Schuster, Natalia Toro, and Itay Yavin. Terrestrial and Solar Limits on Long-Lived Particles in a Dark Sector. *Phys. Rev.*, D81:016002, 2010.
- [181] Geraldine Servant and Timothy M.P. Tait. Elastic scattering and direct detection of Kaluza-Klein dark matter. *New J.Phys.*, 4:99, 2002.
- [182] Geraldine Servant and Timothy M.P. Tait. Is the lightest Kaluza-Klein particle a viable dark matter candidate? *Nucl.Phys.*, B650:391–419, 2003.
- [183] Mikhail A. Shifman, A. I. Vainshtein, and Valentin I. Zakharov. Remarks on Higgs Boson Interactions with Nucleons. *Phys. Lett.*, B78:443, 1978.
- [184] Torbjorn Sjostrand, Stephen Mrenna, and Peter Skands. PYTHIA 6.4 Physics and Manual. *JHEP*, 05:026, 2006.



- [185] Tracy R. Slatyer, Nikhil Padmanabhan, and Douglas P. Finkbeiner. CMB Constraints on WIMP Annihilation: Energy Absorption During the Recombination Epoch. *Phys. Rev.*, D80:043526, 2009.
- [186] Paul J. Steinhardt and Michael S. Turner. Saving the Invisible Axion. *Phys. Lett.*, B129:51, 1983.
- [187] Matthew J. Strassler. Possible effects of a hidden valley on supersymmetric phenomenology. 2006.
- [188] Matthew J. Strassler and Kathryn M. Zurek. Echoes of a hidden valley at hadron colliders. *Phys. Lett.*, B651:374–379, 2007.
- [189] (ed.) 't Hooft, Gerard, (ed.) Itzykson, C., (ed.) Jaffe, A., (ed.) Lehmann, H., (ed.) Mitter, P.K., et al. Recent Developments in Gauge Theories. Proceedings, Nato Advanced Study Institute, Cargese, France, August 26 - September 8, 1979. *NATO Adv.Study Inst.Ser.B Phys.*, 59:1–438, 1980.
- [190] Zachary Thomas, David Tucker-Smith, and Neal Weiner. Mixed Sneutrinos, Dark Matter and the CERN LHC. *Phys.Rev.*, D77:115015, 2008.
- [191] S. Torii et al. High-energy electron observations by PPB-BETS flight in Antarctica. 2008.
- [192] David Tucker-Smith and Neal Weiner. Inelastic dark matter. *Phys. Rev.*, D64:043502, 2001.
- [193] Matteo Viel, Julien Lesgourgues, Martin G. Haehnelt, Sabino Matarrese, and Antonio Riotto. Constraining warm dark matter candidates including sterile neutrinos and light gravitinos with WMAP and the Lyman- alpha forest. *Phys. Rev.*, D71:063534, 2005.
- [194] D. Walsh, R. F. Carswell, and R. J. Weymann. 0957 + 561 A, B - Twin quasistellar objects or gravitational lens. *Nature*, 279:381–384, 1979.
- [195] Steven Weinberg. Gauge and Global Symmetries at High Temperature. *Phys. Rev.*, D9:3357–3378, 1974.
- [196] Christopher Wiebusch et al. Physics Capabilities of the IceCube DeepCore Detector. 2009.
- [197] Frank Wilczek. Decays of Heavy Vector Mesons Into Higgs Particles. *Phys. Rev. Lett.*, 39:1304, 1977.
- [198] Katsuji Yamamoto. PHASE TRANSITION ASSOCIATED WITH INTERMEDIATE GAUGE SYMMETRY BREAKING IN SUPERSTRING MODELS. *Phys. Lett.*, B168:341, 1986.
- [199] Kathryn M. Zurek. Multi-Component Dark Matter. *Phys. Rev.*, D79:115002, 2009.
- [200] F. Zwicky. Spectral displacement of extra galactic nebulae. *Helv. Phys. Acta*, 6:110–127, 1933.